Faculdade de Engenharia da Universidade do Porto

Study of intestinal homeostasis by means of organ-on-chip technologies

Joana Inês Carlos Pimenta

Master's Thesis

Mestrado Integrado em Bioengenharia - Biotecnologia Molecular

Supervisor: Marta Alves da Silva, PhD, i3S

Co-supervisor: Pedro Costa, PhD, Biofabics

Co-supervisor: Bruno Pereira, PhD, i3S

November 2020

Study of intestinal homeostasis by means of organ-on-chip technologies

Joana Inês Carlos Pimenta

Mestrado Integrado em Bioengenharia - Biotecnologia Molecular

November 2020

Funding

This work was funded by Fundação para a Ciência e Tecnologia (FCT) through the project grant POCI-01-0145-FEDER-031538. This work has also been supported by the following entities: Portuguese funds through FCT in the framework of the project "Institute for Research and Innovation in Health Sciences" (POCI-01-0145-FEDER-007274); NORTE-01-0145-FEDER-000029, Norte Portugal Regional Programme (NORTE 2020), under the PORTUGAL 2020 Partnership Agreement, through the European Regional Development Fund (ERDF); FEDER - Fundo Europeu de Desenvolvimento Regional funds through the COMPETE 2020 - Operacional Programme for Competitiveness and Internationalisation (POCI), Portugal 2020.

FCT Fundação para a Ciência e a Tecnologia
MINISTÉRIO DA CIÊNCIA, TECNOLOGIA E ENSINO SUPERIOR

INSTITUTO DE INVESTIGAÇÃO E INOVAÇÃO EM SAÚDE
UNIVERSIDADE DO PORTO

Resumo

O intestino delgado é o órgão humano onde decorre a parte mais significativa da absorção de nutrientes e fármacos. O epitélio intestinal tem uma das taxas de renovação mais altas do corpo humano, que é suportada pelas células estaminais do intestino (CEIs) $Lgr5^{+}$. Na base das criptas intestinais, as CEIs estão protegidas do ambiente hostil do lúmen intestinal e recebem sinais das populações celulares vizinhas que ativam vias de sinalização associadas com a estaminalidade e proliferação. Gradientes de fatores de crescimento formam-se ao longo do eixo cripta-vilosidade e contribuem para a compartimentalização de zonas de proliferação e de diferenciação. O conhecimento sobre a biologia das CEIs e dos componentes do nicho estaminal possibilitaram a criação de protocolos para o desenvolvimento de organoides intestinais. Organoides intestinais são modelos *in vitro* tridimensionais que recriam a organização celular e parte da funcionalidade do intestino delgado. No entanto, algumas desvantagens podem ser apontadas a este modelo como a limitação de tamanho, a falta de controlo da morfologia e a reduzida complexidade do modelo.

A microfluídica surgiu da aplicação das técnicas de microfabricação à manipulação de fluidos à escala micrométrica. Recentemente, abordagens de microfluídica têm sido acopladas à cultura de células, criando modelos *in vitro*, compactos e modulares com caraterísticas facilmente controláveis. Modelos *intestine-on-chip* podem incorporar a simulação de movimentos peristálticos, gradientes de oxigénio e co-culturas com células endoteliais, imunológicas e bactérias da microbiota, por exemplo. Muitos sistemas *intestine-on-chip* usam linhas celulares imortalizadas ou células dissociadas derivadas de organoides, mas sistemas baseados em organoides inteiros são pouco comuns.

O presente trabalho focou-se em desenvolver estratégias de microfluídica para a otimização da cultura de organoides intestinais derivados de ratinho, com vista à construção de um modelo intestinal-organoid-on-chip biomimético. Dispositivos de microfluídica foram produzidos por impressão 3D na empresa Biofabics e testados com cultura de organoides, com e sem fluxo de meio de cultura. Nesta dissertação, a otimização de condições experimentais, como a concentração de matrigel, tempo de polimerização e taxa de fluxo para a perfusão de meio, assim como a adaptação de designs de microfluidica para aumentar a eficiência destas experiências são descritos. O crescimento de organoides foi monitorizado através de microscopia de time-lapse e a expressão de marcadores relevantes de estaminalidade e diferenciação foi analisada. Os organoides intestinais foram cultivados com sucesso num dos dispositivos desenvolvidos, sem fluxo de meio, e mantiveram-se viáveis depois de 4 dias. Organoides cultivados no dispositivo pareceram amadurecer mais rapidamente que os organoides cultivados em condições tradicionais. A permeabilidade aos gases e o encaixe dos elementos do dispositivo têm de ser melhorados de forma a permitir experiências com perfusão contínua de meio de cultura. Adicionalmente, foi desenhado um dispositivo de microfluídica para o desenvolvimento de organoides com estrutura tubular.

Sumariamente, este trabalho descreve a fase inicial de desenvolvimento de um modelo *in vitro* do intestino delgado baseado em microfluídica e que pode poderá no futuro ser aplicado no estudo de doenças gastrointestinais, biologia de células estaminais e testes a fármacos no âmbito da medicina personalizada.

Abstract

The small intestine is the human organ where the most significant part of nutrient and drug absorption takes place. The intestinal epithelium has one of the highest turnover rates in the body that is supported by $Lgr5^+$ intestinal stem cells (ISCs). In the base of intestinal crypts, ISCs are protected from the hostile environment of the intestinal lumen and receive cues from neighboring cell populations that activate signaling pathways associated with stemness and proliferation. Growth factor gradients are created along the crypt-villus axis and enable the compartmentalization of proliferation and differentiation zones. The knowledge of ISC biology and the components of the stem cell niche paved the way for the determination of protocols for developing intestinal organoids. Intestinal organoids are 3D *in vitro* models that recreate the cellular organization and part of the functionality of the small intestine. However, some shortcomings can still be pointed to this model, such as limited size, lack of control over morphology, and low complexity.

Microfluidics arose from the application of microfabrication techniques to fluid manipulation at the micrometric scale. Recently, microfluidic approaches have been coupled with cell culture, creating self-contained and modular *in vitro* models with easily controllable features. Intestine-on-chip models can incorporate peristalsis simulation, oxygen gradients, and co-culture with endothelial, immune cells, and bacteria from the microbiota. Many intestine-on-chip systems use immortalized cell lines or dissociated cells from organoids, but reports of systems based on whole organoids are scarce.

This work focused on engineering microfluidic strategies to optimize mouse-derived intestinal organoid culture, aiming to the development of a biomimetic intestinal-organoid-on-chip model. Microfluidic devices were produced by 3D printing in Biofabics and tested with organoid culture, with and without fluid flow. Optimization of experimental conditions, such as matrigel concentration, polymerization time, and flow rates for medium perfusion, as well as adaptation of microfluidic designs to improve the efficiency of the experiments are reported in this dissertation. Organoid growth was monitored by time-lapse microscopy and gene expression profiles of relevant stem and differentiation markers were analyzed. Intestinal organoids were successfully cultured in one of the microfluidic devices developed, without fluid flow, and remained viable after 4 days. Organoids cultured in the device appeared to mature faster than organoids grown in standard conditions. Further optimization of gas permeability and lid fitting in the microfluidic system is required to enable experiences with fluid flow. Additionally, a microfluidic design to support organoid development in tubular shape was projected.

In summary, this work describes the initial phase of development of a microfluidic-based *in vitro* model of the small intestine that can potentially be applied to gastrointestinal disease studies, stem cell biology research, and drug testing in personalized medicine.

Agradecimentos

Antes de mais, agradeço aos meus orientadores neste trabalho, Marta Alves da Silva, Bruno Pereira e Pedro Costa por todo o conhecimento que me transmitiram ao longos dos últimos meses e a sua constante disponibilidade para ajudar. Gostaria de agradecer ao grupo Differentiation and Cancer, do Instituto de Investigação e Inovação em Saúde (i3S), por me ter acolhido durante estes meses para a realização da minha dissertação de final de curso. Agradeço também à Biofabics por me dar a oportunidade de realizar a tese num ambiente de interface entre a academia e a indústria. Agradeço ao Ricardo Ribeiro por toda a ajuda, disponibilidade e motivação que me deu e também à Vanessa Machado por ter sido uma tábua de salvação em alguns momentos complicados.

Agradeço também à equipa de Advanced Light Microscopy do i3S, em particular, Paula Sampaio e Maria Azevedo, pelo apoio nas experiências com o microscópio de Time-lapse.

Um grande obrigada aos meus pais, por todos os esforços que fizeram e ainda fazem por mim. Por serem mais pacientes comigo do que eu própria e nunca porem entraves aos meus sonhos e ambições. Por terem sempre um ombro (e ouvido) amigo nos momentos mais difíceis. Obrigada por tudo.

Irei para sempre recordar estes últimos 5 anos em que aprendi muito não só sobre Bioengenharia mas sobretudo a trabalhar sob pressão, espírito crítico e a não ter medo de desafios, porque tudo se faz. Acredito que mais do que nos formar para uma profissão, a faculdade endurece-nos e prepara-nos para os desafios que nos aparecerão pela frente. Por isso, tenho de dar um enorme obrigado à FEUP, a minha faculdade de coração, onde sempre me senti em casa e fui muito muito muito feliz. Ficam as saudades das salas de estudo, do bar de minas e dos cachorros do bar da biblioteca, assim como, dos bons momentos diurnos e noturnos passados na AEFEUP. Agradeço também ao ICBAS, principalmente pelas vistas maravilhosas para o rio Douro, pelos beagles e pelos pavões. Agradeço também a todos os professores que tive ao longo destes 5 anos que de uma forma ou de outra, contribuíram para o meu desenvolvimento intelectual, científico e pessoal. Tenho muito orgulho em ter estudado nas melhores faculdades da melhor universidade do país e se voltasse atrás no tempo a minha escolha teria sido a mesma.

Não posso deixar de agradecer também ao NEB-FEUP/ICBAS e a todos os membros com quem tive o prazer de trabalhar nestes 3 anos. O NEB acabou por ser, para mim, uma verdadeira escola, onde conheci pessoas muito diferentes e tive a oportunidade de aprender o que é trabalhar em equipa por um mesmo objetivo. O NEB obrigou-me a sair da minha zona de conforto e ensinou-me que com pouco se consegue fazer muito. Ensinou-me a sonhar alto e a correr riscos. Porque, de facto, quando se trabalha com a alegria e a dedicação que o NEB tem, tudo é possível. Obrigada, em particular, aos meus colegas da Direção do ano de 2019/2020, a Ana e o Gu, porque, se não fosse com eles, eu nunca teria aceitado este desafio. Obrigada por nunca nos termos chateado ou deixado que os problemas do NEB se sobrepusessem à nossa amizade. Aprendi mais com vocês do que possam imaginar e admiro-vos imenso. E orgulho-me também por termos cumprido a nossa promessa de nunca dizer mal do NEB.

Agradeço também a todos os amigos que tive o prazer de encontrar durantes estes anos que tornaram esta viagem mais fácil e divertida. A começar pela Ana, o Gu, o Álvaro e a Nati, um grande obrigada por serem os mais antigos e por todas as memórias que fizemos juntos. Seja de viagens, sessões de estudo, campismos, conversas profundas e noites de festa, só ficam histórias para contar, umas hilariantes, outras menos. Podia escrever aqui um livro sobre a nossa amizade e as nossas aventuras. Destaque para o grupinho de Glasgow e os momentos de terror verdadeiro que vivemos na nossa casa infestada pela personagem roedora coletiva Speedy González, também

conhecida por Schrödinger, e para as várias torradas diárias que causavam sempre o disparo do alarme de incêndio. Não esquecerei também as viagens que fizemos juntos pela Escócia, nem a vez que acampamos no meio de um monte, debaixo de uma tempestade e com temperaturas negativas, na ínfima esperança de ver as auroras boreais. Valeu pela vista matinal incrível do Loch Lomond. Um beijinho especial para a Nati, por ser a minha parceira fiel de Biotec e confidente próxima de todo o tipo de problemas e questões da vida. Obrigada pela amizade e por toda a paciência que tens para mim. Agradeço também à Violeta, pelo seu espírito livre contagiante. Passando aos amiguinhos de Biomédica: Obrigada às Gémeas Nónó e Raquel por ajudarem sempre a trazer um pouco de bom senso e sensibilidade feminina a este grupo disfuncional, por serem parceiras na compra online de bikinis e pelos gossips, claro. Obrigada ao Pedrão por ter acordado para a vida e mudado para o MIB, onde veio tornar os seus e nossos dias, sem dúvida, mais divertidos. Ao Migas, que apesar de falar pouco, diz sempre a coisa certa. Ao Vizinho, Pedro Dias, Pierre Jours, Pedrini, pelas viagens de metro e as boleias onde às vezes só falamos das cadeiras e do stress da faculdade, como os dois nervosinhos que somos, mas ocasionalmente também da vida em geral. Obrigada ao Meneses, por ser um amigo extremamente preocupado e presente, que não deixa que ninguém se sinta esquecido e que me ajudou muito ao longo destes anos. Também ao Bruno, por ver as coisas sempre por uma perspetiva diferente da do resto das pessoas e pela paciência que tem para ensinar novos jogos de tabuleiro aos amigos. Por fim, um obrigado ao pessoal de Biotec. Primeiro, às Biotecas Marta, Mónica e Nati por todos os almoços e intervalos, os trabalhos de grupo e pelos momentos de desespero coletivos em que dissemos mal das cadeiras, da matéria, dos trabalhos e dos professores, sem esquecer também dos livros comprados em conjunto e do nosso cacifo partilhado (499). Obrigada por terem tornado estes últimos 3 anos numa experiência mais agradável. Um beijinho também para a Andreia e a Bea que tive o prazer de conhecer melhor neste último ano. Adoro-vos a todos, do fundo do coração e espero que continuemos a ser amigos por muitos mais anos. Foi bom.

Aos amigos extra-faculdade, que ao longo dos últimos anos foram indo e vindo. Um principal obrigada à Ana por ser quase uma irmã, por sofrer os meus problemas comigo, e vice-versa, e porque sei que se um dia lhe ligar a meio da noite a pedir ajuda, ela não vai hesitar. Obrigada por tudo amiga. Agradeço também ao Luís por me saber sempre animar, por ser uma das pessoas mais fortes que conheço e me inspirar todos os dias a querer ser melhor.

Um obrigada também ao Iago por ser um anjo que apareceu na minha vida e que me aceita tal e qual como eu sou, porque ele é igual. Por me motivar a sonhar alto e por toda a compreensão e paciência que tem comigo. No fundo, agradeço-lhe por não desistir de mim, nunca.

Este é um fim de curso, sem dúvida, anti-climático. Neste ano particularmente complicado, ficaram a faltar muitos momentos marcantes, como o Cartolanço, a semana da Queima das Fitas e o Cortejo, que idealizamos durante tantos anos. É como se não nos pudéssemos despedir destes últimos anos que foram tão importantes para nós. O valor e a importância da conclusão desta etapa perdem parte do seu significado. Fica apenas o sonho de um dia ainda vir a ser cartolada e de poder descer os Clérigos de cartola e bengala, de braço dado com os meus amigos da faculdade, tal como merecemos.

A todos, um enorme obrigada.

Joana Pimenta

"Whether you think you can
or you think you can't,
you are right."

Henry Ford

Contents

List of Figures

List of Tables

List of Abbreviations

2D	Two-dimensional
2PP	Two-photon polymerization
3D	Three-dimensional
APC	Adenomatous polyposis coli
BMP	Bone morphogenetic protein
CEIs	Células estaminais do intestino
CBC	Crypt-base-columnar cell
CF	Cystic fibrosis
CFTR	Cystic fibrosis transmembrane conductance regulator
CO	Cardiac output
Col	Collagen
CYP2C9	Cytochrome P450 2C9
CYP3A4	Cytochrome P450 3A4
DC	Dendritic cell
dH_2O	Distilled water
DKK-1	Dickkopf-1
DMEM	Dulbecco's Modified Eagle Medium
DMSO	Dimethyl sulfoxide
DTR	Diphtheria toxin receptor
EC	Endothelial cell
EC50	Half maximal effective concentration
ECM	Extracellular matrix
EDTA	Ethylenediamine tetraacetic acid
EdU	5-ethynyl-2'-deoxyuridine
EGF	Epidermal growth factor
EGFP	Enhanced green fluorescent protein
EIEC	Pathogenic strain of *Escherichia coli*
ELISA	Enzyme-Linked Immunosorbent Assay
ER	Estrogen receptor
ESC	Embryonic stem cell
FACS	Fluorescence activated cell sorting
FBS	Fetal Bovine Serum
FDA	Food and Drug Administration
FDM	Fused deposition modeling
FITC	Fluorescein isothiocyanate
FSC	Forward scatter
FZD	Frizzled
GFP	Green fluorescent protein
GFP-EC	Non-pathogenic strain of *Escherichia coli* marked by GFP expression
GPQ-W	Glycine-Proline-Glutamine-Tryptophan

H&E	Hematoxylin and eosin
HEPES	4-(2-hydroxyethyl)-1-piperazineethanesulfonic acid
HIMEC	Human intestinal microvascular endothelial cell
HUVEC	Human umbilical vascular endothelial cell
IBD	Inflammatory bowel disease
IgA	Immunoglobulin A
iPSC	Induced pluripotent stem cell
ISC	Intestinal stem cell
ISEMF	Intestinal subepithelial myofibroblast
LGG	*Lactobacillus rhamnosus* GG
LGR5	Leucine-rich repeat-containing G-protein couple receptor 5
Lgr5^{EGFP}	*Lgr5-EGFP-IRES-creERT2*
LPS	Lipopolysaccharide
Lyz1	Lysozyme 1 gene
MJM	Multi-jet modeling
mMph	Mucosal macrophage
NOG	Noggin
NSF	National Sanitation Foundation
PBS	Phosphate-buffered saline
PBMC	Peripheral blood mononuclear cell
PC	Polycarbonate
Pcna	Proliferating cell nuclear antigen gene
PDMS	Polydimethylsiloxane
PE	Phycoerythrin
PEG	Polyethylene glycol
PET	Polyethylene terephthalate
PMMA	Poly(methyl methacrylate)
PPARγ	Peroxisome proliferator-activated receptor
qRT-PCR	Quantitative real-time polymerase chain reaction
RGD	Arginine-Glycine-Aspartate
RIF	Rifampicin
ROCK	Rho-associated protein kinase
rpm	Rotations per minute
RSPO	R-spondin
SLA	Stereolithopgraphy
SSC	Side scatter
TA	Transit-amplifying
TCF	T-cell factor
TEER	Transepithelial electrical resistance
VD3	1,25-dihidroxyvitamin D3

Chapter 1

Introduction

1.1 The small intestine

1.1.1 Anatomy and function

The digestive tract consists of a sequence of organs that form a tubular system. The characteristics of each organ in the digestive system are inherently related to their functional demands. Overall, the main activities of the digestive system are food reception, storage, transport and processing, absorption of nutrients, protection from external factors and evacuation. The small intestine is a critical organ in this system, not only due to its dimensions (5 meters is the mean length in a living human adult [44]), but also because of its major role in absorption. It is divided in 3 parts:

- **Duodenum**: receives the digestion product from the stomach as well as the digestive juices from the pancreas and liver and neutralizes gastric acids;
- **Jejunum**: composed of circular folds decorated with villi and where the largest percentage of absorption occurs;
- **Ileum**: the final part of the small intestine before the connection to the large intestine, responsible for the absorption of the remaining nutrients and bile [26].

1.1.2 Microanatomy

The peculiar microanatomy of the small intestine wall makes it resistant to continuous aggression by mechanical stress, pH variation or pathogens, while performing nutrient absorption and without compromising tissue homeostasis. The lining of the intestine wall shows a succession of circular and semilunar folds of mucosa and submucosa, called *plicae circulares* (Figure 1.1a) [70]. The absorptive surface of the small intestine mucosa is composed of millions of villi - protuberances in the epithelium projecting up to 1 millimeter inside the intestinal lumen (Figure 1.1a and Figure 1.1b). In addition, each epithelial cell in the villus is decorated with up to 1000 microvilli, protruding 1 micrometer from the surface of the villi [42]. Each villus is sided by tissue infoldings, the crypts of Lieberkühn, forming the crypt-villus structure (Figure 1.1b).

The continuous folds in the intestinal epithelium allow an increase in the surface area of the intestine of about 60-120 times, boosting the efficiency of the absorption process [44]. Additionally, these structures are densely supplied with blood and lymph vessels that rapidly transport the nutrients to the rest of the organism.

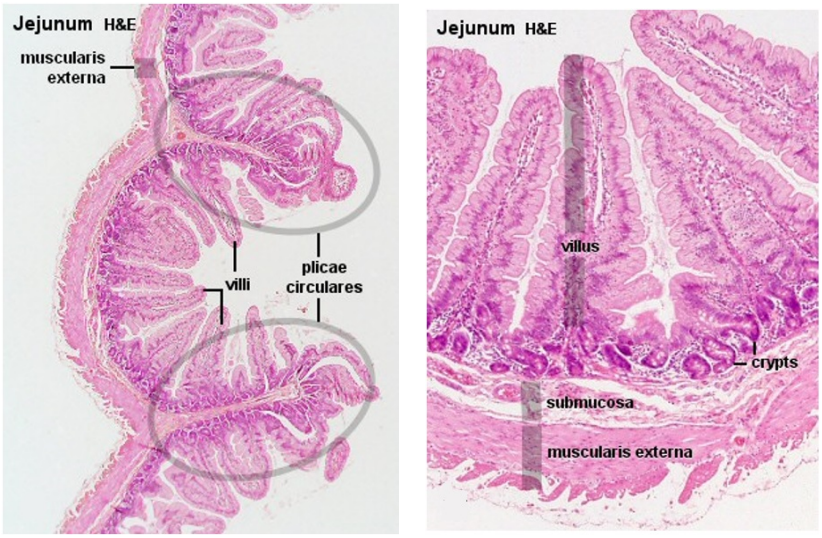

(a) **(b)**

Figure 1.1: Hematoxylin and eosin staining of the jejunum. (a) *Plicae circulares* covered with villi. (b) Villi and crypts of Lieberkühn are part of the intestinal mucosa. The submucosa and *muscularis externa* are located below the mucosa. Images adapted from [86].

1.1.3 Histological characterization

There are 6 types of differentiated cells in the small intestine mucosa:

- **Enterocytes**: tall columnar cells with an oval nucleus in the basal end. The apical part of the enterocyte shows a striated border consisting of a layer of microvilli covered by glycocalyx through which nutrients are internalized by the cells, denominated brush border [70]. Their function is mostly absorptive.

- **Goblet cells**: intraepithelial mucin-secreting glands important for protecting and lubricating the epithelial surface. Goblet cells have a polarized morphology, having organelles in the basal part while the apical end is rich in vesicles containing mucins. This distribution of organelles makes mucin secretion to the mucosa more efficient [105].

- **Paneth cells**: exocrine cells with large eosinophilic granules in the apical cytoplasm. Their main role is to secrete anti-microbial peptides such as lysozyme and phospholipase A, regulating the microenvironment of the intestinal crypts and protecting neighboring cells from pathogens [70]. Moreover, they release signaling factors to the stem cell niche.

- **Enteroendocrine cells**: cells that secrete hormones to the intestinal lumen and apically display chemoreceptors that recognize nutrient levels to regulate hormone release basally [70].

- **M (microfold) cells**: specialized epithelial cells covering the lymphoid tissue in the ileum mucosa, the Peyer patches. M cells apically show microfolds. On the basal side these cells have intracellular pockets occupied by lymphocytes and antigen-presenting cells that communicate with the lymphoid tissue below, through an especially porous basement membrane. M cells uptake antigens in the intestinal lumen that are transported to the antigen-presenting cells and presented in the lymph nodes where an immune response can be triggered [70].

- **Tuft cells**: rare cell type in the intestinal epithelium, characterized by long and blunt microvilli protruding from a narrow apex and a highly developed tubulovesicular system in the supranuclear position. The exact role of tuft cells in the intestine is still to be defined however, these cells express chemosensory proteins, suggesting an association with the nervous system. Other reports, associate tuft cells to epithelial recovery upon damage and to type 2 immune response against parasitic infection in the intestine [81, 7].

Covering the villi there is a simple columnar epithelium of enterocytes, intercalated with goblet cells. The core of the villus is composed of connective tissue that starts at the lamina propria and contains several different cell types such as fibroblasts and lymphocytes, capillaries, and a central lymphatic vessel. Below the intestinal mucosa, the submucosa and a muscle layer called *muscularis externa* can be found (Figure 1.1b).

In order to maintain homeostasis under the hostile conditions of the intestinal environment, the small intestine epithelium has one of the highest turnover rates of the whole body – 3 to 6 days in humans [22]. An increased rate of cell proliferation is demanded to ensure the epithelium is regenerated rapidly upon lesion, especially because the intestinal tissue acts as a barrier that protects the body from possible pathogens in ingested food. The high level of proliferation demanded in the small intestine is maintained by a population of intestinal stem cells (ISCs) that reside at the bottom of the crypts. ISCs are multipotent stem cells, meaning they can differentiate in every cell type present in the intestine and self-renew in the long term. Their location at the bottom of the crypt provides a degree of protection from the intestinal lumen and the aggressive processes that take place.

1.1.4 Microbiota

The term microbiota refers to the population of microorganisms - bacteria, fungi, archae, virus and protozoans - that reside in a particular environment [46]. The intestinal microbiota is especially important in humans due its extensive metabolic capacity and substantial functional plasticity, being considered by some specialists as an additional organ [4, 8, 28, 60]. Although a majority of microorganisms is considered pathogenic and triggers immunological reactions in the human body, the microbiota is composed of commensal microorganisms, i.e., microbes that establish a symbiotic relationship with the intestinal mucosa and benefit human health. On the other hand, diseases such as inflammatory bowel disease, allergies, obesity, diabetes, and cancer have been associated with altered bacterial diversity. These data suggest that a varied microbiota population correlates with an intestine that is healthier and more resistant to environmental agents [100]. The human gastrointestinal tract comprises over 100 trillion microorganisms [16]. The microbiota is a dynamic

population that shows spatial and temporal differences of number of microbes, distribution and species present. Its diversity is influenced by age, diet and antibiotics.

Some of the colonic microorganisms in intestinal microbiota metabolize indigestible nutrients, since they express enzymes that are not present in the human body. Fermentation of carbohydrates and indigestible oligosaccharides by colonic organisms results in short chain fatty acids that are powerful energy sources for the host. Microbiota can also metabolize xenobiotics and interfere with pharmacokinetics, either enhancing or reducing their effect. As an example, digoxin triggers the expression of a cytochrome-encoding operon in *Eggerthella lenta*, which causes inactivation of the drug [41]. The maintenance of normal intestinal homeostasis requires the immune system to establish a balance between the toleration of commensal microorganisms and prevention of pathogenic overgrowth. In fact, the intestinal microbiota seems to contribute to antimicrobial protection. Microbial metabolites and structural components induce synthesis of antimicrobial proteins like cathelicidins, C-type lectins, defensins as well as mucin glycoproteins and IgA [46].

1.2 Intestinal Stem Cells

1.2.1 History

Although the presence of a stem cell compartment in the intestine has been hypothesized since the 1950s, its exact location and organization have been a quite controversial topic in stem cell biology [9]. Crypt-base-columnar cells (CBCs) were first described by Cheng and Leblond, in 1974, as a cell population located at the bottom of the crypt and capable of differentiating into four cell types of the intestinal epithelium [18]. However, the stemness of this population of cells was only confirmed in 2007 with the work of Barker *et al.* [10]. Previous reports had already proposed the leucine-rich repeat-containing G-protein coupled receptor 5 gene (*Lgr5*) to be a target of Wnt signaling, the main pathway associated with crypt biology, and described a unique pattern of expression of the gene. *Lgr5* was expressed in response to Wnt signaling and when the signal was deactivated, *Lgr5* expression was lost. In addition, this gene was found to be highly expressed in the crypt and not in the villi [102, 103]. Therefore, using *in situ* hybridization on a *Lgr5-LacZ* mice model, the authors were able to detect $Lgr5^+$ CBCs interspersed with Paneth cells. In order to further determine their stemness, a *Lgr5-EGFP-IRES-creERT2* knock-in mouse model was used for lineage tracing experiments, revealing that the CBC showed long-term maintenance and self-renewing capacity, originating enterocytes, Paneth cells and goblet cells. The results confirmed that $Lgr5^+$ was a marker of ISCs [10].

1.2.2 $Lgr5^+$ ISCs

Concerning morphology, the $Lgr5^+$ ISC is relatively broader at the base, demonstrating a reduced number of organelles and a flat nucleus. The apical cytoplasm is compacted between the neighboring Paneth cells and extends to the lumen displaying some microvilli [10]. In mice, there are 4 to 6 ISCs in each crypt, interspersed with Paneth cells (Figure 1.2) [68]. Each ISC divides every 24 hours giving rise to transit-amplifying (TA) cells and ISCs. While the latter remains undifferentiated in the bottom of the crypt, the former goes through several rounds of

division before committing to differentiation at the crypt-villus junction. Differentiated cells are continuously pushed upwards on the epithelial layer in direction to the villus top (Figure 1.2).

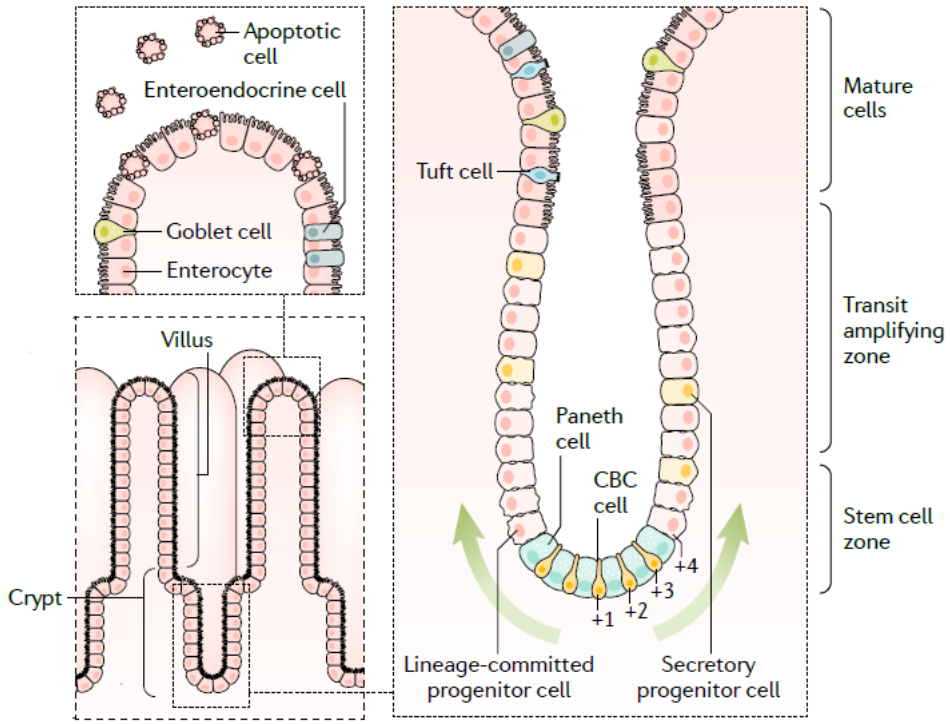

Figure 1.2: Schematic representation of the crypt and villus. CBCs can be found at the bottom of the crypt, interspersed with Paneth cells. CBCs divide generating TA cells and ISCs. Cells in the villi are fully differentiated in enteroendocrine, enterocyte, goblet, or tuft cells. Image adapted from [32].

The Paneth cell is an exception to this rule, as it is the only differentiated cell type that is located in the crypt. The energetic rate of proliferation generated at the crypt is compensated by recurrent apoptotic processes at the top of the villi.

Dedifferentiation processes have been described in the intestinal crypt, as a response to injury-driven loss of ISCs. Repopulation of the intestinal epithelium can be conducted by both absorptive and secretory progenitors that fall back in the niche when necessary. Although the mechanisms that enable dedifferentiation of intestinal epithelium cells are not totally defined, they seem to be a consequence of a permissive open chromatin state present in these cells [32].

1.2.3 +4 cell population

For an extended amount of time, +4 cells, located next to the uppermost Paneth cell between the bottom of the crypt and the progenitor region, were believed to be the only stem cell population present in the intestine. In 2007, Barker *et al.* [10] proved that the *Lgr5*$^+$ and +4 cell populations were distinct, based on their different sensitivities to irradiation. However, the hierarchical positioning of *Lgr5*$^+$ cells and +4 cells is still a controversial topic. Many efforts have been made towards the discovery of +4 cell markers, such as *Bmi1*, *mTert* and *Hopx*, but, on the contrary of *Lgr5*$^+$ cells, none of the identified +4 cell markers distinguish a homogeneous

population [95]. On the other hand, the contribution of +4 cells to intestinal physiology is quite established. In 2012, Yan *et al.*, conducted a systematic comparison between *Lgr5*$^+$ and *Bmi1*$^+$ cells functionality in homeostasis and injury repair, using *Lgr5-eGFP-IRES-CreERT2* and *Bmi1-CreER;Rosa26-YFP* mouse models [112]. This study concluded that *Bmi1*$^+$ cells had minimal contribution for homeostatic intestinal regeneration and were insensitive to canonical Wnt signaling, unlike *Lgr5*$^+$ cells. Notably, through a radiation injury model of 12 gray, the authors demonstrated complete ablation of *Lgr5*$^+$ ISCs, but not of *Bmi1*$^+$ ISCs. In fact, this population went through intensive proliferation post-irradiation, as observed by lineage tracing. Similarly to what had already been demonstrated with single *Lgr5*$^+$ cells [84], this study proved that single *Bmi1*$^+$ cells were capable of generating all intestinal epithelial cell types, including *Lgr5*$^+$ ISCs. In conclusion, the 4+ cell is a slowly cycling intestinal multipotent stem cell, exhibiting self-renewal and capability of differentiation in the various cell types on the intestine, mainly in injury settings. Therefore, it acts as a quiescent, reserve stem cell compartment, with higher resistance to radiation than *Lgr5*$^+$ cells.

1.2.4 The intestinal stem cell niche

Wnt is a signaling pathway associated with stemness and cancer. *Lgr5*$^+$ ISCs maintenance is entirely dependent on canonical Wnt signaling and the expression of several Wnt target genes such as *Sox9*, *Ascl2*, *EphB2* and *Axin2* is detectable on these cells [88]. As previously demonstrated, transgenic expression of Dickkopf-1 (DKK-1), a Wnt pathway antagonist, results in depletion of the *Lgr5*$^+$ ISCs population [112]. Besides, T-cell factor 4 (TCF4), the main effector protein in Wnt signaling, has proven to be essential in the maintenance of small intestine homeostasis [104]. LGR5 has seven transmembrane domains and is a high affinity co-receptor of R-spondin (RSPO) growth factors, secreted soluble proteins. When RSPOs are not present, the transmembrane E3 ubiquitin ligases RNF43/ZNRF3 antagonize Wnt signaling by targeting Frizzled (FZD), the Wnt ligands receptors, for degradation. On the contrary, when RSPOs bind to LGR5, RNF43/ZNRF3 is sequestered, so it is unable to target FZD receptor for degradation [64] (Figure 1.3). Therefore, the Wnt ligand/FZD complex stabilizes at the cell surface, inhibiting degradation of β-catenin by adenomatous polyposis coli (APC) destruction complex. β-catenin keeps accumulating and migrates to the nucleus where it binds to TCFs and regulates gene expression. This generates a complex feedback mechanism of Wnt pathway signaling amplification depending on the presence of RSPOs and Wnt ligands. The capability of a Wnt ligand to activate signaling is dependent on RSPOs [32].

In the intestine, the epithelial Wnt ligands required by *Lgr5*$^+$ ISCs are produced by Paneth cells, in the form on WNT3. Wnt ligands show poor solubility meaning that this type of signal is commonly transferred by close cell-to-cell contact. In fact, cell organization in the crypt base ensures that each ISC contacts with at least one Paneth cell, facilitating growth factor diffusion [32]. Along with proliferation and cell division from the crypt to the villus, Wnt signalling activity diminishes, forming a gradient (Figure 1.4). This gradient is dynamic since it depends on proliferation speed of ISCs and Wnt availability [32].

Epidermal growth factor, or EGF, is another key growth protein in intestinal crypts, as it stimulates stem cell proliferation [84] and its receptor is highly expressed in *Lgr5*$^+$ cells.

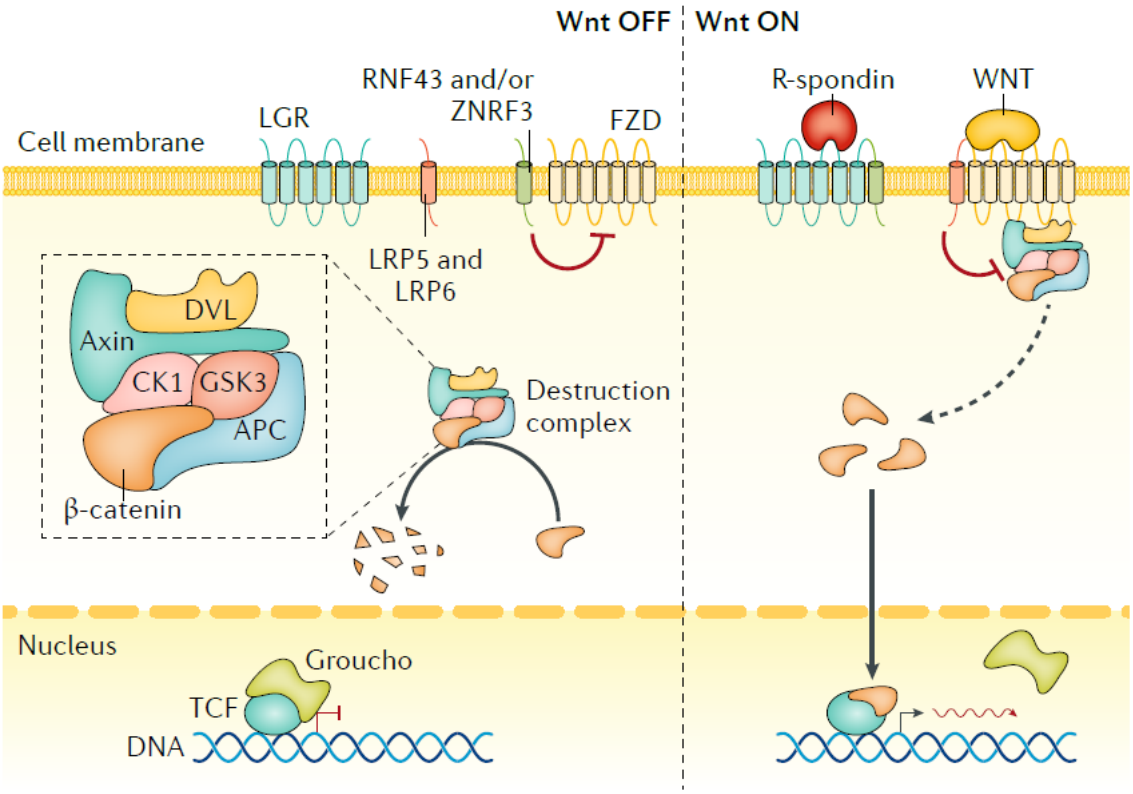

Figure 1.3: The Wnt pathway. Wnt signaling allows β-catenin to bind to TCF and regulate gene expression. Image adapted from [32].

Inactivation of EGF pathway does not compromise stem cell identity even though it turns stem cells quiescent [12].

Notch is also an important signaling pathway in the stem cell niche, particularly, for the maintenance of the crypt compartment and regulation of stem cell self-renewal. Notch is a single transmembrane receptor that requires direct membrane contact between two cells and is involved in cell fate differentiation. Cells with Notch receptors can bind cells with Notch ligands, such as DLL1 or DLL4. Besides contributing to the stem cell niche, Notch seems to be a key regulator of cell fate, since its blockade causes a reduction of secretory cells in the intestine [94]. The Notch gradient along the crypt-villus axis is opposite to that of bone morphogenetic proteins (BMPs) and similar to Wnt, with progressive loss of activity in the villus direction (Figure 1.4).

BMPs are a group of growth factors associated with cell differentiation. The binding of BMPs to their receptors in the cell membrane, triggers a signaling cascade inside the cell that will culminate in the regulation of gene expression. In the intestine, BMP2 and BMP4 inhibit proliferative signals in the stem cell niche and stimulate differentiation. Therefore, myofibroblast and smooth muscle cells below the crypt release BMP inhibitors, such as Noggin (NOG), originating a gradient of BMP along the crypt-villus axis [32] (Figure 1.4).

Paneth cells are major actors in the intestinal stem cell niche, providing signaling factors such as WNT3, WNT11, EGF, TGFα and the Notch ligand DLL4 [82]. However, when this cell type is depleted, intestinal homeostasis is not impaired, suggesting there must be a non-epithelial contribution to the niche [54]. Several reports have described that peri-cryptal mesenchymal and

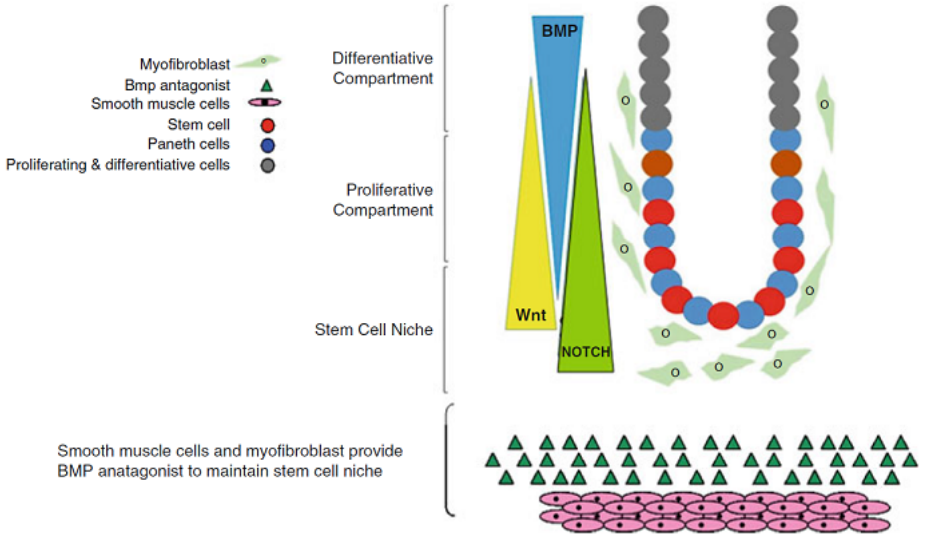

Figure 1.4: The intestinal stem cell niche. The main signaling pathways in the niche are Wnt and Notch, while BMP is blocked. The three signals establish different gradients along the crypt-villus axis. Subepithelial myofibroblasts and smooth muscle cells contribute to the niche. Adapted from [94].

smooth muscle cells also release important factors to the niche. As an example, PDGFRα marker identifies a myofibroblast population that secretes RSPO3 to the stem cell niche [38] and *Foxl1* marks mesenchymal cells that produce RSPO3, WNT2B, WNT4, WNT5A and GREM½ (a BMP antagonist) [5]. Accordingly, body-wide ablation of Wnt leads to ISCs death, harming the regeneration of intestinal tissue, but epithelial-specific ablation of Wnt signalling shows no impact on intestinal homeostasis [101]. The relevance of non-epithelial populations in the stem cell niche is now becoming recognized, and appears to result from a collective effort of cells with distinct phenotypes and functional redundancy.

1.3 Organoids

1.3.1 Definition and history

Tridimensional cell cultures, such as organoids, overcome the main problem of standard cultures, which is the lack of extracellular matrix (ECM) support that results in an inaccurate recreation of the physiological microanatomy of native tissues. As a result, the biochemical and mechanical cues the cells receive are different and influence their behavior and communication with other cells. Therefore, results obtained on studies using 2D cultures may not be entirely reliable. Generally, in comparison to 2D cultures, 3D cultures show greater cell viability, more physiologically relevant protein expression profiles and higher proliferation rate [57].

An organoid is an *in vitro* 3D structure that resembles a living organ. Organoids derive from pluripotent or multipotent stem cells that proliferate, self-maintain, and self-organize, through spatially restricted lineage commitment, following processes similar to the development *in vivo*.

This way, an organoid is a miniaturized version of a real organ, with preserved tridimensional microanatomy. An organoid must fulfill at least two conditions [62, 29]:

1. Be able to self-renew;

2. Contain several types of cells from the original organ;

Moreover, they partially reproduce the cellular spatial organization and function of the original organ. The formation of an organoid requires non-committed cells that can fulfill the abovementioned conditions. Additionally, to support the tridimensional development of the organoid, a hydrogel matrix that resembles the natural extracellular environment of the tissue can be included. Normally, these systems also require the presence of molecular signals that recapitulate the signaling pathways that are activated in the tissues *in vivo* to modulate the growth, differentiation and expansion of the organoid.

In 1987, one of the first organoids in history was successfully developed by Li *et al.* [65]. The authors tried to use an Engelbreth-Holm-Swarm matrix, nowadays commercially known as Matrigel, to culture primary mouse mammary epithelial cells. In 2D culture, these cells rapidly lost the ability to produce and secrete milk. By using an ECM mimic, the gene expression profile and tissue morphology recreated the *in vivo* scenario, with the formation of ducts, ductules and lumina, resembling mammary secretory alveoli. Following the pioneer work of Li and coworkers, a variety of organs like the liver, stomach, kidney and intestine have been reproduced in the form of organoids.

Organoids are promising platforms in the study of developmental biology and disease modeling. Moreover, they can be important tools in drug testing, perhaps reducing the burden of animal testing in the pharmaceutical industry. In the area of personalized medicine, organoids created with patient cells might pave the way for future organ replacement therapy with auto-transplantation. In addition, personalized drug screening will enable the creation of tumor-tailored therapeutics, in the case of cancer patients. Drug screening using patient cells is a much more advantageous approach than the use of immortalized cell lines, which do not include the personal characteristics of the patient's tumor, display additional genomic instability due to immortalization, and do not recreate the behavior or morphology of the tumor.

1.3.2 Intestinal organoids

In 2009, Sato and colleagues, successfully developed the first self-renewing, non-transformed, intestinal organoid culture, displaying crypt-villus structures similar to those *in vivo* (Figure 1.5). There were two key factors for the success of this protocol. First, the utilization of Matrigel, a natural matrix rich in laminin, just like the crypt base. Second, a cocktail of growth factors and signaling molecules to recreate the cues present in the stem cell niche, composed of RSPO1, an agonist of the Wnt pathway that is essential for the growth and maintenance of intestinal organoids, EGF to stimulate intestinal proliferation, and NOG that potentiates crypt formation and blocks the BMP pathway that leads to differentiation [84].

First, the authors isolated mouse crypts and suspended them in Matrigel. Over passages, the crypts showed normal development, presenting crypt fission events as well as Paneth and $Lgr5^+$ stem cells at the bottom of the crypt. Further expansion created organoids with dozens of crypt domains surrounding a central lumen, lined by a villus-like simple epithelium. The expression

profile remained identical to the one verified in freshly isolated crypts. Through a *Lgr5–EGFP–ires–CreERT2* mouse model crossed with the Cre-activatable Rosa26–LacZ reporter, the authors confirmed the presence of single labelled cells that induced lineage tracing over the following days, both in fresh isolated crypts and in established organoids. Next, *Lgr5-GFP*^{hi} cells were isolated and seeded at 1 cell per well, with the addition of the anoikis inhibitor Y-27632, and a Notch-agonistic peptide. 6% of these cells developed into organoids (Figure 1.5b and 1.5c) that were visually indistinguishable from those derived from whole crypts and presented enterocytes, enteroendocrine, goblet, Paneth and *Lgr5*$^{+}$ stem cells. In 2011, Sato *et al.* reported the adaptation of this protocol to the development of human intestinal organoids [83]. Both reports were a landmark in organoid studies because they created a platform for long-term intestinal organoid cultures, circumventing dependency on fibroblasts, and confirmed that a single stem cell, in this case, the *Lgr5*$^{+}$ ISC, is able to generate a self-organizing intestinal epithelial structure with preserved morphology.

Besides their potential to be maintained for a long period of time – up to 350 days [73] – intestinal organoids might also be cryopreserved using vitrification, a method that prevents tissues from damage by rapidly cooling them. Post-cryopreservation viability is of around 90% for human and mouse-derived intestinal organoids [96]. More recently, Watson *et al.* reported the development of human intestinal organoids derived from embryonic stem cells (ESCs) and induced pluripotent stem cells (iPSCs) that successfully engrafted mice *in vivo*. Such findings further underscore the potential of organoid technology in organ replacement therapies by using patient-derived organoids that can be conserved in biobanks and used upon necessity [107].

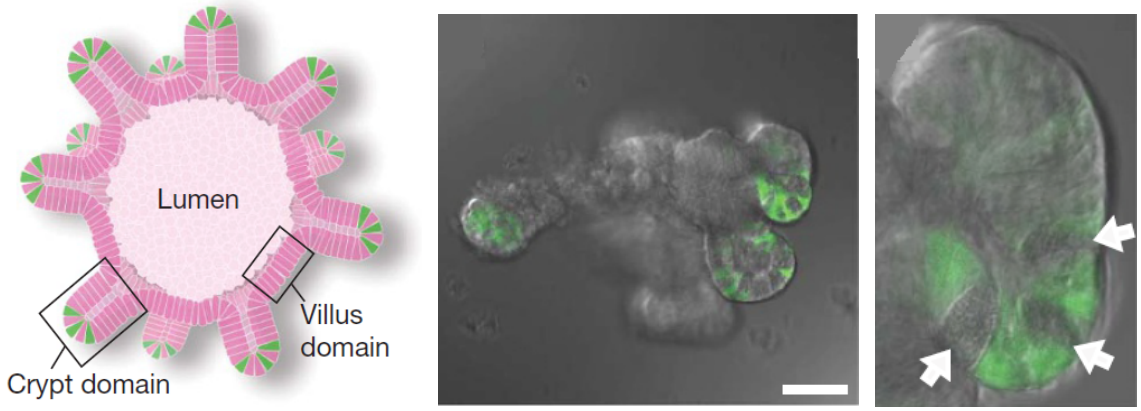

(a) **(b)** **(c)**

Figure 1.5: The intestinal organoid. (a) Schematic representation of an intestinal organoid, comprising a lumen surrounded by epithelium with invaginations. Such invaginations are crypts with *Lgr5*$^{+}$ ISCs depicted in green. (b) Confocal image of an intestinal organoid derived from a single *Lgr5-GFP*^{hi} cell at 14 days after sorting. *Lgr5*$^{+}$ ISCs are marked with GFP. Scale bar: 50 µm. (c) Higher magnification of b. White arrows point to Paneth cells. Images adapted from [84].

In our group, murine intestinal organoids were recently employed to study the impact of deleting the RNA-binding protein MEX3A on intestinal homeostasis [75]. The results on the characterization of a *Mex3a* knockout mouse model show that MEX3A is critical for the maintenance of the *Lgr5*$^{+}$ ISC pool *in vivo* in mice. *Mex3a* null mice displayed increased postnatal mortality and growth retardation, while *Lgr5*$^{+}$ ISCs population was decreased and

intestinal microarchitecture was largely altered. Moreover, *ex vivo* organoids derived from *Mex3a* null mice had a longer maturation period, when compared to wild-type-derived organoids. To assess a possible correlation between increased peroxisome proliferator-activated receptor, $PPAR_{\gamma}$, signaling in the crypt and the decrease in $Lgr5^{+}$ population, intestinal organoids derived from wild-type and *Mex3a* mice were treated with $PPAR_{\gamma}$-selective agonists. Although both types of organoids were reduced in size and number, this effect was exacerbated in knockout-derived organoids, given that $Lgr5^{+}$ mRNA expression levels and organoid initiation efficiency upon passage were severely reduced. These data established a link between MEX3A depletion and a trigger in $PPAR_{\gamma}$ signaling, uncovering a novel regulatory pathway in ISCs maintenance.

Intestinal organoids have also been developed to study diverse pathologies that affect the digestive tract. For instance, cystic fibrosis (CF) is the most common monogenetic recessive disease in the Caucasian population and is caused by mutations in the Cystic Fibrosis Transmembrane Conductance Regulator gene (*Cftr*). CF causes aberrant fluid transport and abnormal mucus formation that affects the functionality of multiple organs, including the intestine. CF shows a huge variability between patients, with more than 2000 CFTR variants reported in the Cystic Fibrosis Mutation Database, and many other genetic modifiers and environmental agents can contribute for such variability [23]. As a result, some of the modulators for CF do not work for every patient. Patient-derived intestinal organoids can be extremely helpful to investigate the clinical benefit of various drugs and to design therapies for identical mutations groups. The development of a human primary intestinal organoid with CF was reported by Dekkers *et al.* in 2013, who designed a robust assay for the quantification of CFTR function in the organoid [24]. This work paves the way for more extensive studies of CF disease and the introduction of patient-derived CF organoids in the clinic that can be employed in personalized medicine.

Although intestinal organoids can have many useful applications and the technology behind their development is rapidly progressing, there are still some challenges in the field. First, the culture of stem cell-derived intestinal organoids requires biomolecules that mimic the stem cell niche cues. These factors are normally provided through conditioned media produced on-site, which reduces reproducibility of the experiments. Moreover, most intestinal organoids produced to date only include epithelial cells, leaving other physiologically relevant tissues, such as neural tissue, mesenchyme, endothelium, immune cells and even the microbiota unrepresented. Therefore, such a simple model may not be sufficient to recreate certain intestinal pathologies intrinsically linked to different cell types, for instance, the response to infection [23]. From the perspective of auto-transplantation, for example, these systems lack neural and endocrine signaling of satiety, as well as production of immunoglobulins [62]. Furthermore, due to the absence of blood circulation, the nutrition and oxygenation of cells is solely dependent on diffusion processes, which limits the possible maximum size of the organoid [23]. Due to the type of morphology the organoid acquires, it is difficult to expose the cells to growth factor gradients. Intestinal organoids are also heterogeneous in size and shape and may display incorrect spatial arrangement of different parts of the organ, due to the absence of anterior-posterior and dorsal-ventral embryonic axes [62]. Finally, the enclosed lumen that results from the self-organization of the intestinal epithelial cells does not enable the incorporation of peristalsis movements and fluid flow, to simulate peristalsis, blood flow and shear stress in the gut [6]. As a result, cell debris and secretions produced by epithelial cells, accumulate

in the lumen. Likewise, the presence of an enclosed lumen significantly hinders the analysis of the intraluminal environment, studies of transport and absorption across the intestinal barrier and co-culture with microbiota in the apical surface of the epithelium. Recently, a high-throughput microinjection platform was developed to overcome this challenge in intestinal organoid culture. The technology reported by Williamson and colleagues in 2018, has the ability of reproducibly entrap different molecules and bacteria inside the intestinal organoid lumen [109].

In summary, even though some shortcomings might be pointed out to intestinal organoid models, they are promising tools in the field of tissue engineering with a wide range of applications. Some of the aforementioned issues might be solved with the use of microfluidics, which will be covered in the next section.

1.4 Organ-on-chip

1.4.1 Biofabrication

In the context of tissue engineering, the term biofabrication was defined in 2016 by Groll *et al.* as *"the automated generation of biologically functional products with structural organization from living cells, bioactive molecules, biomaterials, cell aggregates such as micro-tissues, or hybrid cell-material constructs, through Bioprinting or Bioassembly and subsequent tissue maturation processes"* [39]. Biofabrication combines additive manufacturing technologies with different biomaterials and biological elements to create increasingly more complex and faithful 3D *in vitro* models of native tissues and organs. The biofabrication process grants a high degree of design flexibility to the model, enabling the incorporation of more features that help recapitulating the original microenvironment of the tissue. In organoid cultures, particularly, biofabrication is used to improve the characteristics of ECM, as well as to produce scaffolds for tissue culture. Both factors contribute to an accurate representation of tissue architecture, and to support cell proliferation, organization, migration, and differentiation.

The limited oxygen and nutrient diffusion rate across organoids can be overcome by using flow perfusion bioreactors and microfluidic devices. On the other hand, growth factor concentrations can be controlled both spatially and temporally by using biomaterials capable of sustained release for a certain amount of time or that initiate the release upon exposure to certain stimuli [85]. All in all, the combination of biofabrication and organoid culture produces physiological relevant and versatile 3D *in vitro* models and will largely contribute to their clinical translation.

1.4.2 3D printing of microfluidic devices

Microfluidics is an interdisciplinary field inspired by microfabrication techniques that focuses on the analysis and manipulation of fluids at a sub-millimeter scale. Microfluidic devices are composed of microchannels and chambers where fluid flows in laminar condition. The different fluidic mechanics attainable with microfluidics approaches might be the solution for some of the problems associated with "macro-sized" laboratory experiments [6].

Soft lithography is the most commonly used method for microfluidic device fabrication. The term soft lithography refers to a group of techniques, e. g., replica molding (Figure 1.6a), microcontact printing (Figure 1.6b), micromolding (Figure 1.6c) and microtransfer molding

(Figure 1.6d). The basic principle in soft lithography is the replication of a microfabricated mold, containing the contrary geometry or pattern of the intended polymeric material. In this process, an elastomer, like, polydimethylsiloxane (PDMS) and a curing agent are mixed. The mixture is then shed into a master mold, where it is heated and becomes solid. After a few hours, the mold can be peeled off, creating an elastomeric stamp. In replica molding, micromolding and microtransfer printing, a polymeric solution fills the empty spaces created in the mold. In microcontact printing, the elastomeric stamp is coated with ink that is pressed against a substrate. After 24 hours, the polymer can be peeled off from the stamp and the final product reveals the intended geometry or pattern [111]. This method is interesting for biomedical applications due to the use of PDMS, a biocompatible, flexible, gas permeable and optically transparent polymer. Besides, resolutions from a few microns to hundreds of nanometers can be obtained using soft lithography [111].

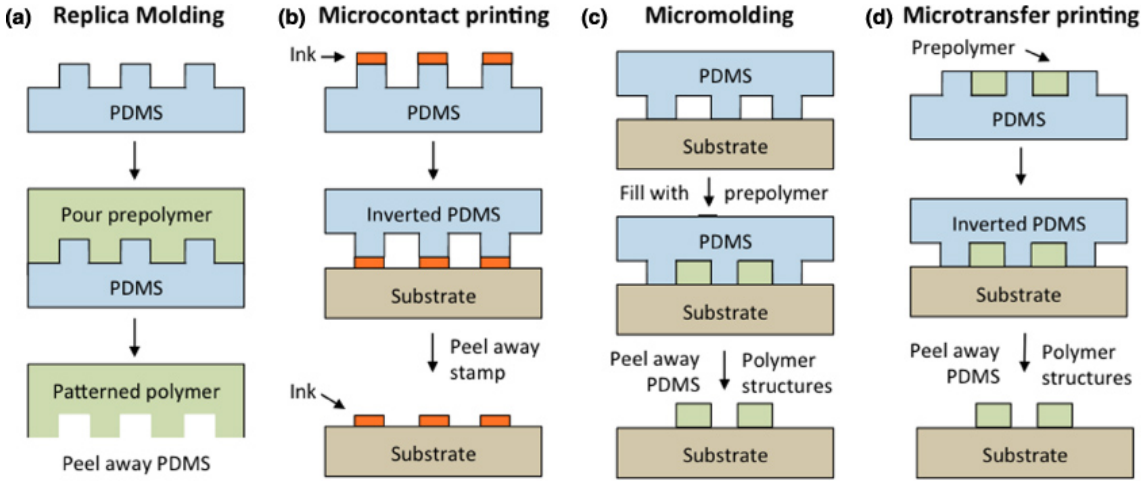

Figure 1.6: Representation of the main steps of four soft lithography techniques: (a) Replica Molding, (b) Microcontact printing, (c) Micromolding and (d) Microtransfer printing. Adapted from [66].

However, over recent years, rapid prototyping techniques have been emerging as alternatives to lithography methods, due to their low cost, simplicity, design flexibility and improved resolution. One of those is 3D printing, a group of manufacturing methods based on layer-by-layer material deposition that forms a three-dimensional object. The object is built according to a 3D digital model that is sectioned in 2D slices and thus can be interpreted by a printer. Stereolithography (SLA), fused deposition modeling (FDM), multi jet modeling (MJM) and two-photon polymerization (2PP) are examples of 3D printing techniques [31].

FDM is the most common technique used for 3D printing, for being inexpensive. As an extrusion-based method, it uses a nozzle to print 2D layers of materials that get progressively stacked. In FDM, the printing material is melted in the nozzle and printed on top of the previous layers, where it binds before cooling. Biocompatible thermoplastic materials, such as polycarbonate, polystyrene and polylactic acid, as well as polymer composites and nanocomposites can be printed with FDM. This technique does not require much space for operation and prints with high speed. On the downside, FDM is not the most suitable technique for microfluidic device fabrication, since 3D printed products are leak prone and its resolution is not sufficient for making microfluidic channels [31]. In spite of that, this technique has been

employed, for instance, for the production of a microfluidic immunosensor for three prostate cancer biomarkers [47]. The results of the assay of serum samples of 6 prostate cancer patients correlated with the ones obtained with ELISA quantification.

In MJM, the material used is a photosensitive resin which is ejected from an inkjet printhead onto the previously printed layer. Then, a light source is used to cure the resin, while a sacrificial layer of material that is not cured can later be removed from the print [108]. This process shows high printing accuracy and allows utilization of different materials in the same build. On the other hand, MJM has low resolution, requires expensive material and uses patent-protected resins [31]. A microfluidic device coupled with FDA-approved microdialysis probes was developed using MJM. The biosensor was employed to subcutaneously measure glucose and lactose levels in real-time in cyclists [36].

2PP is a 3D printing technique which uses femtosecond laser pulses to induce a two-photon absorption phenomenon, creating a three-dimensional object from a photoactivable material. Two photons are absorbed simultaneously by the photo-activated material in the voxel where the pulse laser is focused on, turning it from liquid to solid. This is a nonlinear phenomenon that confers this technique a higher resolution, meaning that sub-100 nm features can be produced [31]. For the same reason, 3D structures can be assembled within the volume of the sample, without printing material layer-by-layer, which can be useful for printing functional elements directly on pre-assembled microfluidic devices [108]. However, 2PP requires expensive equipment and its speed is considerably low. A placental barrier microfluidic model was developed with 2PP [67]. This technique was utilized to produce the basal membrane out of GelMOD-AEMA, a modified gelatin polymer, directly on the preassembled microfluidic device. This way, two separate cell culture compartments were created, simulating the interface between the fetal compartment and the maternal syncytium.

SLA was one of the first 3D printing techniques developed. SLA is a layer-by-layer printing process where a vat of resin is irradiated with a structured light source to induce polymerization of a photopolymer. There are two light exposure methods in stereolithography: SLA, which uses a focused light-emitting diode laser to cure spots in the surface of the resin vat; and digital light processing that utilizes a projector that exposes the entire surface simultaneously to the light source but masks the desired pattern using digital micromirror display technology [31]. There are two possible setups in SLA: free surface (Figure 1.7a) and constrained surface (Figure 1.7b). The difference between them is the incidence of light on the sample. In the free surface configuration, the light is irradiated from above the resin vat and the stage where printing takes place descends progressively to lower the cured resin (Figure 1.7a). In the constrained surface, the setup is inverted with the light source coming from below the vat and the cured resin gradually ascending along the printing process (Figure 1.7b). The last configuration is favorable, since it requires smaller amounts of resin to print, avoids contamination and formation of oxides. Overall, SLA is a rapid technique that can achieve high resolutions despite not being as suitable for printing of multiple materials as techniques like MJM and FDM. Applying stereolithography to microfluidic device fabrication is possible by using biocompatible resins [31].

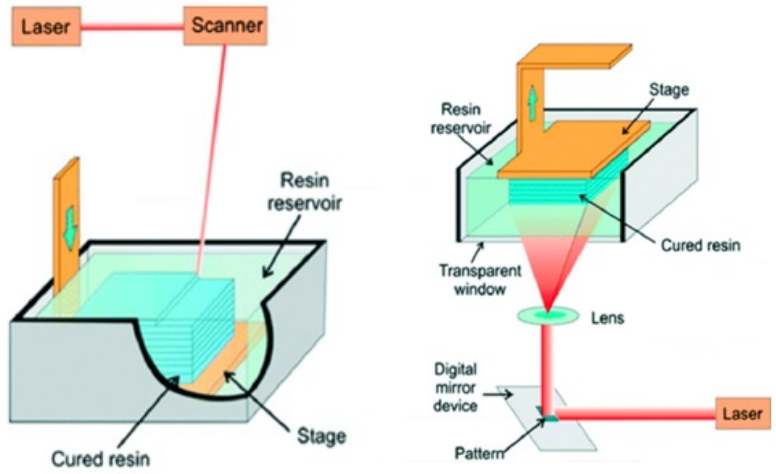

(a) **(b)**

Figure 1.7: Configurations of equipment for stereolithography 3D printing: (a) free surface and (b) constrained surface. Adapted from [31].

In fact, a model of arterial thrombosis was developed by stereolithography 3D printing of stenotic arteries molds, derived from computed tomography angiography data of both healthy and stenotic arteries [20]. The molds were then used for PDMS-based soft lithography to assemble microfluidic chips. The thrombosis-on-a-chip model successfully simulated thrombosis on stenotic vessels but not on healthy vessels. Stereolithography has also been used in the fabrication of entire microfluidic devices as, for instance, the bovine oviduct-on-chip reported by Ferraz and colleagues in 2017 [30]. This device displayed a U-shape to enhance cell contact area as well as to allow live-cell imaging and perfusion of the system. Besides, a polycarbonate membrane was included in the device to enable independent perfusion of apical and basolateral compartments of the culture. As a result, bovine oviduct epithelial cells maintained polarization in the long-term and simulated proper sperm and oocyte interactions such as fertilization.

Table 1.1 presents a comparison of these four techniques, in terms of their advantages and disadvantages. When developing a microfluidic platform, factors such as resolution, cost, speed and available equipment need to be balanced out to select the appropriate technique.

Table 1.1: Analysis of the advantages and disadvantages of four 3D printing techniques employed in microfluidic device fabrication. Based on information gathered from [31].

.

Technique	Advantages	Disadvantages
Fused Deposition Modeling	Low cost Small space requirements High printing speed Manufacturing ease Widely accessible	Sensitivity to compressive stress fracture Leakiness Low resolution No control of surface roughness
Multi Jet Modeling	High accuracy Multi-material print	Expensive Proprietary resins Low resolution
Two-photon Polymerization	Nanoscale resolution Non-linearity	Expensive Low speed
Stereolithography	High printing speed Low cost Good resolution	Not compatible with multi-material print

1.4.3 Microfluidic platforms for cell culture

Microfluidics enables the creation of revolutionary platforms for cell culture. In conventional cell culture, the environment is static, meaning that the contact with soluble factors, nutrients, chemical compounds, and metabolites is limited by diffusion. However, *in vivo*, blood flow delivers these substances to the cell. The perfusion created in microfluidic devices mimics the function of blood circulation in tissues, allowing communication between different tissues and biochemical environments through microchannels or porous membranes [6]. The features and structure of microfluidic chips are completely tunable so that a variety of components can be included for a better representation of complex physiological environments. Examples of variables that might contribute to this are: 1) co-culture of different types of cells; 2) establishment of chemical gradients and physical stimulation, like cardiac cyclic compression and peristaltic movements in the digestive system; 3) incorporation with biomaterial-derived scaffolds to support 3D cell cultures. Taking this range of possibilities into account, microfluidic devices permit a reductionist representation of an organ's functions, creating organ-on-chip systems.

Organs-on-chip are designed considering the characteristics of the organ's functional units; therefore, they include the different cell types of the organ, recapitulate the structural organization, as well as organ-specific physical and biochemical microenvironment. As a result, organ-on-chip platforms provide a more precise control of cell cultures [74]. Microfluidic devices, and organ-on-chip systems in particular, are portable, cost-efficient, and require small quantities of reagents, which makes them ideal for high-throughput experiments. Instruments for cell monitoring, electrochemical measures, analysis of metabolites and biomarkers, can be coupled to these devices, facilitating laboratory tasks [74]. On the other hand, thanks to spatial and

temporal manipulation of these systems, they can be employed in the study of cell-fate specification, differentiation and disease modeling [74].

Chapter 2

Intestine-on-chip systems: state of the art

2.1 Introduction

In recent years, researchers started applying microfluidic technology to model the human intestinal physiology, thereby creating intestine-on-chip models. In fact, the introduction of microfluidics in the field contributed to circumvent many issues associated with previous models.

Culture of intestinal epithelial cells in Transwell insert systems is still the golden standard for a variety of studies concerning the intestine, being commonly used in pharmacological assays during preclinical testing of drugs. Transwell systems are routinely maintained as static cultures, without media flow or applied mechanical strain. Formation of villi-like structures in this model is not attainable, suggesting that epithelial differentiation is not fully recapitulated, which raises questions about the reliability of permeability results obtained with this model. Moreover, another issue with this approach is the common use of Caco-2 cells, which are derived from a human colorectal adenocarcinoma [80]. Although experiments using immortalized cell lines have various advantages like cost-effectiveness, unlimited supply and longer periods of culture, these cells are derived from tumors and, therefore, present phenotype and genotype alterations that significantly limit their physiological relevance [50]. Transwell cultures have also been employed to model the host-microbiota interaction in the intestine. Due to the lack of media flow, these experiments cannot be maintained for more than a few hours without bacterial overgrowth and epithelial cell death [79]. In the case of organoids, as discussed before, the difficult access to the lumen significantly hinders the potential experiments and results that can be retrieved from this model and is not descriptive of the physiological morphology of the intestine.

One of the first intestine-on-chip models was created by Kimura *et al.* in 2008 [55]. The device is a two-compartment PDMS culture chamber, in which the two chambers are separated by a polyester semipermeable membrane. Caco-2 cells were cultured on top of the membrane and fluid flow was ensured by two stirrers embedded in the device that were controlled by rotating magnets under the device (Figure 2.1). Two optical fibers were incorporated in the apical and basolateral side of the device for fluorescence measurements. Caco-2 cells were cultured for 30 days and formed a tight monolayer on day 9. Transport of rhodamine 123 was assessed by fluorescence measurements

in both sides of the device, confirming that rhodamine 123 migrated from the basolateral to the apical area, thus displaying polarized transportation. Although this study was preliminary, it was a first clue to the relevance of fluid flow in intestinal epithelial differentiation. Nevertheless, the model did not show any particular improvement over the standard Transwell insert culture since it lacks the recreation of intestinal morphology that is necessary for normal intestinal functions, such as absorption of nutrients or regeneration of the epithelium.

This chapter will provide an overview of several intestine-on-chip approaches and their solutions for some of the problems associated with other models. It will start by the description of various applications of one specific microfluidic device that combines fluid flow with peristalsis-like motion and allowed studies from basic biology to modeling of intestinal inflammation and host-microbiota interaction. Then, it will present different designs of microfluidic devices that were employed as intestinal models for diverse purposes.

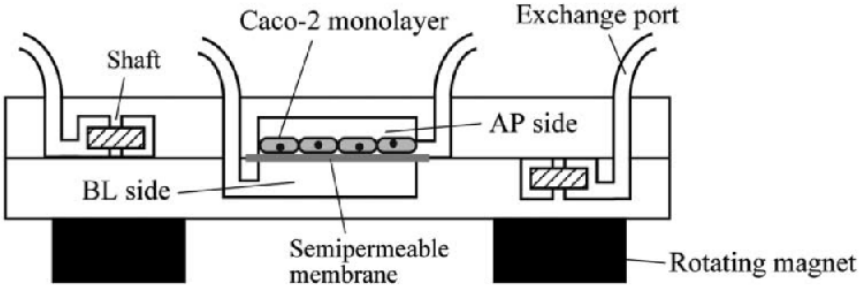

Figure 2.1: Schematic representation of the microfluidic design used in [55].

2.2 Intestine-on-chip model with peristalsis-like mechanical stimulation

2.2.1 Immortalized cell lines

In 2012, Kim *et al.* described a revolutionary gut-on-chip system that introduced two relevant factors in *in vitro* intestinal models: co-culture of an intestinal cell line, Caco-2, with microorganisms from intestinal microbiota, and peristalsis-like stimuli, enabling a deeper understanding of how both factors contribute to a healthy intestine [51]. The authors built a PDMS microfluidic device consisting of two channels vertically stacked, sided by two hollow vacuum chambers. Separating the channels, a 30 µm thick porous membrane coated with an ECM solution of rat type I collagen (Col-I) and Matrigel was incorporated (Figure 2.2).

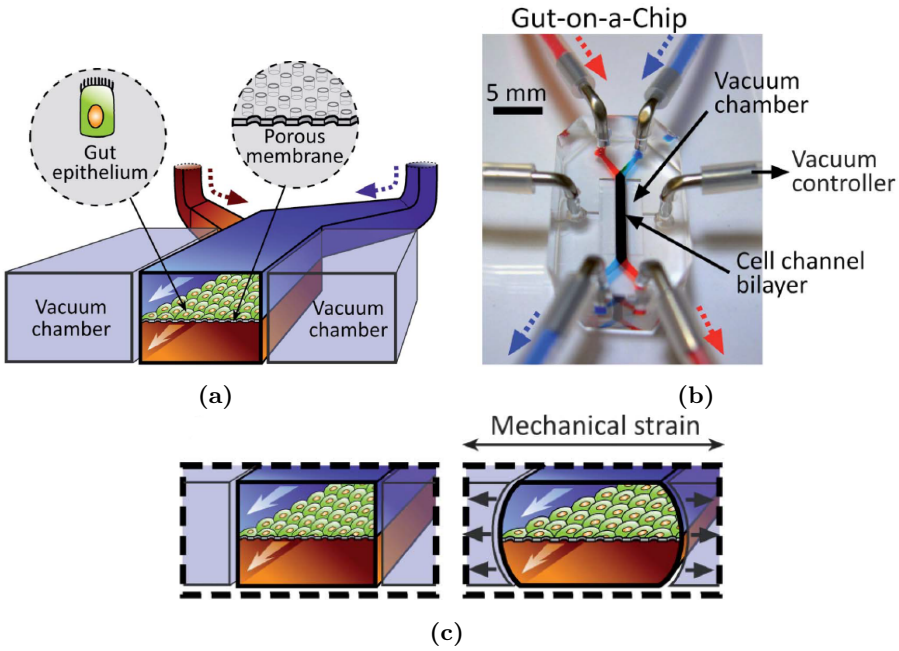

Figure 2.2: Gut-on-chip device developed in [51]. (a) Cross section schematic representation of device's structure, comprising two vacuum chambers, two flow chambers and a porous membrane separating them. (b) Top view photograph of the Gut-on-chip and the positioning of its inlets. (c) Representation of deformation of the device in response to cyclic mechanical strain.

This microfluidic design will from now on be referred to as Gut-on-chip. After the attachment of Caco-2 cells to the top surface of the ECM-coated membrane, culture medium was continuously perfused through the upper channel at a constant flow rate. After one day, the medium started flowing through both channels at the same rate. The simulation of intestinal peristaltic movements was performed through cyclic suction applied to the vacuum chambers, resulting in unidirectional elongation of the porous membrane. The flow rate, as well as the frequency and strain percentage of the mechanical stimuli applied in this system, were set to values like the ones intestinal tissues experience *in vivo*. In this study, three conditions were compared: (a) a Transwell insert system, with a porous polyester membrane pre-coated with the same ECM hydrogel, the golden standard of Caco-2 cells culture; (b) the novel gut-on-chip system with fluid flow alone and (c) the same system with fluid flow and cyclic mechanical strain. In (b) and (c) cell polarization and differentiation occurred after just 3 days whereas in (a) the phenomenon was only observed after 21 days (Figure 2.3). After longer periods of culture in exposure to fluid flow and mechanical strain, Caco-2 cells forming a monolayer surprisingly organized in villi-like folds. The authors concluded that fluid flow was a critical determinant for accelerating intestinal cell polarity and differentiation, and peristaltic movement simulation enhanced those responses.

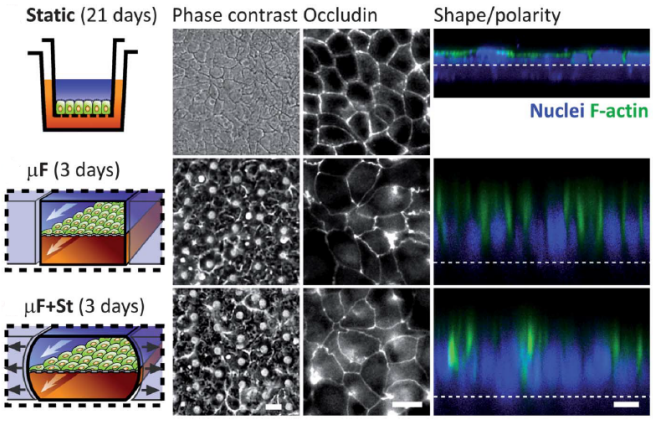

(a) Static: static culture in Transwell insert, **µF** culture in microfluidic device with fluid flow (30 µL h^{-1}); **µF+St** culture in microfluidic device with fluid flow and cyclic mechanical strain (10%; 0.15 Hz). On the left, a representation of the culture systems is depicted. On the center, fluorescence microscopy images demonstrate distribution of occludin in the epithelial monolayers. On the right, confocal imaging of a vertical cross section of the epithelium showing cell shape and polarity through staining of the nuclei (blue) and F-actin (green).

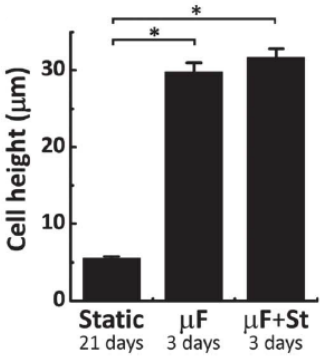

(b) Average height of Caco-2 cells after culture in static Transwell system, in microfluidic device with (µF) or without (µF + St) cyclic mechanical strain. (* $p < 0.001$).

Figure 2.3: Comparison of cell morphology in three different conditions. Adapted from [51].

The mimicking potential of the Gut-on-chip was further explored in 2013 by Kim & Ingber, who demonstrated that intestinal morphology and cytodifferentiation *in vivo* were accurately recapitulated in the device [52]. EdU (5-ethynyl-2'-deoxyuridine) labeled cells migrated upwards in the crypt-villus axis, suggesting that undifferentiated Caco-2 cells remain in the crypt niche and generate daughter cells that suffer differentiation along the villus (Figure 2.4) [52]. Moreover, the distribution and frequency of each intestinal epithelial cell type in the Caco-2 crypt-villus structures were identical to the observed *in vivo*.

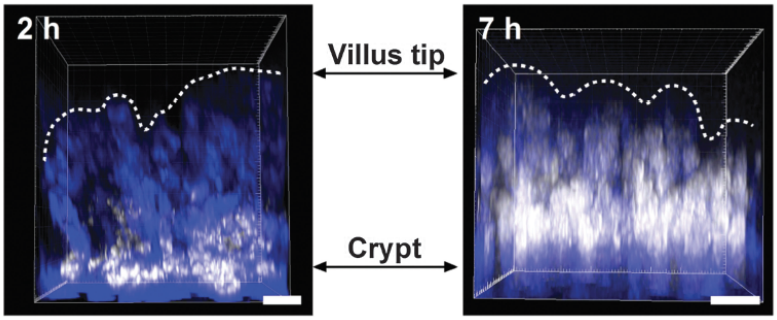

Figure 2.4: Fluorescence microscopy images that demonstrate formation of crypts and villi (outlined by the white dotted line). Staining with Edu for 2 hours marked proliferative cells exclusively at the bottom of the crypt. Washing out for 5 hours shows stained cells along the villi. Scale bar: 20 µM. Adapted from [52].

The co-culture of Caco-2 cells with commensal bacteria *Lactobacillus rhamnosus GG* (LGG) under cyclic mechanical strain and fluid flow inside the device was successful, with both populations remaining viable after 96 hours [51]. Gut-on-chip circumvented the bacterial overgrowth issue by

providing continuous perfusion which eliminates non-attached LGG and dilutes acidic metabolites. Interestingly, this study underscored the importance of the microbiota in intestinal homeostasis, since transepithelial electrical resistance (TEER) measured in the gut-on-chip culture significantly increased over time, which translates to an improvement of intestinal barrier integrity. Such an increase demonstrates that the microbiota releases biochemical cues that stimulate epithelial cells and enhance their functions, contributing to a healthier intestine.

In recent years, the Gut-on-chip device has been used as an *in vitro* model of intestinal inflammation [53, 92]. In 2016, Kim *et al.* explored the potential of this system to decode the complex interplay of various cell types in intestinal inflammation, which is characterized by villi destruction and compromised epithelial barrier integrity [53]. Particularly, in inflammatory bowel disease (IBD), immune cells vastly accumulate in the intestinal mucosa, and that was mimicked in the device through the introduction of peripheral blood mononuclear cells (PBMCs). Interestingly, when a non-pathogenic strain of *Escherichia coli* (GFP-EC) and/or lipopolysaccharide (LPS) were added to the simple intestinal epithelial culture, formed by Caco-2 cells, the hallmarks of intestinal infection were not observed. On the other hand, when PBMCs were introduced in the model, together with GFP-EC and LPS, there was a significant loss of barrier integrity as well as destruction and shortening of the villi. Moreover, while the independent co-culture of a pathogenic strain of *E. coli* (EIECs) provoked damage on the intestinal epithelium and overgrown the culture in 24-36 hours, when PBMCs were present, this effect was significantly aggravated (Figure 2.5).

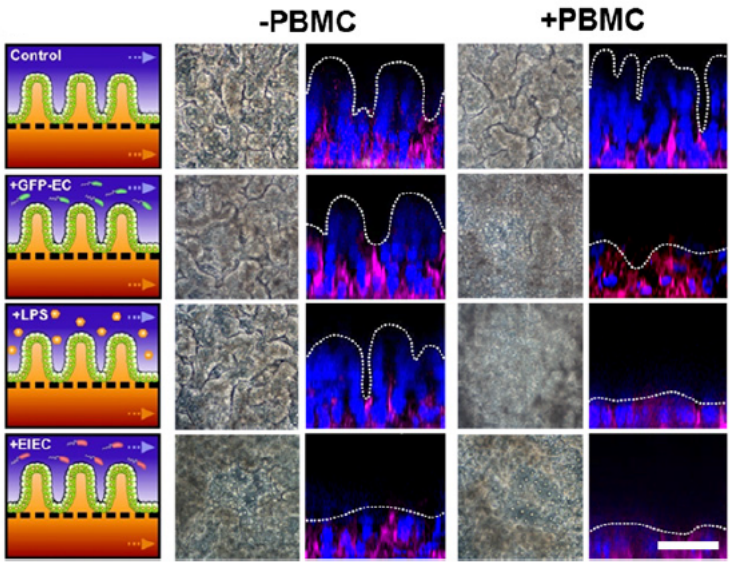

Figure 2.5: Morphological analysis of intestinal villus damage in response to addition of GFP-EC, LPS, and EIEC in the absence (-PBMC) or presence of immune cells (+PBMC). Schematics of experimental setup, phase contrast images (horizontal view, taken at 57 h after onset), and fluorescence confocal micrographs (vertical cross-sectional views at 83 h after onset) are sequentially displayed. F-actin and nuclei are coded with magenta and blue, respectively. Adapted from [53].

Similarly, in 2018, the same microfluidic *in vitro* model of intestinal inflammation prompted the discovery that barrier dysfunction is one of the most critical triggers that initiates the onset of inflammation in the gut [92]. Accordingly, this report suggests that a "leaky gut" patient

is significantly more vulnerable to microbial infections and aggressive immune activity due to intensified permeability of the epithelial barrier, which can turn into a chronic inflammation.

2.2.2 Primary cells

With the objective of developing a more physiologically relevant model of the human intestine, in 2018, Workman *et al.*, used the Gut-on-chip design for culturing intestinal epithelium derived from iPSCs [110]. iPSCs were directed to form endoderm, epithelium and, ultimately, intestinal organoids. Organoids were dissociated into single cells and cells positive for epithelial cell adhesion molecule (EpCAM/CD326) were seeded on the upper channel, on top of a Matrigel-coated PDMS membrane (Figure 2.6).

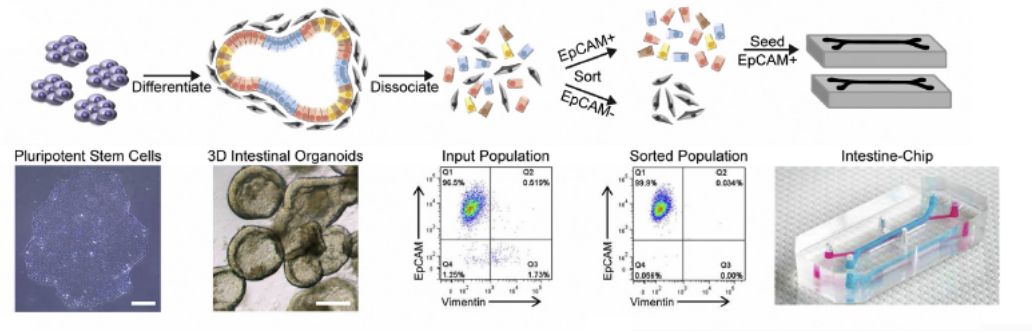

Figure 2.6: Schematic of the protocol for isolation of epithelial cells from intestinal organoids derived from iPSCs and their incorporation in the Gut-on-chip device. Adapted from [110].

After 14 days of fluidic culture, cells organized into villi-like structures. Moreover, the intestinal lineage of these cells, the formation of brush borders and the presence of all four major intestinal epithelial subtypes and ISCs was also confirmed. With this work, the compatibility of the Gut-on-chip device with the culture of iPSC-derived intestinal epithelial cells was proved and the protocol for using organoid-derived cultures was optimized. Preliminary tests suggested that the behavior of this model in inflammation settings might represent *in vivo* conditions more faithfully, when compared to the Caco-2 cells model [110].

Accordingly, in 2018, Kasendra and colleagues [49] constructed an *in vitro* model of human duodenum with fragments of organoids derived from biopsy samples. This model consisted of a combination of microfluidic technology with organoid-based methods for culture of primary epithelial cells in an epithelial-endothelial interface. Organoids established from donor crypts were enzymatically dissociated into fragments, which were seeded on the microfluidic device. The fragments organized in an epithelial monolayer after 6 days of culture with fluid flow and developed villi after 8 to 12 days. Co-culture with endothelial cells accelerated the formation of the monolayer to 2 days. In line with what was previously demonstrated with Caco-2 cells [54, 52], this microfluidic device supported differentiation into multiple intestinal lineages. Additionally, the transcriptomic profile found in this model more closely resembled the profile of the duodenum *in vivo*, for all three donors enrolled in this study. Besides, the simulation of an endothelial barrier makes the primary-epithelium Gut-on-chip an interesting tool for the study of nutrient, drug transport and malabsorption-related diseases, in a patient-specific manner, being an important step for the future of personalized medicine. This work was followed-up by a

thorough characterization of the primary-epithelium Gut-on-chip as a model to study drug transport, drug metabolism and drug-drug interactions [48].

The previous studies demonstrated that primary intestinal epithelial cells on the Gut-on-chip simulated the duodenum tissue *in vivo* more accurately than other intestinal models. These data reflect the potential of this model as a tool for pre-clinical drug assessment and also for decoupling the effect of factors like age, sex, disease and diet on metabolism, clearance and bioavailability of xenobiotics. Nonetheless, strategies to improve reproducibility and standardization of protocols need to be developed, so that this model can be introduced in the pharmaceutical industry, as an alternative to animal testing.

Other applications of the primary-epithelium Gut-on-chip have been reported in the literature. Jalili-Firoozinezhad and colleagues developed a new approach to reproduce the interface of epithelial and endothelial tissue, while creating an oxygen gradient that simulates the conditions *in vivo* and enables the co-culture of aerobic and anaerobic microorganisms from the human microbiota (Figure 2.7) [45]. Infant-derived microbiota was co-cultured with primary human cells isolated from organoids derived from human ileum. The upper channel, where microorganisms and epithelial cells were cultured, was maintained in hypoxic condition, while the lower channel was lined with human intestinal microvascular endothelial cells (HIMECs) and perfused with oxygenated medium. Bacterial richness assessed in this model was similar to values detected in intestinal aspirates.

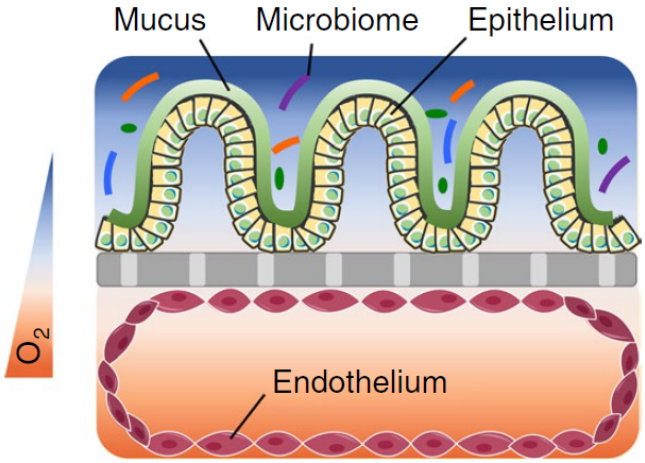

Figure 2.7: Schematic representation of the culture conditions in [45]. Intestinal epithelial cells are cultured on top of a porous membrane and self-organize in villus-like structures. A layer of mucus released by the cells in the epithelium forms around the undulating structure. Microbiota is present in the luminal portion of the model. Endothelial cells line the whole bottom channel, establishing a tissue-tissue interface with the epithelium through the porous membrane. An oxygen gradient is formed across the device, with higher levels of O_2 in the endothelial channel that decrease along the luminal channel.

The primary-epithelium Gut-on-chip device was also used to study intestinal epithelial morphogenesis [91]. DKK-1, a Wnt antagonist, was found to be predominantly secreted to the basal chamber and its removal by fluid flow in this compartment triggers 3D morphogenesis, i. e., restoration of villi-like microarchitecture, in Caco-2 cells and primary intestinal epithelium. Another interesting finding was that FZD9, a Wnt ligand receptor, is involved in such response

and its expression level correlates with flow rate and epithelial differentiation. Further work should consist in analyzing the contribution of morphogens secreted by subepithelial mesenchymal cells for epithelial differentiation in the intestinal microenvironment. The main drawback of this work is that, in its current form, the primary-epithelium Gut-on-chip does not recreate the crypt/villus compartmentalization of the native organ [49], limiting the extrapolation of the findings in this study to the *in vivo* condition.

2.3 Organoplate ® Caco-2

The company Mimetas produces a commercially available intestine-on-chip model that consists of a 384-well plate-shaped microfluidic device where 40 gut models are grown in tubular shape, the Organoplate ® Caco-2 [2] (Figure 2.8a). Caco-2 cells are seeded in the left channel, a Col-I-based ECM gel is introduced in the middle channel and the right channel contains the culture media (Figure 2.8c). The channels connect with each other in the center through two capillary pressure barriers (Figure 2.8b) [99]. In order to simulate perfusion, the plate is placed in OrganoFlow® L, a rocking system developed by the same company [1]. On a first report in 2017, Caco-2 cells cultured in this device showed proper polarization, confirmed by the presence of tight junctions and brush borders, and drug-induced alteration of epithelial barrier integrity was assessed [99]. Furthermore, in 2019, Organoplate ® Caco-2 was employed to construct an inflammatory bowel disease (IBD) *in vitro* model, by exposure of Caco-2 cells to a mixture of pro-inflammatory cytokines [13]. Cytokine production and compromised barrier function, two characteristic consequences of IBD, were successfully recreated in the model.

In summary, Organoplate® Caco-2 is a microfluidic device optimized for high-throughput experiments which, from the perspective of drug development and testing, is a valuable feature, reducing cost, time, and reagent consumption of screening experiments. Its format is compatible with common lab instruments, plate readers and imaging systems, making it a microfluidic platform easy to implement and that does not require pumps or tubes. Moreover, Mimetas has developed OrganoTEER® which enables on-chip measurement of TEER in real-time, which is ideal for intestine-on-chip models [3]. The downside of the Organoplate ® Caco 2 is also the use of an immortalized cell line. In addition, although the cells form a monolayer around the left channel, only a section of those cells are in direct contact with the ECM mimic. At last, there has been no description of the formation of crypts or villi-like structures in this device.

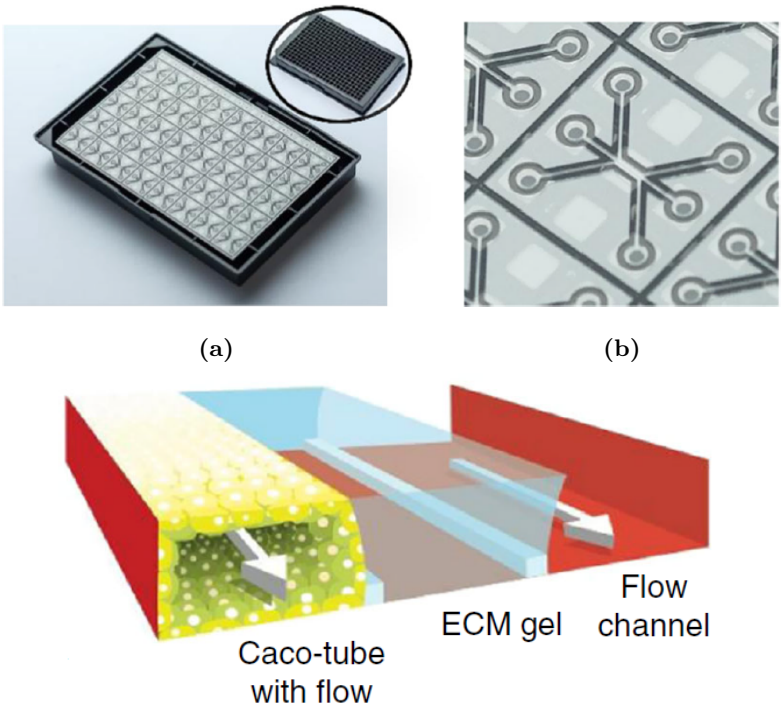

Figure 2.8: Organoplate ® Caco-2 *in vitro* model. (a) Photograph of the plate containing 40 small microfluidic systems incorporated. (b) The microfluidic system consists of 3 channels that communicate in the center. (c) Schematic representation of culture conditions with cell culture in the left channel, ECM-like gel in the central channel and media flow in the right channel. Adapted from [99].

2.4 Intestine-on-chip models for pharmacological studies

A different microfluidic device for intestine-on-chip culture using Caco-2 cells was applied to the determination of permeability coefficients of lipophilic prodrugs of the chemotherapeutic agent 7-ethyl-10-hydroxycamptothecin or SN38 [77]. Caco-2 cells were cultured on top of a polycarbonate (PC) membrane coated with Matrigel, sandwiched between two PDMS layers (Figure 2.9a). After a 5-day culture under dynamic flow of medium, cells formed a 3D undulating monolayer with microvilli. The compounds of interest were perfused through the apical chamber and their concentration on the basal chamber was measured to determine the transport through the membrane and consequently their permeability coefficient (Figure 2.9b). As expected, the most lipophilic prodrug exhibited the highest permeability coefficient.

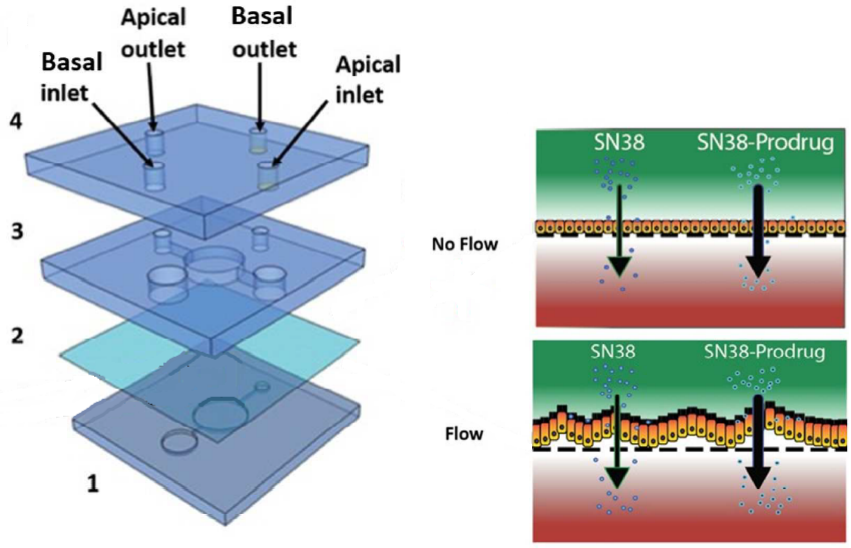

(a) **(b)**

Figure 2.9: Intestine-on-chip for intestinal permeability studies of SN38-prodrugs. (a) Representation of the four layers of the device: 1 – PDMS basal chamber, 2 – PC membrane, 3 – PDMS apical chamber, 4 – PDMS top layer. (b) Scheme of SN38 and SN38-prodrugs transport across the epithelial layer, in static (top) and microfluidic (bottom) conditions. Adapted from [77].

A four-chamber intestine-on-chip using Caco-2 cells was developed in 2018 to model drug metabolism in the intestine [40]. The chip consisted of three layers: a microfluidic channel layer, containing 4 parallel culture chambers, a tridimensional porous nitrocellulose membrane and an unstructured PDMS layer for support. The channels were coated with Col-I and media flow was continuous (Figure 2.10). Nitrocellulose membrane was chosen due to its porous structure, biocompatibility and protein-binding capability that might benefit cell adhesion. Caco-2 cells cultured in this device formed an epithelial monolayer with well-developed tight junctions as well as mucus secretion. Expression of villin and sucrase-isomaltase, two indicators of intestinal epithelium differentiation, was increased in this dynamic device in comparison to a planar culture in polystyrene.

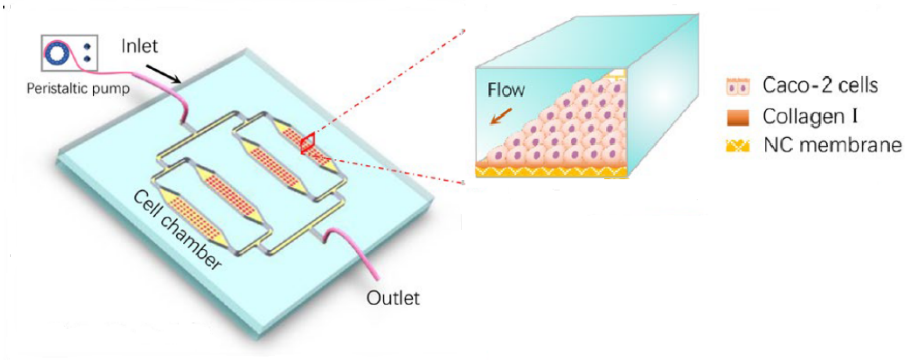

Figure 2.10: Four-chamber intestine-on-chip model. A nitrocellulose membrane coated with Col-I supports epithelial growth. The cells receive continuous media flow from the inlet and waste is removed through the outlet. Adapted from [40].

2.5 Intestine-on-chip models of host-microbiota interaction

Human-microbial crosstalk – HuMiX – is an *in vitro* microfluidic model of the host-microbiota interface in the human intestine [90]. The device comprises three co-laminar microchannels: a perfusion microchamber, a human epithelial cell culture microchamber and a microbial culture microchamber, enabling the creation of an oxygen gradient (Figure 2.11). Caco-2 cells were cultured on a collagen-coated polycarbonate membrane and formed a monolayer. To prove the potential of HUMiX to sustain culture of obligate anaerobic microorganisms, *Bacteroides caccae* were successfully co-cultured with LGG in the microbial chamber in equal proportions. Overall, the data obtained in anaerobic conditions was more consistent with the data obtained in the human intestine, proving that oxygen concentration has an effect on the activity of epithelial cells. Taking these results into account, the anaerobic condition is more representative of the intestinal setting and should be employed in following studies. On the downside, in HuMiX, commensal microbes are separated from the epithelial layer by a nanoporous membrane, which is not truly representative of the colonization by microbiota *in vivo*, usually concentrated on the apical surface of the epithelium.

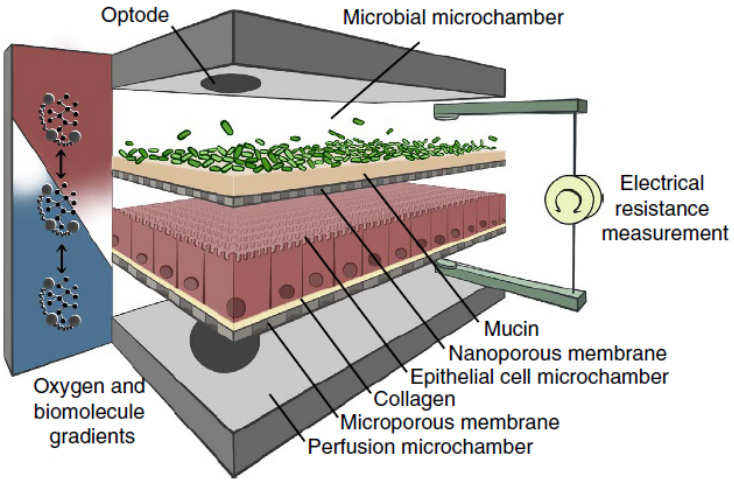

Figure 2.11: Diagram of the HuMiX model. There are three chambers: microbial, epithelial and perfusion, separated by porous membranes. An oxygen gradient is established with levels increasing from the microbial chamber to the perfusion chamber. Adapted from [90].

Maurer *et al.* developed a microfluidic model of the human intestine, MOTiF, combining endothelial and epithelial cell layers with mucosal macrophages and dendritic cells, that supported formation of villus and crypt-like structures in an immunocompetent environment [69]. Caco-2 cells and human umbilical vascular endothelial cells (HUVECs) were cultured on opposite sides of a porous polyethylene terephthalate (PET) membrane. Primary monocytes that later differentiated into mucosal macrophages (mMphs) and dendritic cells (DCs), were seeded on top of the confluent endothelial layer. In response to exposure to LPS on the luminal side of the model, DCs migrated to the epithelial cell layer and matured, while mMphs populated the endothelial layer. The presence of LPS in the lumen induced immunotolerance, but the exposure to LPS on the endothelial side triggered a release of proinflammatory cytokines and an impairment of the integrity of the epithelial

and endothelial layers (Figure 2.12). Upon colonization of the epithelial layer with the probiotic bacteria LGG, exposure to LPS on either side of the model, did not trigger any harmful effects on the cell layers and barrier integrity was improved. This is a very complete microfluidic model of the intestine that reproduces the complex interactions established between the different cell populations that coexist in the intestine. The immunotolerance observed is a crucial requirement for the stable colonization of living microorganisms of the microbiota.

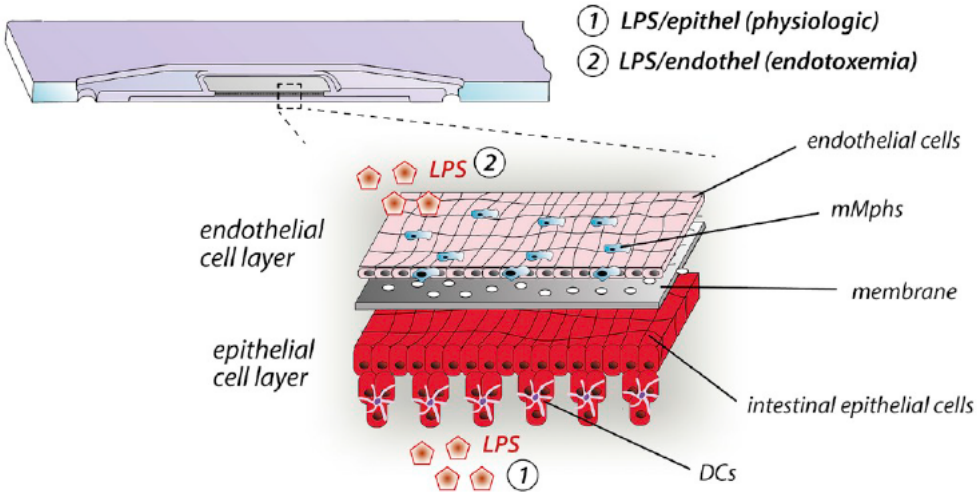

Figure 2.12: Schematic of the MOTiF intestine-on-chip model, composed of an epithelial, an endothelial layer, mMphs and DCs to assess the impact of LPS stimulation on the luminal (1) and endothelial (2) compartment. Adapted from [69].

2.6 Intestinal organoid-on-chip

Envisioning to overcome one of the main challenges associated with intestinal organoids, the lack of fluid flow inside the lumen, Sidar and colleagues developed the GOFlowChip [93]. This is a PMMA millifluidic device that sustains long-term internal perfusion of iPSC-derived human intestinal organoids. The device is composed of three layers: a middle layer that contains the organoid embedded in Matrigel and a channel for extraluminal flow, and the upper and lower chamber that enclose the middle one. Extraluminal flow was ensured by the introduction of liquid in and out of holes in the upper chamber. Intraluminal flow was achieved using tapered glass capillaries that were inserted into the organoids (Figure 2.13). After continuous intraluminal flow for over 20 hours, the signs of waste accumulation inside the organoid (darkening and opacity) significantly decreased as intraluminal flow washed away the cell debris out of the organoid. Organoid viability was not affected by capillary porting or culture in the device. This is an innovative approach to organoid culture that confers facilitated access to the lumen and allows its continuous perfusion, while the cells receive nutrients from the extraluminal channel, simulating the vasculature surrounding intestinal tissues. Organoid viability - which in static culture does not surpass 7 or 8 days without passaging - might be extended in this system. Additionally, different types of medium can be introduced into the different channels to mimic blood supply and luminal content.

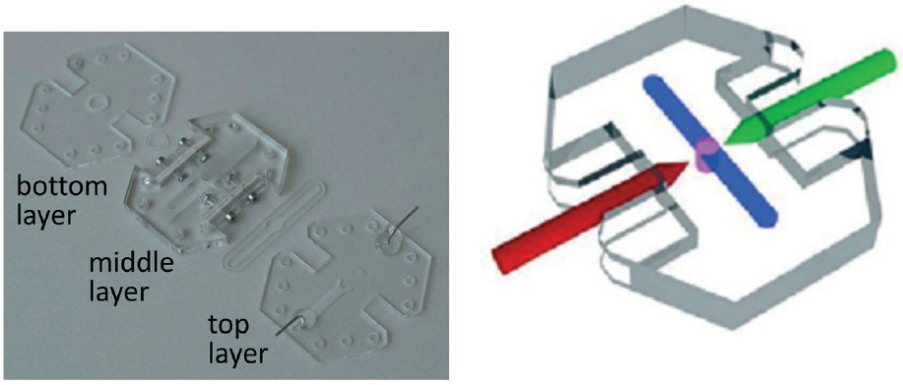

(a) **(b)**

Figure 2.13: The GOFlowChip. (a) The three layers that compose the chip, the top layer has inlets for the medium, the middle layer contains the organoid and the bottom layer encloses the device. (b) Schematic representation of organoid puncture. Adapted from [93].

2.7 Summary

Two-dimensional cell culture does not correctly recreate the structure and organization of native human tissue which has three-dimensional complexity. *In vivo*, cells are embedded in a matrix of proteins and proteoglycans that assures cell nutrition, migration, differentiation, and proliferation. Besides, cells are in close contact with other cell types and are exposed to specific biochemical cues that vary with time and space, with homeostasis and disease. Another factor that has been considered recently in the literature is the impact of different types of physiological mechanical stress on cell differentiation. Tissue morphogenesis and homeostasis are a result of a multitude of factors that interplay to recreate complex cellular and physiological processes. Constructing a reliable *in vitro* model that recapitulates the totality of variables that influence cell behavior is far from reach. On the other hand, recent tissue engineering research has been focused on developing *in vitro* models that provide a three-dimensional structure to cell culture where more components that are relevant in the native microenvironment of organs can be added, and the control over culture conditions is enhanced. Organ-on-chip technologies have proved their potential in mimicking complex organ environments, in a self-contained, miniaturized model. One of the organs that has been successfully mimicked using microfluidics approaches is the small intestine.

Over the last 15 years, several research groups have applied microfluidic technology to establish increasingly more sophisticated intestine-on-chip models, *in vitro* 3D models of the human intestine. A summary of those reports and a comparison of their features can be found in Table 2.1.

The variety of designs reported in the literature is considerable, however, one particular design stands out among the others, the Gut-on-chip [51]. Various researchers based their work on this device to create models of the human-microbiota interaction [51, 53, 92] and of intestinal pathologies [92, 53]. The Gut-on-chip presented two main significant advances from Transwell systems. First, it proved that fluid flow is a determinant factor for the organization of Caco-2 cells in folds [51] that show crypt-villus compartmentalization [52] and that peristalsis-like mechanical simulation further enhances that organization. Second, the device enabled long-term co-culture of microorganisms

from the microbiota with Caco-2 cells because the presence of continuous fluid flow washed out excess bacteria.

Concerns about Caco-2 cell line physiological relevance prompted groups of researchers to incorporate primary cells in the Gut-on-chip. The compatibility of the device with iPSCs and primary duodenum tissue culture was demonstrated recently [110, 49] and the suitability of primary intestinal epithelial cells for microfluidic models has been corroborated, given that such type of culture is genetically and functionally more faithful to the human living intestine. However, in these microfluidic approaches, the cell seeding protocol promoted the formation of a monolayer where differentiated cells and stem cells were, seemingly, randomly distributed and the intestinal tridimensionality was partially lost [49]. In their current form, these models might not be suitable for studying signalling pathways associated with stemness, biomolecular gradients that drive differentiation or intestinal pathologies since they may produce inaccurate findings. In spite of that, the primary-epithelium Gut-on-chip has been adapted to the simultaneous co-culture with aerobic and anaerobic intestinal commensals [45] and has been applied in the research of triggers that drive epithelial morphogenesis in a microfluidic setting [91].

Alternative designs of intestine-on-chip models, with different microarchitectures and made of different materials were also reported in this Chapter. So far, there has been no other example of peristalsis simulation in intestine-on-chip platforms.

Nonetheless, important breakthroughs were also achieved with some of these models, for example, the development of a system to introduce fluid flow inside an enclosed intestinal organoid, avoiding waste accumulation and simulating luminal flow (GOFlowChip) [93]. This system permits analysis of luminal content, establishment of chemical gradients (oxygen or growth factors) and molecule transport analyses. The GOFlowChip can be optimized to culture intestinal organoids for regenerative medicine applications, in a patient-specific manner. Furthermore, it is the only example of an organ-on-chip compatible with culture of whole intestinal organoids, instead of organoid-derived fragments. An alternative microfluidic design enabled the co-culture of six different cell populations in a model that intended to recreate the immunological activity in the intestinal mucosa and how it is modulated by the presence of commensals [69]. The host-microbiota interaction results from the interplay of endothelial, epithelial and immune populations, therefore, models should become progressively more complete for an accurate representation. To date, the Organoplate ® Caco 2 is the only commercially-available alternative system to the Gut-on-chip, however, its versatility and physiological relevance are still limited in comparison to other approaches reported in the literature.

The use of Matrigel is recurrent in intestine-on-chip models to provide three-dimensional support to cell growth and simulate the native ECM. However, Matrigel is an animal- and tumor-derived matrix [19, 56] which significantly hinders its application in clinical settings, for instance, in regenerative medicine. Due to its biological nature, the relative quantities of its components may vary from batch to batch, affecting the reproducibility of experiments. Thus, Matrigel should be gradually replaced by synthetic hydrogels optimized for cell culture.

From the perspective of biofabrication, Table 2.1 demonstrates that most intestine-on-chip devices are still produced by soft lithography. Microfluidic device fabrication using 3D printing techniques is faster, less expensive and more versatile in terms of geometry than soft lithography. Moreover, it is a straightforward technique that encompasses less experimental steps. As a result,

Table 2.1: Comparison of diverse features and applications of intestine-on-chip models reported in the literature.

Reference	Intestinal cells	Co-cultured cells	Peristalsis simulation	Oxygen gradient	Device material	Membrane material and matrix	Fabrication technique	Main observations
Kim et al., 2012	Caco-2 line	*Lactobacillus rhamnosus*	Cyclic elongation of the membrane	No	PDMS	PDMS Matrigel Col-I	Soft lithography	Fluid flow accelerates intestinal epithelial differentiation and organization into villi-like structures Mechanical stimulation enhances the response to fluid flow Long-term co-culture with commensal bacteria
Kim & Ingber, 2013	Caco-2 line	No	Cyclic elongation of the membrane	No	PDMS	PDMS Matrigel Col-I	Soft lithography	Presence of four intestinal epithelial cell types Increased proliferative activity in the base of the crypt
Kim et al., 2016	Caco-2 line	PBMCs *E. coli* Microbiota	Cyclic elongation of the membrane	No	PDMS	PDMS Matrigel Col-I	Soft lithography	Inflammatory bowel disease (IBD) model
Shim & Kim et al, 2018	Caco-2 line	PBMCs *E. coli* Microbiota	Cyclic elongation of the membrane	No	PDMS	PDMS Matrigel Col-I	Soft lithography	Barrier dysfunction is the critical trigger of inflammation onset in the gut
S. Jalili-Firoozinezhad et al., 2019	Caco-2 line Organoid-derived primary epithelium	Intestinal microbiota samples ECs	Cyclic elongation of the membrane	Yes	PDMS	PDMS Matrigel Col-I	Soft lithography	Establishment of an oxygen gradient compatible with co-culture of anaerobic commensals
Shin et al., 2019	Caco-2 line Organoid-derived primary epithelium	No	Cyclic elongation of the membrane	No	PDMS	PDMS Matrigel Col-I	Soft lithography	DKK-1 and FZD9 mediate 3D morphogenesis of the intestinal epithelium in the Gut-on-chip
Workman et al., 2018	Caco-2 line iPSC-derived primary epithelium	No	No	No	PDMS	PDMS Matrigel	Soft lithography	Development of an iPSC-derived intestine-on-chip More accurate response to inflammatory stimuli comparing to the Caco-2 model
Kasendra et al., 2018 and Kasendra et al., 2020	Caco-2 line Organoid-derived primary epithelium	HIMECs	Cyclic elongation of the membrane	No	PDMS	PDMS Matrigel Col-I	Soft lithography	Transcriptomic profile of this model is more similar to the human duodenum, comparing to Caco-2 cell model
Organoplate ® Caco-2 by Mimetas Triestch et al., 2017 and Beaurivage et al., 2019	Caco-2 line	No	No	No	Glass and proprietary polymers	Phaseguide™	Unknown	High-throughput platform First commercially available model Epithelial barrier integrity studies
Pocock et al., 2017	Caco-2 line	No	No	No	PDMS	Polycarbonate Matrigel	Soft lithography	Determination of permeability coefficient across the intestinal barrier
Guo et al., 2018	Caco-2 line	No	No	No	PDMS	Nitrocellulose Col-I	Soft lithography	Metabolic efficiency of Caco-2 cells upon exposure to verapamil and ifosfamide Four parallel cell culture chambers
Shah et al., 2016	Caco-2 line	*Lactobacillus rhamnosus GG* *Bacteroides caccaer*	No	Yes	Polycarbonate	Polycarbonate Collagen Mucin	Computer controlled milling Laser cutting Bolting	Co-culture with commensal organisms alters gene expression in Caco-2 cells Importance of oxygen gradient simulation in intestine-on-chip models
Maurer et al., 2019	Caco-2 line	HUVECs mMphs DCs *Lactobacillus rhamnosus* *Candida albicans*	No	No	Polystyrol	PET	Injection molding	Characterization of immunological response to luminal LPS and endotoxemia Role of probiotics in the protection from opportunistic infections
Sidar et al., 2019	iPSC-derived human intestinal organoids	No	No	No	PMMA	Absent	Laser cutting	Establishment of intra and extraluminal flow in intestinal organoids

3D printed intestine-on-chip devices will emerge in the future and possibly enable optimized designs for intestinal *in vitro* models.

The relevance of microfluidics in intestine modeling is unquestionable since its capability of combining different factors and stimuli in just one culture system allowed an increase in complexity and reliability. Thanks to the modular nature of organ-on-chip platforms, different and more compartments can be added to a single system. In fact, a number of devices can be continuously linked - for example, a stomach-on-chip linked to a liver-on-chip linked to a intestine-on-chip - to simulate whole physiological systems, or even, the human body - body-on-chip. Scaling up and systematization of cell manipulation systems and assays are future challenges associated with the practical application of the intestine-on-chip in pharmaceutical studies and industrial laboratories [15].

In summary, intestine-on-chip systems have contributed to answer relevant questions in the field, allowing for the co-culture with microbiota, endothelial and immune cells. Moreover, they have also shown their potentiality for pharmacological studies, concerning drug transport and absorption in the intestine, bioavailability and drug-drug interactions. By including primary cultures, instead of immortalized cell lines, patient-derived intestine chips may be developed for personalized drug testing.

Investigating the interaction of smooth muscle and neuronal cells with the intestinal microenvironment may be the next applications of intestine-on-chip systems, given that these populations are actively involved in gut motility, for instance. Furthermore, the intestine-on-chip can be further employed to study the intricated morphogenic process of the intestine, helping to unravel specific signaling pathways and biochemical factors that guide differentiation. The complex hierarchy of ISCs could also be investigated with these systems.

Chapter 3

Hypothesis, Strategy and Objectives

As described in the previous chapter, microfluidic strategies have catalyzed the evolution of *in vitro* models of the small intestine, granting them more complexity and a better mimicking potential of physiological conditions. A clear proof was reported by Kim and colleagues, who showed that continuous fluid low accelerates differentiation of Caco-2 cells, inducing them to organize in folds that mimic the microarchitecture of the intestine [51, 52].

As mentioned in Chapter 1, intestinal organoids are 3D models of the small intestine derived from stem cells that undergo a process similar to *in vivo* organogenesis, resulting in a miniaturized version of the small intestine that contains various cell populations of the intestine and recreates its native spatial organization. The versatility of these models is still hindered by their low complexity, uncontrollable size and morphology. Despite the proven advantages of coupling microfluidic approaches to cell culture, intestine-on-chip strategies do not usually focus on whole organoids and, to date, there is only one report of an intestine-on-chip system that is based on whole organoids [93], as described in Chapter 2.

The hypothesis in this dissertation was that intestinal organoid growth and development would be enhanced in continuous fluid flow conditions, as opposed to the static setup of the 24-well plate culture. In collaboration with Biofabics, the strategy was to design 3D-printed microfluidic devices that supported intestinal organoid culture in a Matrigel matrix and that could be coupled with perfusion equipment to perform continuous fluid flow of cell culture medium. Then, organoid development in the device, with and without medium perfusion, would be monitored by time-lapse microscopy and compared. Additionally, differences in the expression of genes associated with stemness, proliferation and differentiation would be analysed by real-time PCR analysis and immunohistochemistry.

Therefore, the main objectives of this dissertation were to:

- Build an optimized microfluidic platform and experimental protocol for performing intestinal organoid culture under continuous perfusion of medium;
- Study the impact of exposure to fluid flow on intestinal organoid development, in particular, regarding morphology and gene expression profile;

- Improve the physiological faithfulness of intestinal organoid models and, ultimately, develop a robust intestinal-organoid-on-chip.

The following two chapters describe the methodologies employed in this work and the results obtained. The results are discussed in Chapter 6 and suggestions for future work can be found in Chapter 7.

Chapter 4

Materials and Methods

4.1 Animal model

Intestinal cells used in this work were derived from wild-type mice or the *Lgr5-EGFP-IRES-creERT2* ($Lgr5^{EGFP}$) knock-in mouse model [10]. Animal experimentation was performed in accordance with the Portuguese National Regulation established by Decreto-Lei 113/2013, which is the national transposition of the European Directive 2010/63/EU for the Care and Use of Laboratory Animals. Procedures were evaluated and approved by the i3S Animal Welfare and Ethics Review Body and by the Portuguese National Authority for Animal Health (DGAV)—project licence code n.º 015434/2017-07-04. Animal manipulation was performed by co-supervisor Bruno Pereira who is certified in animal experimentation (FELASA C course). Mice were bred and maintained at the animal facility of i3S, which is accredited by the Association for Assessment and Accreditation of Laboratory Animal Care (AAALAC), under a standard 12h light/dark cycle, with water and rodent chow available *ad libitum*.

4.2 Intestinal crypt isolation

Mice were dissected to extract mainly the jejunum and ileum portions of the small intestine. The small intestine of $Lgr5^{EGFP}$ or wild-type mice was dissected and flushed with ice-cold PBS, using a blunt intestinal probe attached to a 10 mL syringe. The isolated intestine was cut longitudinally and washed 3 times in a 15 mL tube by vigorous shaking to remove remaining contents. The mucosal side of the tissue was scrapped with a microscope slide, to eliminate villi and expose crypts. The tissue was cut into $5mm^2$ fragments using a razor blade and fragments were incubated in crypt chelating buffer (2 mM EDTA pH 8.0 in PBS) in a 15 mL tube, horizontally, on ice for 1 hour. Digested fragments were washed in 5 mL of ice-cold PBS with manual agitation in order to dissociate the epithelium from the basal membrane. The suspension was filtered through a 70 µm mesh to separate the crypts from the villi. Crypt suspension was centrifuged at 300 x g, at 4ºC for 10 min. Supernatant was eliminated and the crypt pellet was resuspended in ice-cold PBS. Number of crypts per 10 mL was counted at the microscope.

4.3 Intestinal organoid culture

Organoids were cultured as described previously [84] in 24-well culture plates. Approximately 250 crypts/well were mixed with 60% Matrigel growth factor reduced (Amsbio), 10% NOG, 10% RSPO1, and 50 ng/mL EGF (Peprotech). 40 µL droplets of the mix were seeded in individual wells of a pre-heated plate. The formed domes were incubated at 37ºC for 30 min. After, they were immersed in 500 µL of intestinal organoid complete medium that was replaced every 2-3 days. Medium was composed of Advanced DMEM/F12, 10 mM HEPES, 1x GlutaMAX, 1x B27, 1x N2 (all from Thermo Fischer), 50 ng/mL EGF, 0.2% Primocin (InvivoGen), 10% RSPO1-conditioned medium, 10% NOG-conditioned medium and 0.2% Y-27632 (Stem Cell Technologies). Y-27632 was not added to medium on posterior passages. Conditioned media were produced using HEK293T cells stably transfected with HA-mouse RSPO1-Fc or stably transfected with a mouse NOG-Fc expression vector. For that, Adv. DMEM/F12 supplemented with 10% FBS, 10 mM HEPES and 1× GlutaMAX was conditioned for 1 week with each cell line, filtered through a 0.22 µm syringe filter, and individual working aliquots maintained at -20°C. Intestinal organoids were passaged every 3-7 days, by dissolving Matrigel domes with 800 mL of ice-cold Advanced DMEM/F12. The suspension was collected to a 15 mL tube that was centrifuged for 5 min at 300 x g. Supernatant was discarded and the pellet was resuspended in Advanced DMEM/F12 and the seeding process was repeated.

4.4 Sample preparation for Fluorescence-activated cell sorting (FACS)

Control crypts were isolated from wild-type mice and centrifuged for 10 min at 300 x g. Pellet was resuspended in 1 mL PBS. The suspension was divided into two tubes where 3 mL of Accumax were added to dissociate the cells in the crypts. Tubes were incubated for 15 min at 37ºC. *Lgr5*^{EGFP} mice-derived crypts were obtained by dissolving Matrigel domes with intestinal organoids in ice-cold PBS. Resulting suspension was also incubated with 3 mL Accumax for 5-10 min at 37ºC. Both types of samples were centrifuged for 10 min at 300 x g. Pellet was resuspended in FACS buffer composed of 2% FBS and 1 mM EDTA in PBS. Four samples were prepared:

1. **unstained control**: 250 µL cells + 750 µL buffer
2. **anti-CD24 control**: 250 µL control cells + 750 µL buffer + 1 µL anti-CD24 antibody
3. **anti-LGR5 control**: 250 µL control cells + 2.5 µL anti-LGR5 antibody
4. **CD24/LGR5 sorting sample**: 1000 µL cells + 1 µL anti-CD24 + 10 µL anti-LGR5 antibody

All samples were incubated on ice for 40-45 min. Then, they were centrifuged in a microcentrifuge for 5 min at 2500 rpm, 4ºC. Supernatant was discarded and the pellet was resuspended in 500 mL FACS solution and the suspension was passed to a cytometry column. 1000 µL recovery medium for sorted cells (Table 4.1) was prepared with Advanced DMEM/F12 as follows and split into two tubes.

Table 4.1: Composition of recovery medium for FACS-sorted cells

Reagent	**Concentration**
NOG-conditioned medium	10% (v/v)
RSPO1-conditioned medium	10% (v/v)
WNT-conditioned medium	10% (v/v)
Y-27632	0.2% (v/v)
Primocin	0.2% (v/v)
EGF	50 ng/mL

Sorting procedure was conducted by the Translation Cytometry Unit at i3S. The two sorted populations were mixed and seeded in 40 µL Matrigel domes. Mix composition was the same as in normal intestinal organoid plating with the addition of Y-27632 (0.2%), and WNT-conditioned medium (10%). 500 µL of intestinal organoid medium, with equal parts of WNT-conditioned medium and Advanced DMEM/F12, were added to the well and replaced every 2-3 days. The plate was visualized daily in a Zeiss Primovert inverted microscope for two weeks.

4.5 Microfluidic device design

Microfluidic devices were designed in collaboration with Biofabics. Devices are produced from proprietary material using a technique derived from stereolithography. Designs A, B and C were created with the Biofabics Toolbox (https://biofabics-toolbox.com) using "Design tool 4 - Channels through chambers - wells". Dimensions of microfluidic devices A, B, C and D can be consulted in Table 4.2.

Table 4.2: Dimensions of microfluidic devices A, B, C and D.

Parameter	**Design A**	**Design B**	**Design C**	**Design D**
Well diameter (mm)	12	8	6 / 8	-
Well height (mm)	5	5	5	-
Channel length (mm)	10	16	18	23
Channel diameter (mm)	2	1.5	1.5	1.5
Channel to chamber bottom (mm)	0	0	1.0	1.0
Type of chamber	Rectangular	Square	Circular	Circular
Chamber diameter/width (mm)	4.5	4	8	8
Chamber length (mm)	4	4	-	-
Device length (mm)	60	75	75	75
Device width (mm)	32	25	25	25
Inlet/Outlet lid diameter (mm)	-	8	8	-
Inlet/Outlet lid total height (mm)	-	8	10	5
Inlet/Outlet lid base height (mm)	-	3	3	-
Inlet/Outlet internal diameter (mm)	-	1.5	1.5	1.5
Inlet/Outlet external diameter (mm)	-	3	3	3
Lateral lid length (mm)	-	24	26	-
Lateral lid width (mm)	-	10	10	-
Lateral lid height (mm)	-	3	3	-
Type of central lid	-	Square	Circular	Circular
Central lid diameter/width (mm)	-	12	13	13
Central lid height (mm)	-	7	5	5
Central lid transparent diameter (mm)	-	8	8	8
Inlet/outlet PDMS ring outer diameter (mm)	-	-	8	-
Inlet/outlet PDMS ring inter diameter (mm)	-	-	6	-
Central lid PDMS ring outer diameter (mm)	-	-	10	10
Central lid PDMS ring inter diameter (mm)	-	-	8	8

Inlet/outlet pieces and lids were produced by Biofabics using the same material. Central chambers included a coverslip glass at the base, as well as on the lid, to allow visualization by microscopy. Plastic molding lines, diameter 0.9 mm, were inserted through the channels and chambers of the devices to create channels inside Matrigel.

Prior to utilization, devices A, B, C and D and tubes were autoclaved and kept sterile. After use, devices were washed with PBS to dissolve Matrigel and medium remains and then were immersed in a mixture of bleach 20% (v/v) and water for 24 hours, washed abundantly with water, and left to air dry. Tubes were washed by perfusing dH_2O. Before re-utilization, devices and tubes were autoclaved.

Device E was also designed in collaboration with Biofabics. It comprises a central rectangular chamber with dimensions 10 mm x 5 mm x 4 mm. A 0.5 mm diameter porous tube is located inside this chamber for cell seeding. Media inlets and outlets are located at the base of the chamber.

4.6 Dynamic experiments

The system developed for fluid perfusion consisted of:

1. **Aladdin AL-1000HP syringe pump** (World Precision Instruments) in which it was possible to program flow direction, rate, volume to be dispensed and setup complex cycles of injection. Programs for unidirectional and bidirectional flow are displayed in Tables 4.3 and 4.4, respectively. A multi-syringe adapter (Biofabics Lda) was attached to the pump in order to enable the simultaneous operation of multiple (up to twenty) 1 mL syringes;

2. **1 mL syringes** (Braun) compatible with the adapter in the pump;

3. **18G needles** (BD) were attached to the end of the syringes and inserted inside silicone tubes. This diameter was optimal for the diameter of the tubes and smaller diameter needles (e. g. 19G) promoted the formation of air bubbles inside the tubes;

4. **Silicone tubes** (Silex) transported cell culture medium from the syringes in the pump to the microfluidic device. In the microfluidic devices, tubes were attached to inlet lids for medium supply or to outlet lids for disposal of medium. Dimensions: 1.5 mm (inner diameter) x 0.5 mm (wall thickness) x 2.5 mm (outer diameter). These tubes are Food and Drug Administration (FDA) and National Sanitation Foundation (NSF) approved;

5. **Inlet and outlet pieces** were adapters for the connection between the tubes and the microfluidic device. Inlet and outlet pieces were either integrated in a lid (Device B and C) or in the base of the microfluidic device (Device D). Inlets were attached to the tubes injecting medium and outlets were attached to tubes for medium discharge;

6. **Discharge collector** was a 15 mL plastic Falcon tube that received the culture medium perfused out of the microfluidic device.

Before Matrigel polymerization in the device, inlet and outlet lids were inserted into the wells. Then, silicone tubes were attached to each inlet or outlet piece. After Matrigel seeding on the device, tubes were coupled to the needles. For filling the tubes (30-80 cm), before the beginning of the experience, the flow rate employed was 700 µL min^{-1}, and tubes were filled to the base of the inlet lid. Refilling of syringes was performed by putting a clip just ahead of the needle in the tube, so that the medium inside would not leak. Then, the needle was disengaged from the syringe, syringe was removed from the pump, refilled and put in back in the pump support.

A descriptive image of the experimental setup used for dynamic experiments is displayed in Figure 4.1. This photograph was taken during an experiment to evaluate Matrigel resistance to fluid flow, therefore, temperature control was not necessary. In other cases, the setup was assembled inside an environmentally controlled chamber at 37ºC and 5% CO_2.

Table 4.3: Example of pump program for unidirectional flow at 30 µL h^{-1} for 72 hours.

Phase	**Function**	**Rate**	**Volume**	**Direction**
1	Rate	30 µL h^{-1}	2160 µL	Pumping

Table 4.4: Example of pump program for bidirectional flow composed of 10 cycles of 1.5 hours of infusion and 1.5 hours of withdrawal at 100 µL h^{-1}.

Phase	Function	Rate	Volume	Direction
1	LP:ST			
2	Rate	100 µL h^{-1}	150 µL	Pumping
3	Rate	100 µL h^{-1}	150 µL	Withdraw
4	LP:10			
5	STOP			

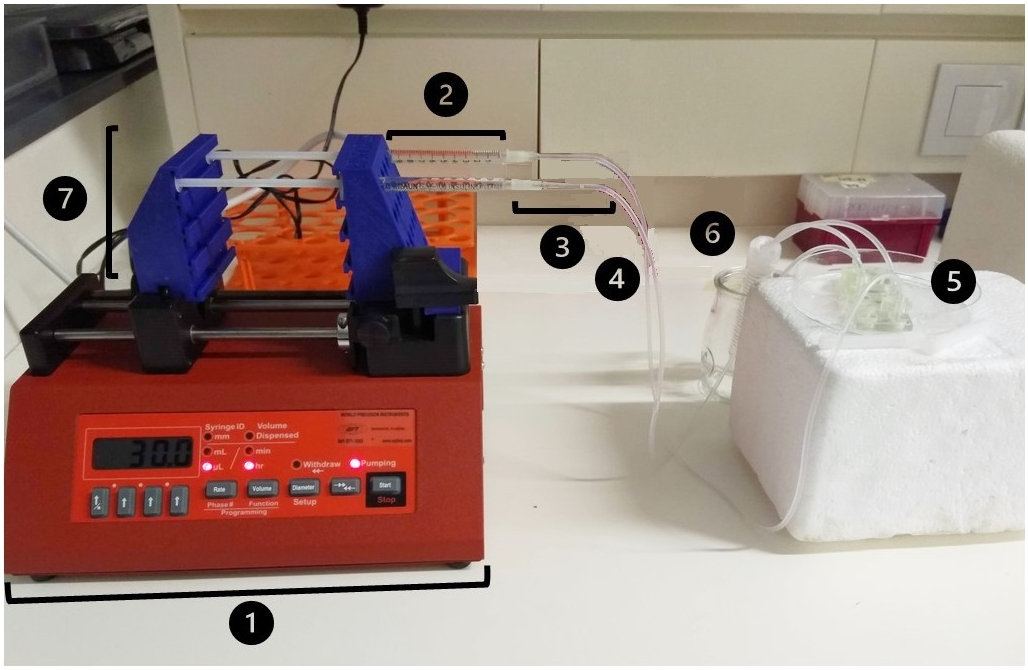

Figure 4.1: Experimental setup for dynamic experiments. (1) Syringe pump. (2) 1 mL syringes. (3) 18G needles. (4) Silicone tubes. (5) Inlet and oulet pieces in the device. (6) Discharge collector tube. (7) Multi-syringe adapter.

4.7 Inverted microscope imaging

If not stated otherwise, all microscopical images were acquired in a Primovert Zeiss inverted microscope coupled to a Axiocam ERC 5s camera. Fiji software was used for image editing, addition of scale bar and measurement of organoid diameter.

4.8 Time-lapse microscopy

All time-lapse imaging experiments were performed on LeicaDMI600 Timelapse microscope (Leica Microsystems, Germany), a motorized inverted epifluorescence microscope equipped with a Hamamatsu FLASH4.0 (Hamamatsu, Japan) camera. Leica Application Suite software (LAS X) was used for operating the microscope, programming the experiment and adjusting intensity,

exposure, positions and z-stack. Phase contrast or brightfield and fluorescence images were acquired with a HC PL FLUOTAR 10x/0.30 Ph1 objective. For phase contrast or brightfield, intensity was set to 10 and exposure to 10 ms. For fluorescence imaging, L5 filter was used, with excitation wavelength 460-500 nm and emission wavelength 512-542 nm. Fluorescence intensity was set to 6 and exposure to 200 ms. Temperature was kept at 37ºC and CO_2 concentration at 5%.

4.9 Real-time PCR

Total RNA was extracted using TRI Reagent according to the manufacturer's guidelines (Sigma-Aldrich). RNA was quantified using a NanoDrop and reverse-transcribed using the Superscript IV Reverse Transcriptase Kit (Life Technologies). Analysis of mRNA expression was performed in an ABI Prism 7500 system using the Power SYBR Green Master Mix (Life Technologies) and specific primer pairs that can be consulted in Table 4.5. Each sample was amplified in triplicate. *18S* rRNA levels were measured for normalization of target gene abundance.

Table 4.5: List of primers used in Real-time PCR

Gene	**Sense Primer**	**Anti-sense Primer**
Lgr5	AGCGTCTTCACCTCCTACCTG	CTTGGGAATGTGTGTCAAAGC
Lyz1	ACAATCGTTGTGAGTTGGCCAG	TAAACACACCCAGTCAGCCAG
Pcna	GGGCTGAAGATAATGCAGACA	TGTACTCCTGTTCTGGGATTC
18S	CGCCGCTAGAGGTGAAATTC	CATTCTTGGCAAATGCTTTCG

Chapter 5

Results

5.1 Intestinal crypt isolation

Intestinal crypts were isolated from *Lgr5*^{EGFP} mice. This mutation causes expression of enhanced green fluorescent protein (EGFP) in *Lgr5*$^{+}$ cells. Only heterozygous animals were used because homozygous mice are not viable [10] due to the insertion of the *Egfp* sequence in the middle of the *Lgr5* gene sequence, silencing *Lgr5* expression. Green fluorescence in the small intestine shows a mosaic pattern, where EGFP is not expressed in every crypt due to allele silencing by an unknown mechanism [87, 11].

In the isolation process, EDTA works as a chelating agent that aids in the detachment of crypts from the basal membrane. The next crucial step in the protocol is a vigorous mechanical agitation. This step should physically release crypts from the intestinal tissue, leaving it with a net-like aspect when visualized in the microscope (Figures 5.1a and 5.1b). Intestinal crypts are U-shaped structures that at the base display cells with large eosinophilic granules, the Paneth cells (Figure 5.1c).

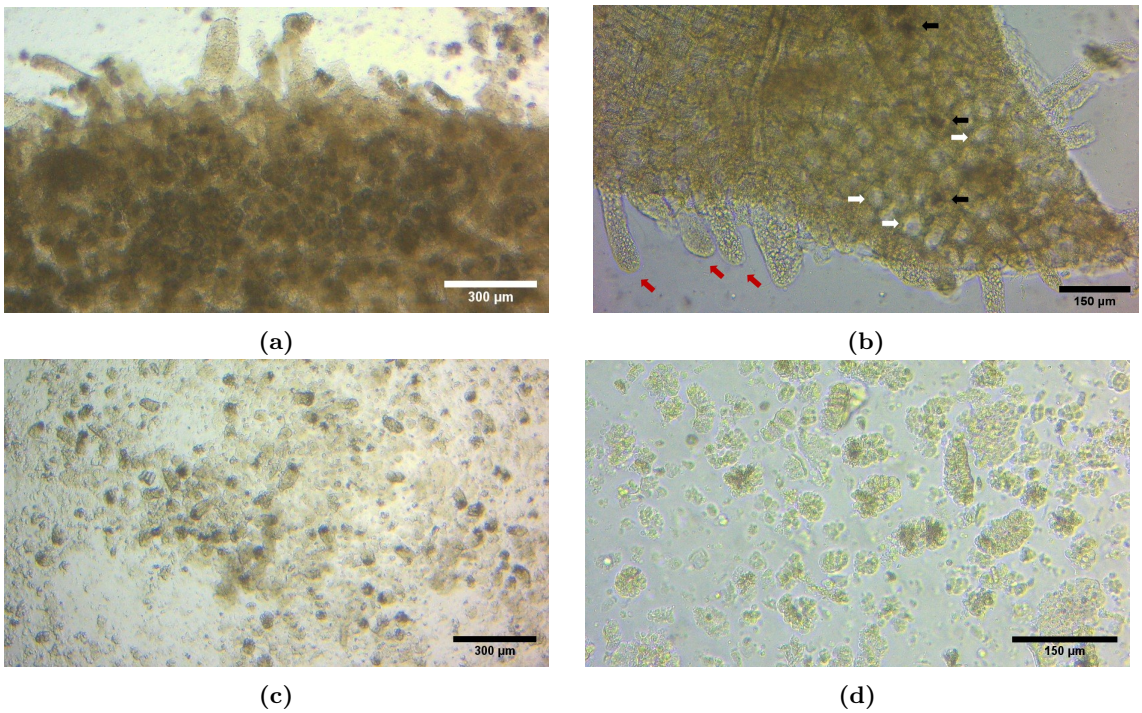

(a) **(b)**

(c) **(d)**

Figure 5.1: Inverted microscope images of the intestinal tissue and isolated crypts. (a) A portion of the intestinal tissue where crypts are still attached to the intestinal wall. Scale bar: 300 µm. (b) Crypt dissociation from the intestinal wall creates a net-like appearance in the tissue. White arrows point to some of the orifices left in the intestinal wall after crypt detachment; black arrows point to crypts that were not separated from the tissue; red arrows point to remaining villi. Scale bar: 150 µm. (c) Isolated crypts after mechanical dissociation and filtration through 70 µm cell strainer. Scale bar: 300 µm (d) Higher magnification image of crypt suspension. Cells with dark granules at the bottom of the crypt are Paneth cells. Scale bar: 150 µm.

Visualization in the ZOE Fluorescent Cell Imager, allowed the identification of $EGFP^+$ cells, at the bottom of the crypts. This observation confirms that *Lgr5* expression is restricted to the crypt base (Figure 5.2) and that the expression pattern of *Lgr5* co-locates with intestinal stem cells. Around 6 $Lgr5^+$ ISCs can be found in each crypt, interspersed with Paneth cells. The results confirm previous findings concerning crypt constitution and organization reported by Barker *et al.*, 2007 [10]. Variegated expression of EGFP between crypts was also verified (Figures 5.2d and 5.2e).

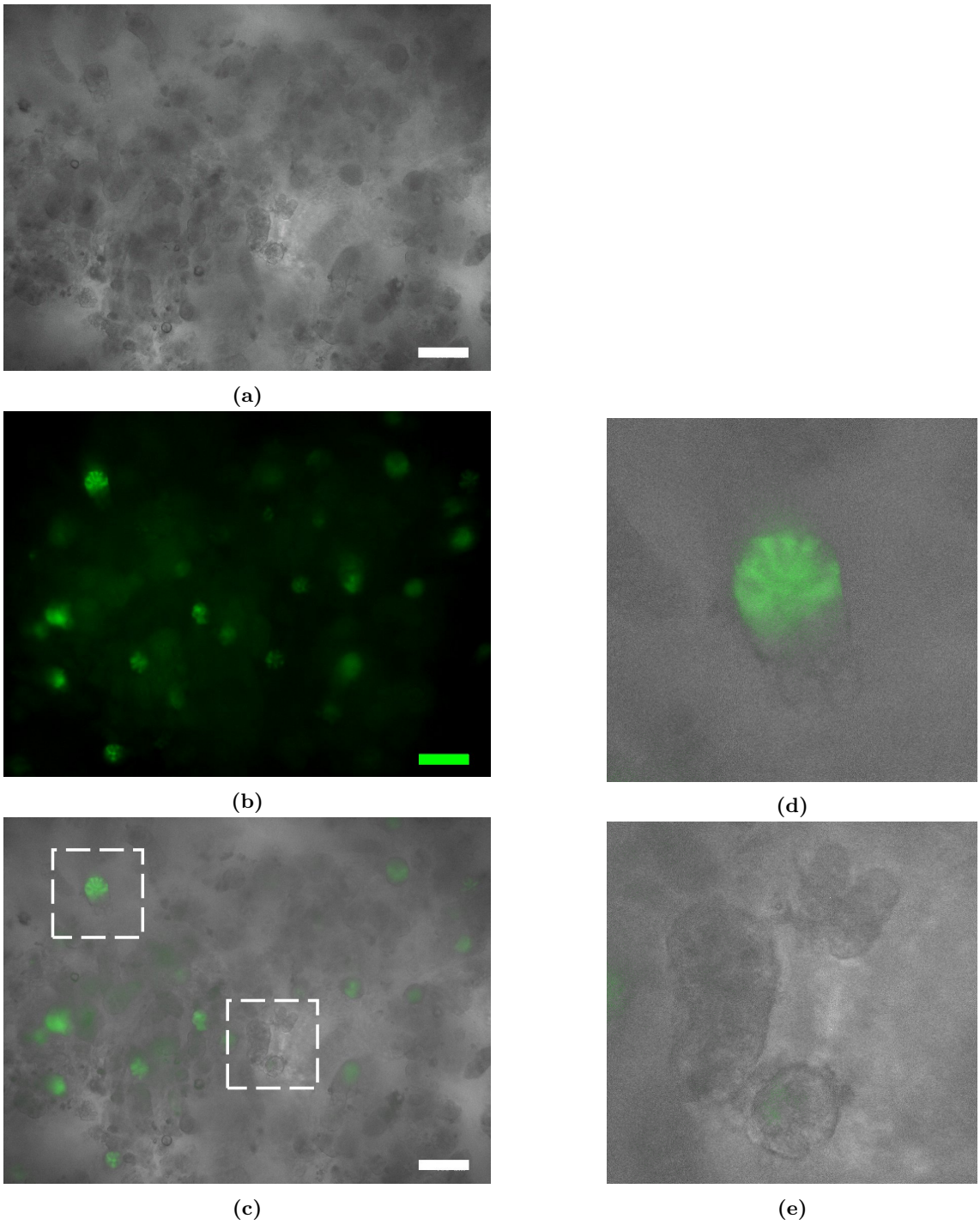

Figure 5.2: EGFP expression in isolated crypts. Images of crypt suspension were acquired using the ZOE Fluorescent Cell Imager in two channels: brightfield and green fluorescence. (a) Brightfield image. (b) Green fluorescence image. (c) Merged image. (d) Crypt expressing EGFP. (e) Crypts negative for EGFP. Scale bar: 100 µm.

5.2 Intestinal organoid culture

To develop intestinal organoids, isolated crypts were embedded in a Matrigel matrix, supplemented with NOG-conditioned medium, RSPO1-conditioned medium, epidermal growth factor (EGF) and primocin, a potent antimicrobial agent active against bacteria, mycoplasma and fungi. After Matrigel polymerization, the dome was immersed in intestinal organoid medium (Figure 5.3). In the first plating after isolation, ROCK inhibitor Y-27632 was added to the medium to prevent dissociation-induced apoptosis, or anoikis.

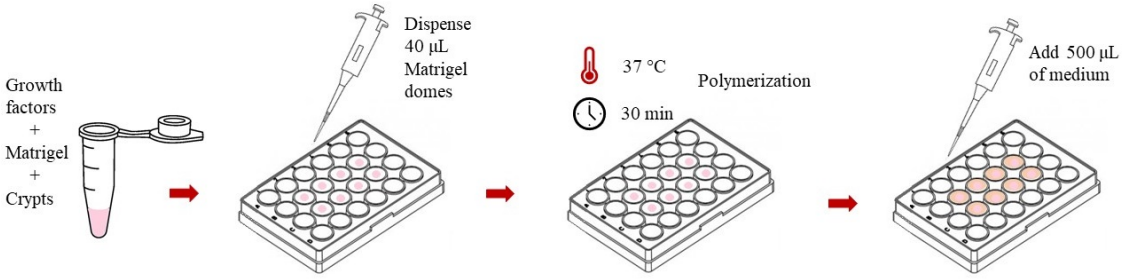

Figure 5.3: Schematic protocol of organoid culture.

Figure 5.4 demonstrates the progressive development of intestinal organoids over 3 days after passaging (day 0). After isolation and embedding in supplemented Matrigel, organoid-derived crypts adopted an enclosed circular structure (Figure 5.4a). After one day, organoids increased in size and a lumen lined by epithelial cells was formed (Figure 5.4b). On the second day, the circular structures started displaying small protrusions, or buds (Figure 5.4c), that consisted of newly-formed crypts. On the following days, organoids kept enlarging and the number of budding events per organoid also increased (Figure 5.4d). Over the days, the organoid lumen accumulated apoptotic cells as a consequence of epithelial shedding and presented a progressively denser and darker center. During passaging, organoids were dissociated into single crypts and the process was repeated. Organoids were passaged every 3-7 days and maintained for several weeks. Frequent passaging of organoids is necessary because nutrient diffusion to cells is limited by the size of the organoid. Previous evidence shows that intestinal organoids maintain a similar expression profile to freshly isolated crypts and display no induction of stress-related genes for at least 8 months of culture [84].

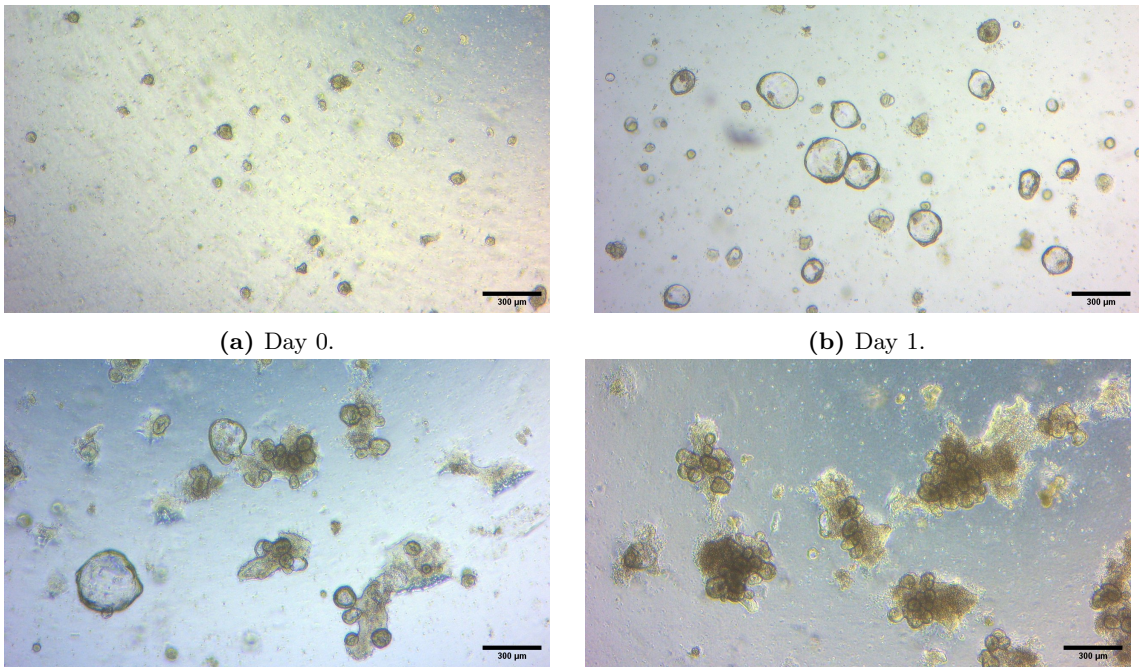

(a) Day 0. **(b)** Day 1.

(c) Day 2. **(d)** Day 3.

Figure 5.4: Intestinal organoid growth in a 24-well plate over 3 days after passaging. Scale bar: 300 µm.

5.3 Optimization of time-lapse microscopy experiments

An initial experiment was conducted to confirm that organoid development could be monitored using the Leica DMI600 Timelapse microscope, as well as to define optimal Matrigel dome volumes and time points for image acquisition. In this experiment, domes of 10, 20, 30, 40 µL of organoids embedded in Matrigel were plated in a 35 mm diameter circular plate. The protocol was the same as for normal passaging in 24-well plates. 3-5 crypts were seeded in each dome. After polymerization, 2 mL of intestinal organoid medium were added to the culture dish. Phase contrast and fluorescence images were acquired every 4 hours for 4 days.

Figure 5.5 displays the images collected in this experiment. Visualization of organoids was possible in the four conditions and dome volume did not seem to affect organoid growth. Additionally, it was possible to monitor EGFP expression by *Lgr5*$^{+}$ cells. As expected, green fluorescence signal is detected primarily in buds which are the analogues to intestinal crypts, where ISCs reside. Green fluorescence in the lumen, most evidently present in the 30 µL condition, is caused by auto-fluorescence of apoptotic cells. This experiment further confirmed that not all organoids or crypts in the same organoid express EGFP due to the variegated expression problem in this mouse model. Time-lapse videos of organoid growth with frames for every time point are available in https://tinyurl.com/intestinalorganoids.

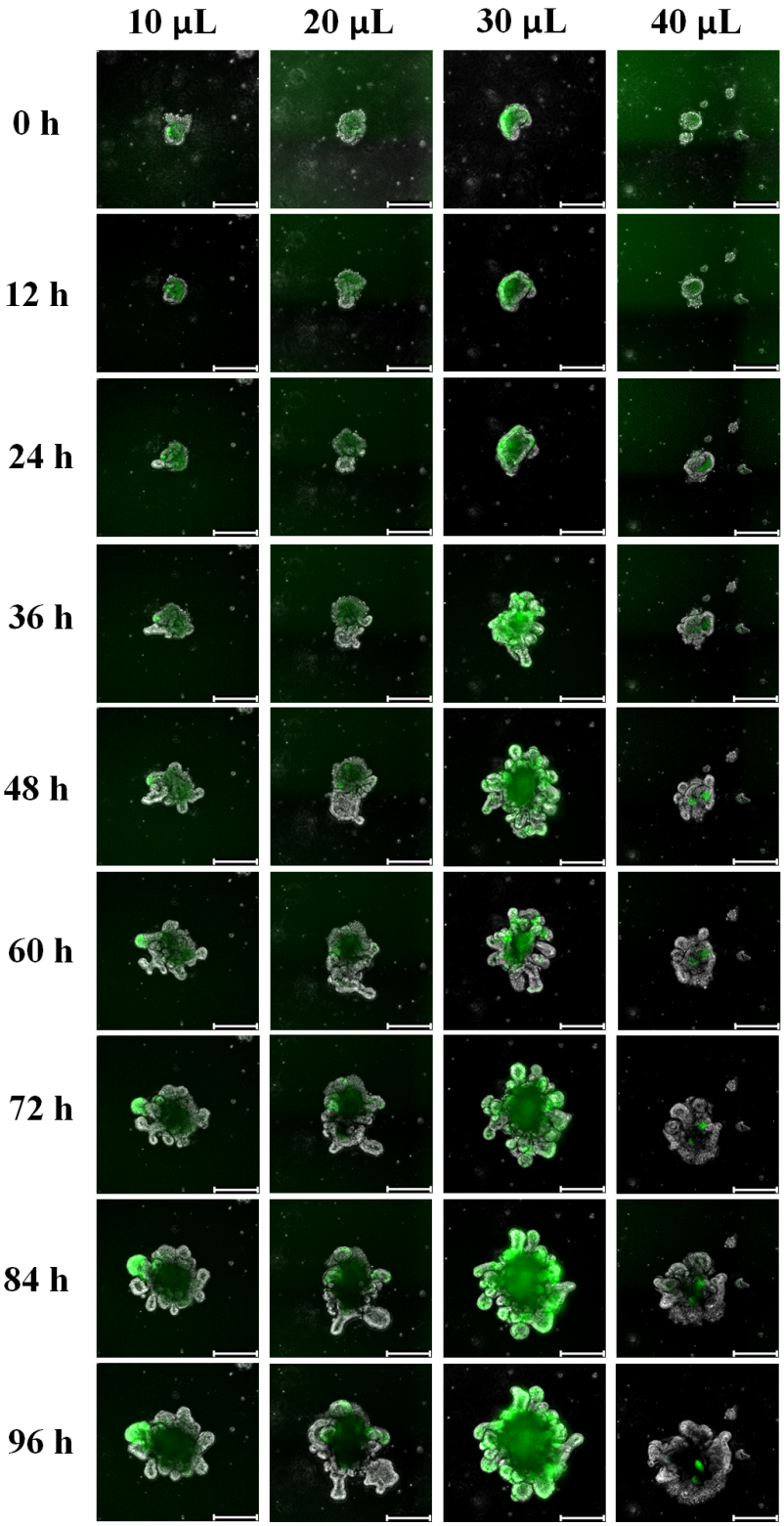

Figure 5.5: Organoid growth and EGFP expression imaged by time-lapse microscopy. Each column corresponds to a different condition: 10, 20, 30 or 40 µL dome volume. Each line represents one time-point: 0 h, 12 h, 24 h, 36 h, 48 h, 60 h, 72 h, 84 h, 96 h. Scale bar: 250 µm.

5.4 Establishment of intestinal organoids from single ISCs

Intestinal organoids can also be generated from single ISCs, marked by *Lgr5* expression [84]. Organoid-derived intestinal crypts were dissociated into single cells that were sorted by FACS. FACS is a flow cytometry-based technique in which cells are sorted based on the expression of selected markers. Antibodies coupled with fluorescent molecules bind to the protein of interest, staining the cell with a fluorescence signal. FACS sorts cells by analysing light scattering and fluorescence information that result from the size and specific marker expression of the cell, respectively.

Cells were incubated with anti-LGR5 and anti-CD24 antibodies. Anti-LGR5 antibody is coupled to a fluorescein isothiocyanate (FITC-A) fluorophore and anti-CD24 is coupled to a phycoerythrin (PE-A) fluorophore. FITC-A has excitation and emission peak wavelengths at 495 nm and 519 nm, respectively, which means its emission is maximized in the green region of the spectrum [106]. The excitation peak wavelength of PE-A is at 565 nm, while maximum emission occurs at 575 nm, corresponding to an orange-yellow color [14]. Anti-LGR5 antibody stained ISCs, while anti-CD24 marked the Paneth cell population [83].

Figure 5.6 displays the results extracted from FACS. Forward scatter (FSC) and side scatter (SSC) information were used to gate the cell population of interest (Figure 5.6a). Forward scattering increases with cell size whereas side scattering depends on the granularity or complexity of the cell. Therefore this step is useful for excluding debris, characterized by very low FSC or low FSC and medium to high SSC. However, optimal gating for cell size and complexity varies between distinct cell samples. The forward scatter area vs. forward scatter height plot was used to exclude cell clusters, like doublets, that normally have larger area but similar height to individual cells (Figure 5.6b).

Figure 5.6c shows a LGR5 FITC-A vs. CD24 PE-A density plot, where two populations were defined for sorting. P3 is the $LGR5^{+}/CD24^{+}$ population and P4 is the population that expresses LGR5 but not CD24 ($LGR5^{+}/CD24^{-}$). Although $LGR5^{+}/CD24^{-}$ is a purer population of ISCs, $LGR5^{+}/CD24^{+}$ cells were also collected because evidence shows that CD24 is expressed by a distinct population of ISCs, the $Hopx^{+}$ facultative ISCs [37]. Besides, P3 population may include doublets of Paneth cells and ISCs. Therefore, by collecting the two populations, the number of ISCs is increased as well as the possible number of organoids that can be generated.

1978 cells were sorted in P3 and 714 cells were sorted in P4. Cell count for each population and their relative and absolute percentages can be consulted in (Figure 5.6d). Given the low number of cells, the two cell suspensions were mixed together.

Matrigel mix for single cell seeding and culture medium were supplemented with WNT-conditioned medium. WNT is an additional activator of the Wnt signalling pathway which is essential for ISCs maintenance [32]. Adding this factor to the medium already supplemented with EGF, RSPO1 and NOG, provides a more faithful recapitulation of the stem cell niche to single ISCs.

No evidence of organoid growth was detected for 14 days after single cell embedding in Matrigel.

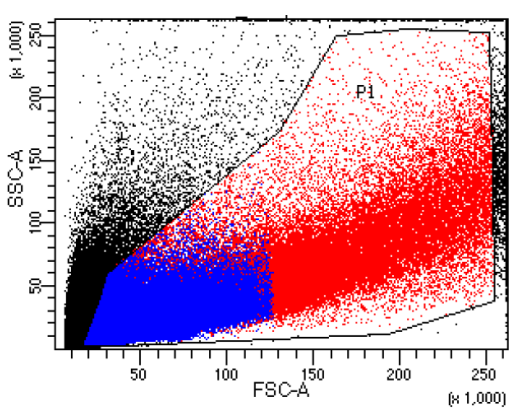

(a)

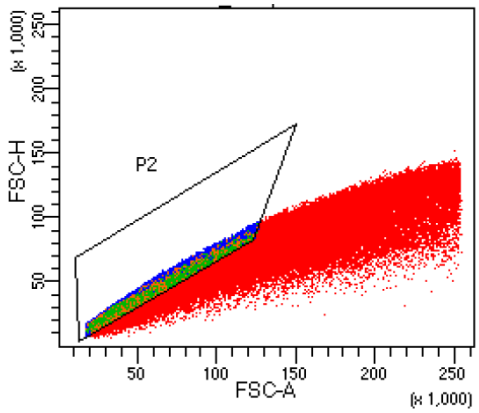

(b)

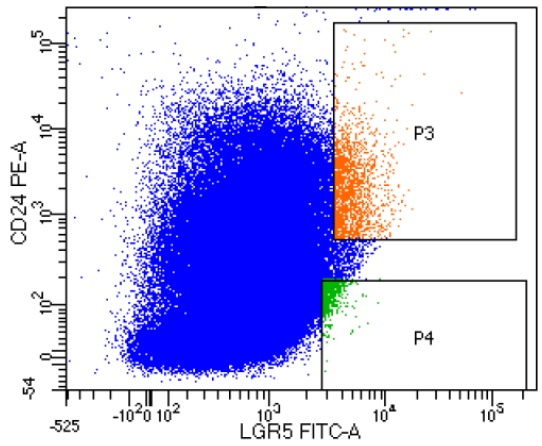

(c)

Tube: Mix

Population	#Events	%Parent	%Total
All Events	516,675	####	100.0
P1	221,117	42.8	42.8
P2	162,120	73.3	31.4
P3	1,978	1.2	0.4
P4	714	0.4	0.1

(d)

Figure 5.6: FACS results. (a) Forward scattering vs. Side scattering plot. (b) Forward scattering area vs. forward scattering height plot. (c) Lgr5 vs. CD24 density plot of organoid-derived single cells. Two distinct cell populations were collected: $LGR5^{+}/CD24^{+}$ (P3) and $LGR5^{+}/CD24^{-}$ (P4). (d) Identification of populations P1, P2, P3, P4 and respective cell count.

5.5 Microfluidic culture of intestinal organoids

The main goal of this work was to investigate if intestinal organoid growth and development would be enhanced by continuous perfusion of medium, as opposed to the static setup of the 24-well-plate culture. For that, we sought to develop microfluidic devices that would incorporate fluid flow into intestinal organoid culture.

For each design, there was an attempt to conduct two types of experiments: static and dynamic. Static experiments consisted of plating the Matrigel mix with organoids in the microfluidic device, adding medium, covering the device with the appropriate lids and maintaining the device in a 37ºC, 5% CO_2 incubator. Dynamic experiments required the perfusion equipment to be connected to the device, so that intestinal organoid medium could be continuously perfused through the system. Therefore, static experiments served as a control for dynamic experiments. The goal was to compare the behavior of the organoid culture in both conditions and to draw conclusions regarding the impact of continuous medium flow in these cultures. When appropriate, results were also compared to intestinal organoid growth in 24-well plates.

5.5.1 Flow rate selection for dynamic experiments

To select an adequate flow rate, a literature search was conducted. In most of the other intestine-on-chip systems reported, single cells are seeded in a two-dimensional layer as opposed to a three-dimensional matrix. That approach aims to simulate luminal flow circulation, while the present system recapitulates extraluminal circulation. Therefore, the selection of a flow rate cannot be based on these reports. Besides, the matrices used are usually a mix of Matrigel with collagen type I and not simply Matrigel, which may result in an alteration of mechanical properties and consequently impact the behavior of the matrix in fluidic conditions. Although some reports focused on recreating the endothelial compartment and simulating extraluminal circulation [49, 48, 45, 69], in those models, the endothelial compartment was separated from the epithelial cells by a matrix-coated membrane and a layer of endothelial cells, a design that is also not comparable to the present system.

Sidar *et al.* developed a method for long-term intra and extraluminal perfusion of human-derived intestinal organoids and estimated the extraluminal flow rate based on the human cardiac output and the percentage of blood that irrigates the gastrointestinal tract [93]. Their conclusion was that optimal flow rates would fall between 20-50 µL h^{-1}. On the other hand, the present intestine-on-chip model uses mouse-derived intestinal organoids. Applying the same rationale to this model, it is possible to calculate blood supply to the mouse intestine. Cardiac output (CO) in mice varies between 10-20 mL min^{-1} [25, 59, 98], and the percentage of CO sent to the small intestine is 13.5% [97] which means the small intestine receives between 1.35 − 2.7 mL min^{-1} of blood flow. Given the average weight of a mouse small intestine, 1932 mg [72], the blood flow per milligram of intestinal tissue is between 41.9 µL h^{-1} mg^{-1} − 83.9 µL h^{-1} mg^{-1}. Considering each 20 µL Matrigel dome weighs approximately 13.5 mg, the blood flow applied should be between 565.6 µL h^{-1} − 1 132.65 µL h^{-1}. These values are extremely high and incompatible with the perfusion equipment available. The reason behind the discrepancy between the optimal flow rate in human-derived and mouse-derived models is a consequence of the high heart rate of mice, that results in a difference in cardiac output per body weight of 9 times [25].

Since it was not possible to establish a direct comparison to any of the previously reported intestine-on-chip models, flow rates used in this dissertation ranged from 0.73 to 100 µL h^{-1}.

5.5.2 Design A

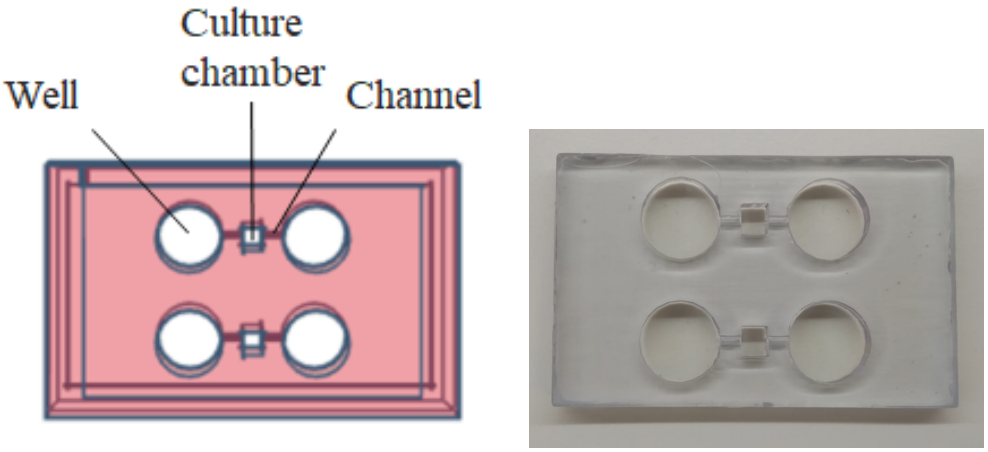

(a) **(b)**

Figure 5.7: Microfluidic device A. (a) The components of microfluidic device A. (b) Photograph of microfluidic device A.

The initial design (Design A) developed in collaboration with Biofabics, consisted of a central rectangular chamber connected bilaterally to two wells by a channel (Figure 5.7). A plastic molding line was inserted through the channel. Organoids were embedded in supplemented Matrigel and this mix was dispensed into the central chamber (culture chamber) and left to polymerize. After polymerization, the tube was removed, creating a channel through the Matrigel dome where intestinal organoid medium could flow (Figures 5.8). A similar system has been used before for culture of bioprinted neural progenitor cells and breast cancer spheroids by Campos *et al.* [17].

First, the volume of Matrigel mix to be dispensed on the culture chamber was optimized. Volumes of 30, 60 and 70 µL were tested. 70 µL was selected as the optimal volume since 30 µL were not enough to fully cover the molding line and 60 µL was just enough. It was visible that, after letting Matrigel polymerize for 30 minutes, the matrix would collapse when the molding line was pulled out of the device. In order to enhance matrix resistance and stiffness, Matrigel concentration was increased from 60% to 90%, and polymerization time was extended from 30 to 60 minutes. In these conditions, no collapse was observed, and medium successfully flowed between wells through the culture chamber, confirming the presence of a channel inside the matrix. Additionally, inverted microscope imaging enabled the visualization of the channel across the matrix (Figure 5.9). The design of the microfluidic device had to be modified so that its dimensions were compatible with the Time-lapse microscope.

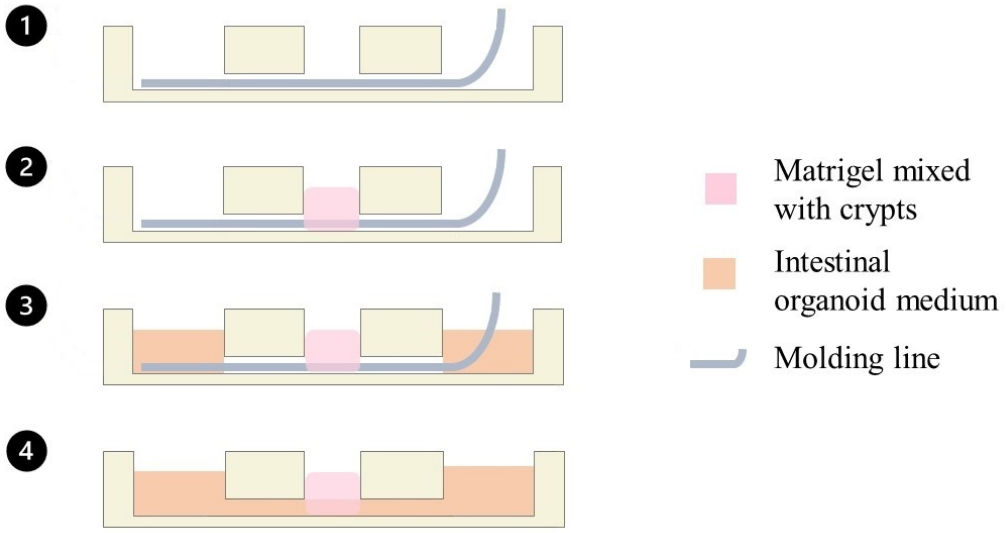

Figure 5.8: Schematic summary of the protocol for forming a channel inside a Matrigel cube. Longitudinal section of the microfluidic device. 1 - A plastic molding line is inserted through the channel in the device; 2 - Matrigel mix containing intestinal crypts and growth factors is dispensed into the culture chamber on top of the molding line; 3 - After 30 minutes, intestinal organoid medium is dispensed on the empty wells; 4 - The molding line is pulled out, creating a channel inside the matrix.

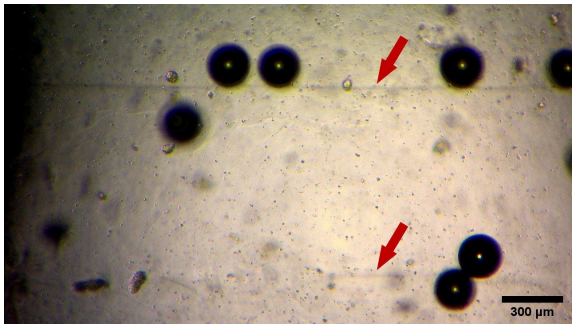

Figure 5.9: Inverted microscope image of the channel inside the matrix, evident by the two parallel horizontal lines indicated by red arrows. Scale bar: 300 µm.

5.5.3 Design B

Microfluidic device B had a similar design to microfluidic device A and its dimensions were adapted to the size of a microscope slide (25 mm x 75 mm). Each device B comprised four culture chambers, each connected to two individual wells (Figure 5.10). This design also aimed to increase the yield of each experiment, by condensing more culture chambers per device. Additionally, two types of lids were developed for this device to minimize medium loss by evaporation and avoid external contamination. Rectangular lids were used to cover adjacent wells, while culture chambers were covered by a square lid with a transparent circular center, to enable microscope imaging

(Figure 5.10b). Parameters such as polymerization time of 1 hour, 90 % Matrigel concentration and 70 µl Matrigel dome volume were maintained in the experiments with device B. Figure 5.11 demonstrates medium flow through the intra-matrix channel inside the central chamber.

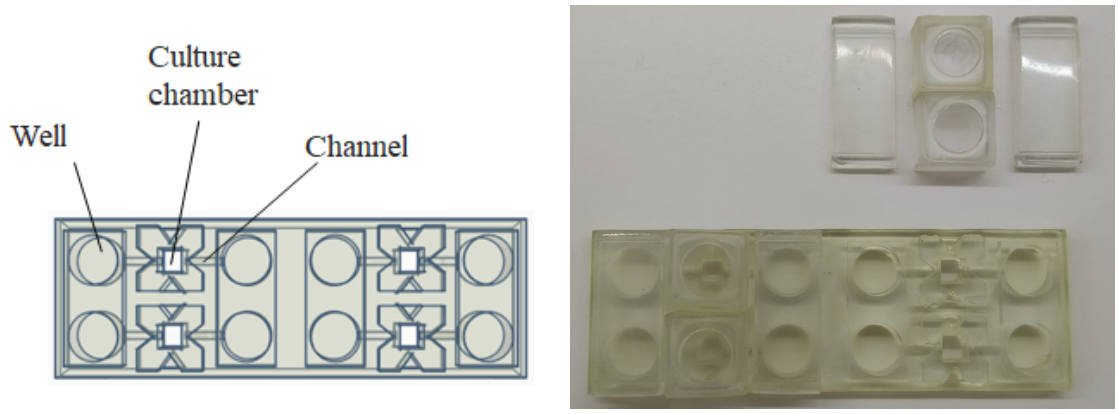

(a) **(b)**

Figure 5.10: Microfluidic device B. (a) Components of microfluidic device B. (b) Photograph of microfluidic device B with (left) and without (right) lids.

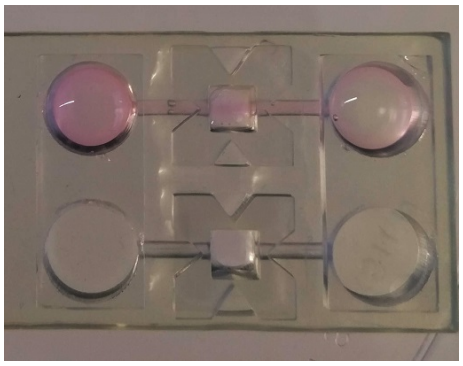

Figure 5.11: Medium flowing through a intra-matrix channel, evidenced by a line of a darker shade of pink inside the culture chamber.

A time-lapse imaging experiment was conducted to monitor organoid development in device B, without fluid flow (static control). 150 µL of intestinal organoid medium were added to each well. Medium evaporated after just 24 hours, causing complete dehydration of Matrigel. In the second attempt to this experiment, 35 mm dishes with distilled water-soaked pieces of paper were put inside the microscope chamber to provide humidity and delay medium evaporation. Over time, organoids appeared to move from the initially defined focal point in all three directions (x, y and z) which was not observed in the previous time-lapse experiment (Section 5.3). This observation suggested that Matrigel was progressively collapsing inside the culture chamber. The presence of a channel inside the gel was hypothesized to decrease gel integrity and resistance, accelerating its degradation. Additionally, organoids lost viability after 48 hours due to a problem in passaging.

Next, the same experiment was repeated in a conventional incubator and the culture was observed in an inverted microscope daily. In contrast to standard culture in the 24-well plate,

where organoids start acquiring buds after 2 days, organoids remained circular until day 4, when they started to lose viability as demonstrated by a loss of structure, decrease in size and a necrotic appearance (Figure 5.12). This result suggests that under static conditions, culture of organoids in device B does not support a normal development of intestinal organoids, compromising their viability.

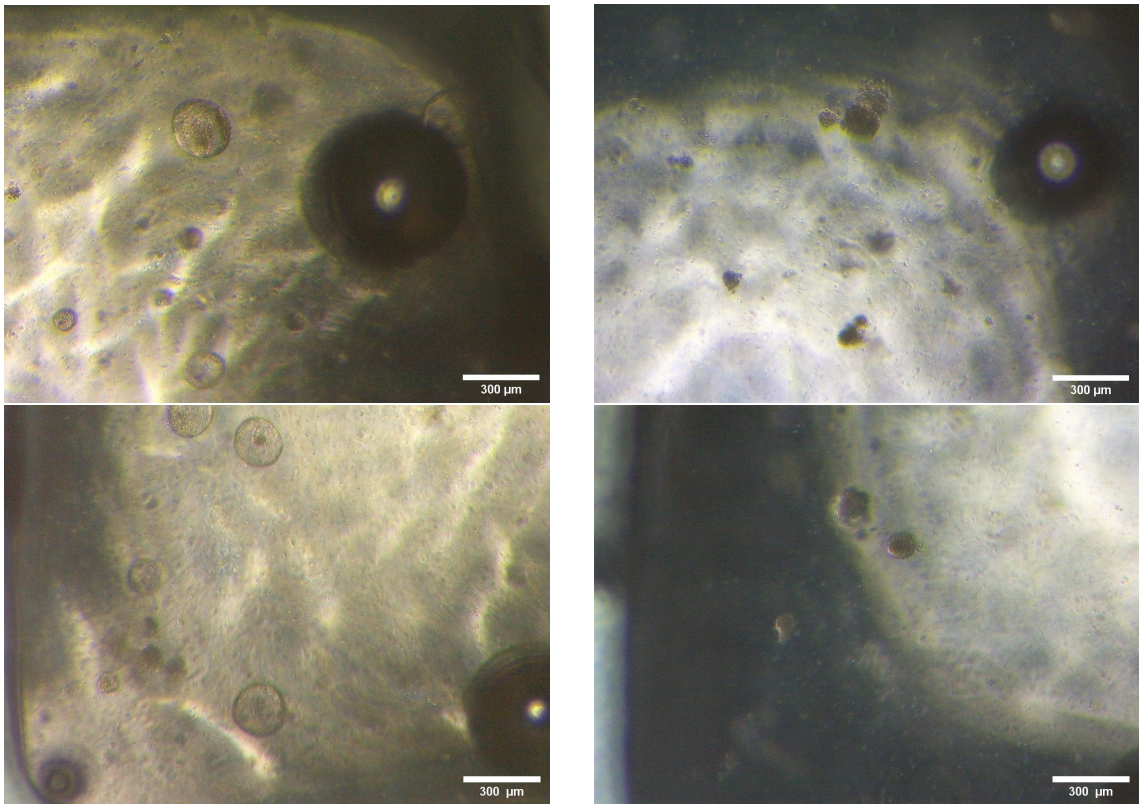

(a) Day 3. **(b)** Day 4.

Figure 5.12: Intestinal organoid growth in static conditions in microfluidic device B at days 3 and 4 after seeding. Each image is representative of 1 culture chamber. Scale bar: 300 µm.

Parallel experiments with fluid perfusion were performed. Lateral rectangular lids were replaced by lids with inlet/outlet pieces that were inserted in the lateral wells. The shape of this lid enables the attachment of silicone tubes that supply intestinal organoid medium (Figure 5.13). Figure 5.14 displays microfluidic device B (without central lid) coupled to the tubing system.

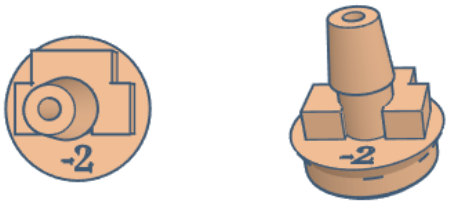

Figure 5.13: Lids with inlet pieces.

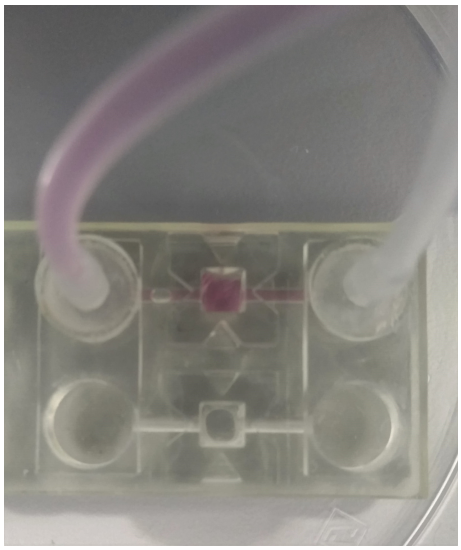

Figure 5.14: Microfluidic device B in a fluidic experiment. Inlet/outlet lids were inserted in lateral wells to enable unidirectional fluid flow of medium from left to right.

For an initial experiment, a flow rate of 100 µL h^{-1} was chosen. After approximately 90 minutes of continuous fluid perfusion, medium was overflowing through the central chamber and Matrigel dome was not intact. In following experiments, lower flow rates were employed (10 µL h^{-1} and 0.73 µL h^{-1}) and the same outcome was verified. At this point, it was impossible to further increase Matrigel concentration to improve matrix resistance to fluid flow or to decrease the flow rate, since 0.73 µL h^{-1} was the minimum limit of the perfusion pump.

The formation of bubbles after the attachment of the tubing equipment to the device was observed. Bubbles travelled from well to well, through the matrix, compressing the matrix against the chamber walls, as depicted in Figure 5.15.

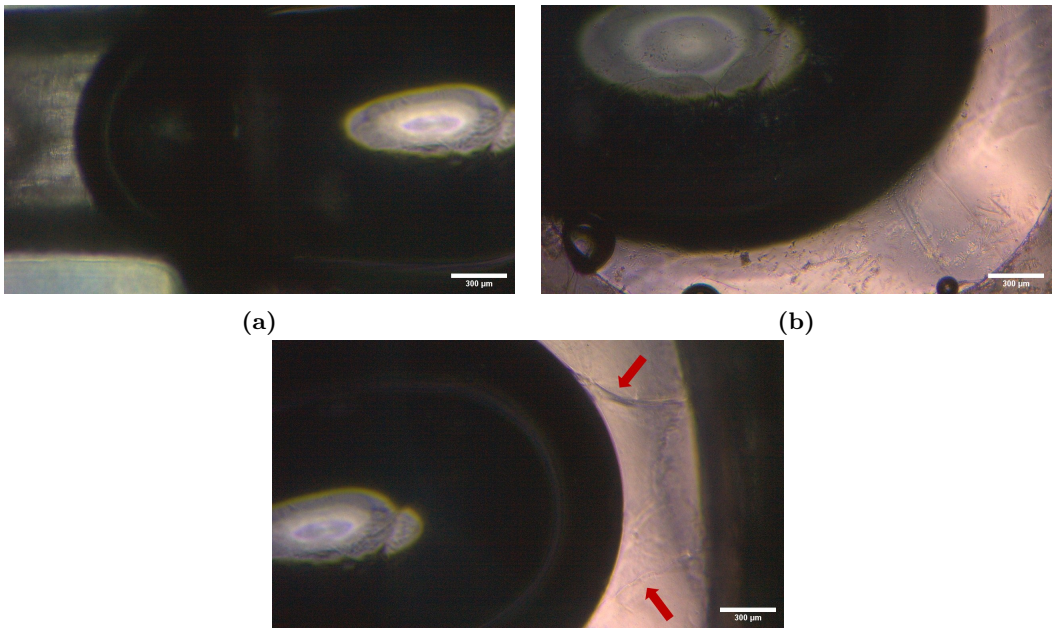

Figure 5.15: Formation of bubbles inside the microfluidic device. (a) A bubble formed in the lateral compartment travels through the channel of the device to the culture chamber. (b) The bubble travels inside the channel inside the matrix, pushing the matrix against the chamber walls. (c) The bubble exerts a high amount of pressure inside the channel, causing it to stretch. Red arrows point to the stretching of the channel around the bubble. Scale bar: 300 µm.

In a new experiment, the tubing was assembled and connected to only one of the wells in the device, leaving the other one open to pull out the molding line after polymerization (Figure 5.16a). In those conditions, the molding line had to be removed before filling the wells with medium. In the absence of medium to fill the channel while the molding line was being pulled out, the structure of the channel was affected (Figure 5.16b). In this condition, unidirectional fluid flow through the device was impossible since there was only one tube attached to the device. In this experiment we used bidirectional flow, which means the pump alternated between infusion and withdrawal of medium every hour. Due to the configuration of the system, there would be no renovation of growth factors during the experiment since the fraction of medium entering and leaving the system would always be the same. Therefore, the flow rate employed in this experiment was increased to 100 µl h^{-1}. Again, Matrigel collapsed after 24 hours of bidirectional perfusion (Figure 5.16c).

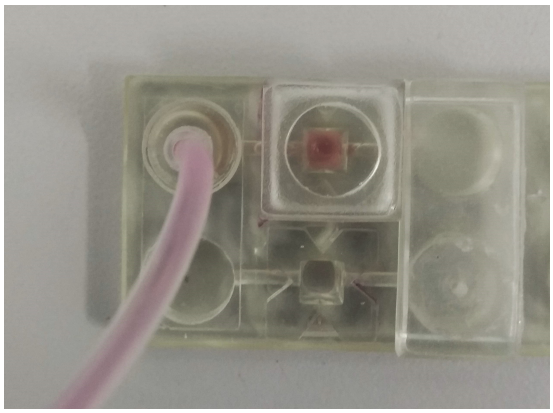

(a)

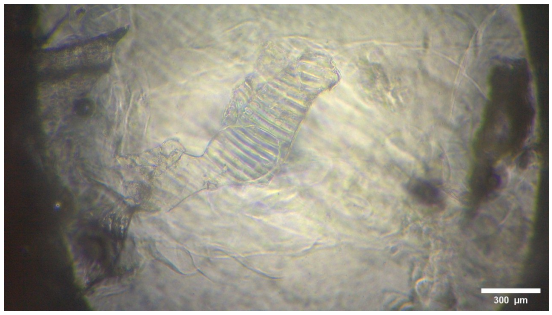

(b)

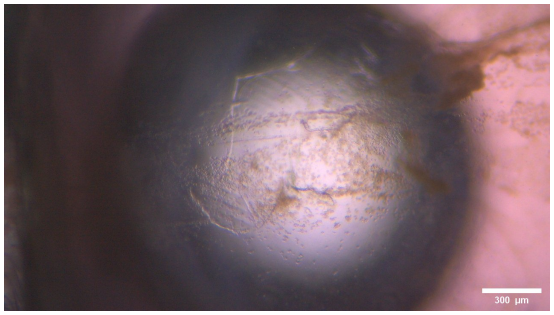

(c)

Figure 5.16: Bidirectional flow experiment. (a) Photograph of microfluidic device B connected to a tube for medium injection and with a lid covering the other well. (b) Inverted microscope image of the channel inside the Matrigel matrix showing partial collapse. Scale bar: 300 µm. (c) After 24 hours of continuous bidirectional perfusion, Matrigel structure was completely collapsed. Scale bar: 300 µm.

Considering the results of the static and dynamic experiences, we concluded that this microfluidic approach was not compatible with the mechanical properties of Matrigel or with intestinal organoid culture and therefore was not a suitable strategy for an organoid-based intestine-on-chip model.

5.5.4 Design C

The design of the microfluidic device was altered to incorporate a different strategy for Matrigel seeding. Microfluidic device C consisted of a central circular chamber with a diameter of 8 mm connected to two lateral wells (Figure 5.17). Central lids and inlet/outlet pieces were redesigned to accommodate a PDMS ring. The presence of a PDMS ring was convenient to seal the chambers and prevent leakage and overflowing of medium in the culture chamber. In the culture chamber, a 20 µL Matrigel dome was seeded. In these experiments, Matrigel concentration was 60%, NOG- and RSPO1-conditioned media concentrations were 10%. Polymerization time was set again to 30 minutes.

The main advantage of using a Matrigel dome is the full immersion of the gel in organoid medium. Additionally, this method is more comparable to the standard culture in 24-well plates, which is helpful to reduce the number of variables in the analysis of the system. The

characteristics of the microfluidic system enable a continuous perfusion of medium to the Matrigel dome, simulating the nutrient supply to the intestine conducted by blood circulation.

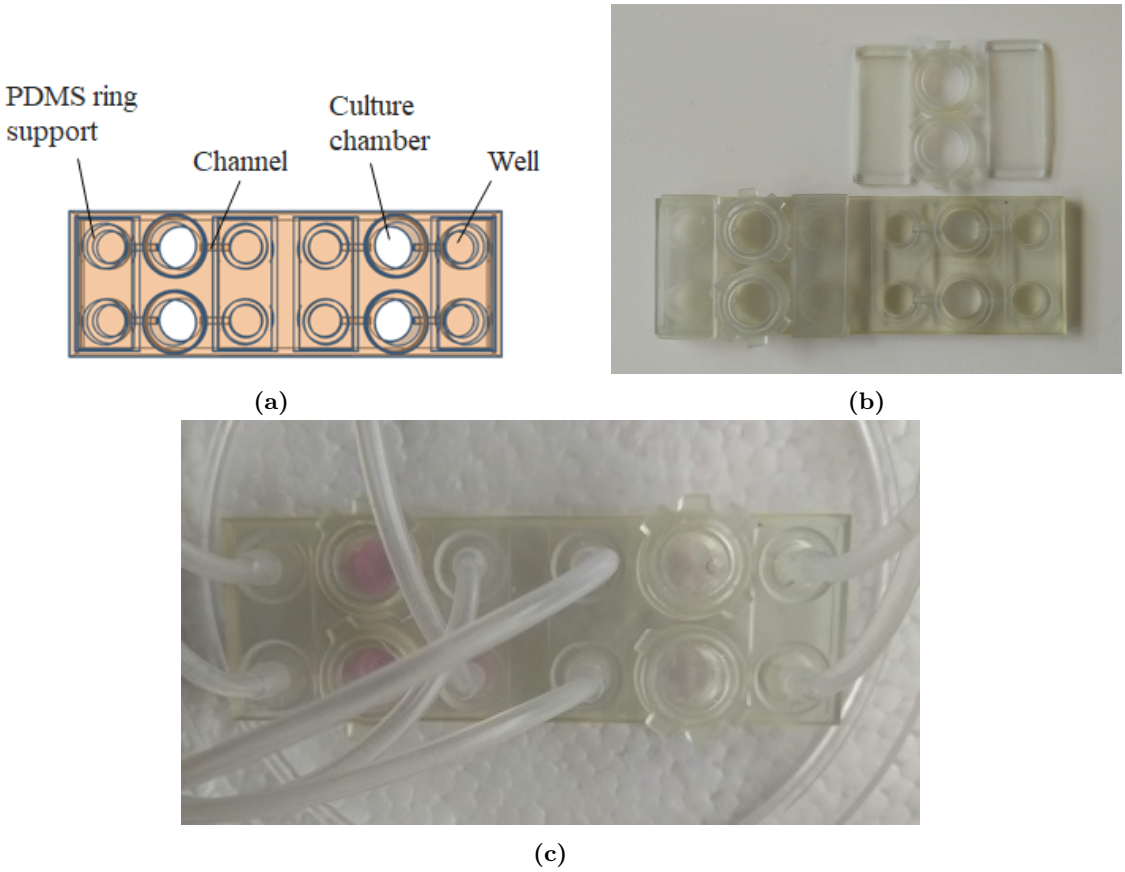

Figure 5.17: Microfluidic device C. (a) Components of microfluidic device C. (b) Photograph of microfluidic device C with (left) and without (right) lids. (c) Microfluidic device B during a dynamic experiment. Inlet/outlet lids were inserted in lateral wells to enable unidirectional fluid flow.

Microfluidic device C was used to perform dynamic experiments at different unidirectional flow rates (10, 20 and 30 µL h^{-1}) and Matrigel resistance was assessed. After 4 days, none of the tested conditions caused Matrigel to collapse. Therefore, this design is more compatible with Matrigel's mechanical properties, preserving the matrix structure for longer than microfluidic device B, which is essential for long-term intestinal organoid culture. On the other hand, similarly to microfluidic device B, this device was very susceptible to medium leakage through inlet/outlet lids, as well as from the central lid. Leakage is a problem since it causes an alteration of the volume of culture medium inside the microfluidic system, prompting two similar culture chambers to have different volumes of culture medium and different quantities of growth factors. Consequently, the reliability and reproducibility of the results might be affected. Medium leakage is also of concern when performing dynamic experiments inside the Time-lapse microscope because of the electrical circuits that surround the stage.

Although this design is suitable for static experiments, where it is beneficial that the lids can be easily removed to replace medium every 2 days and lateral medium reservoirs help to

maintain a sufficient amount of medium to support organoid growth, it is too complex for dynamic experiments.

5.5.5 Design D

To minimize leakage points, inlet and outlet pieces were integrated in the base of the device to circumvent the use of lids with incorporated inlet/outlet pieces. Consequently, medium leakage was reduced and only occurred from the culture chamber lid. The solution was to use a sealing material, in this case, nail polish, to block leakage points.

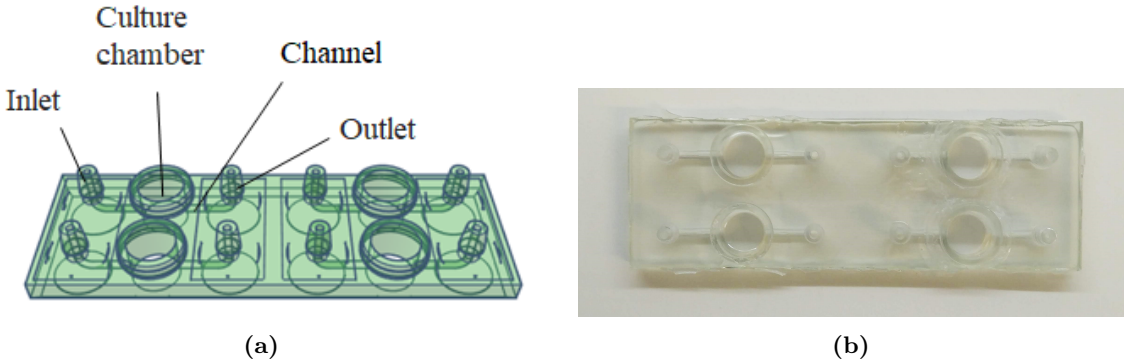

(a) **(b)**

Figure 5.18: Microfluidic device D. (a) Components of microfluidic device D. (b) Photograph of microfluidic device D.

Microfluidic device D was only used for dynamic experiments that were compared to static experiments performed in device C.

5.5.6 Design E

Microfluidic device E was also designed in collaboration with Biofabics for a different strategy to promote organoid development. In this device, a porous cylindrical tube would be coated with intestinal organoids embedded in Matrigel. Then, the coated porous membrane would be sandwiched between two chambers, joined together by magnets. The tube would be immersed in intestinal organoid medium perfused unidirectionally through the inlet and outlet pieces incorporated in the culture chamber. Figure 5.19 displays the design and composition of microfluidic device E.

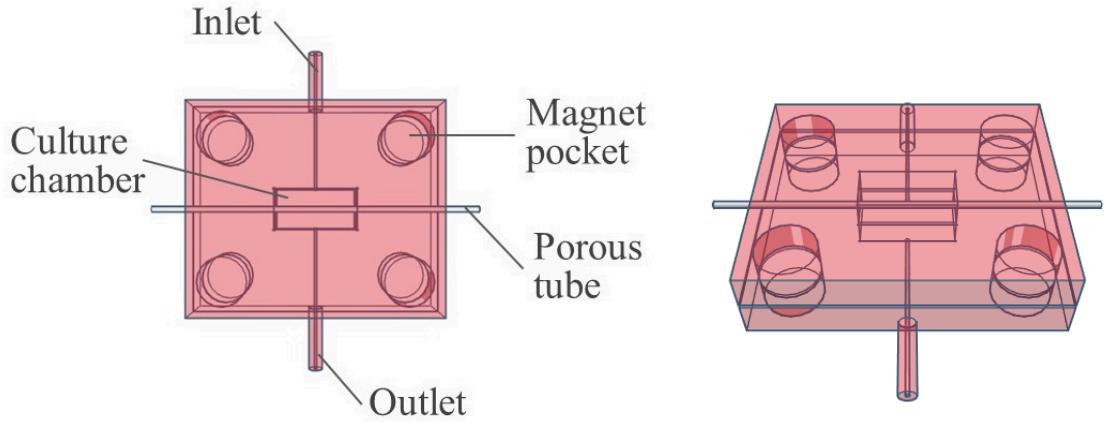

Figure 5.19: Microfluidic device E. (a) Components of microfluidic device E. (b) Perspective of microfluidic device E.

The aim of this design was to investigate if, by being coated on a cylindrical surface immersed in medium, intestinal organoids would rearrange and form tubular structures. This culture system could be an interesting tool in defining protocols for controlling and directing organoid growth into tubular form, improving the physiological resemblance of organoid models to the small intestine. Another advantage of this microfluidic design is the compatibility with co-cultures of different cell populations, such as endothelium or mesenchyme, that could be seeded on the walls of the microfluidic chamber.

This device was not implemented during the reported project due to time constraints.

5.6 Time-lapse monitoring of intestinal organoid growth in microfluidic conditions

Wild-type mouse-derived intestinal organoids were passaged and seeded in 20 µL Matrigel domes with a density of 60-70 organoids/20 µL. 5 domes were plated in a 24-well plate and maintained for four days according to the standard protocol described previously. Organoid growth was monitored by microscopy every 12 hours.

For the static control, four domes were plated in microfluidic device C, overlaid with 400 µL of intestinal organoid medium. The device was covered with the corresponding lids and a PDMS ring was included between the central lid and the culture chamber. The closed device was kept inside a 90 mm Petri dish with an open 35 mm dish with dH_2O to maintain humidity levels and delay medium evaporation. Medium was replaced every 2 days. Organoid growth was monitored by microscopy every 12 hours.

For the dynamic experiment, four domes were plated in microfluidic device D. Initially, 250 µL of intestinal organoid medium were dispensed on the culture chamber to maintain Matrigel hydration for the first hours of continuous fluid perfusion. The culture chambers were closed with the appropriate lids, containing a PDMS ring for isolation. The devices were set in the

time-lapse microscope stage (Figure 5.20c), while the perfusion pump with medium-filled syringes were kept outside the environmentally controlled chamber (Figure 5.20b). Injection tubes were passed through an opening in the chamber and discharge tubes drained medium to a falcon tube inside the chamber. Two 35 mm dishes and one 90 mm dish with dH_2O soaked paper towels were put inside the chamber to provide humidity. The spatial organization of the culture chambers was envisioned to minimize stage movement during acquisition and therefore the obstruction of the camera by the tubes. The flow rate employed was 30 µL h^{-1}. Brightfield images of all 4 Matrigel domes were acquired every two hours.

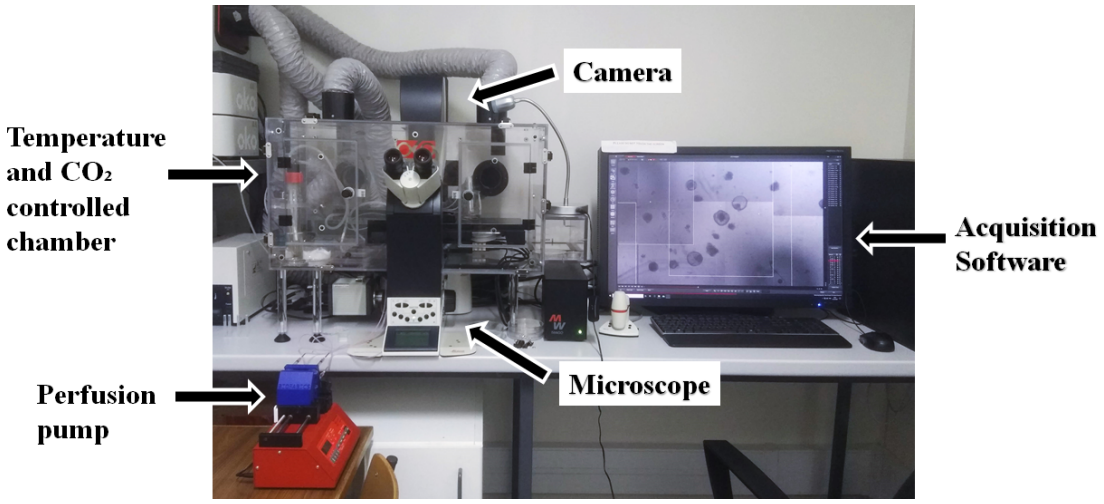

(a)

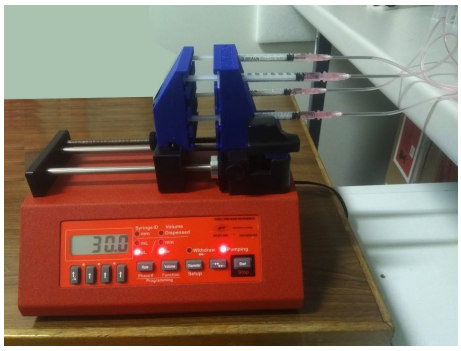

(b)

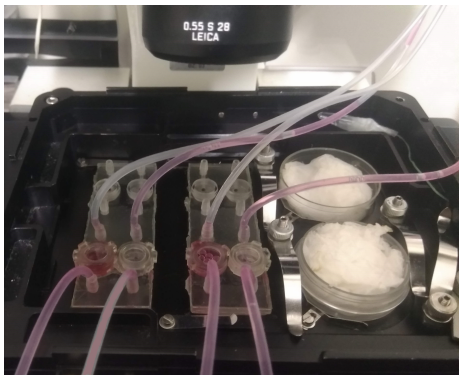

(c)

Figure 5.20: Dynamic experiment inside the Time-lapse microscope. (a) Experimental setup. (b) Perfusion pump injecting medium into the devices. (c) Four chambers were analysed in this experiment.

Figure 5.21 shows the brightfield images acquired every 12 hours during the dynamic experiment. Organoids grown in fluidic conditions increased in size for the first 24 hours of the experience, but budding events were rare, and organoids showed predominantly a circular morphology. From 36 hours up to the end of the experiment, organoids decreased in size, became cystic and acquired a darker appearance, consistent with the accumulation of apoptotic cells. These signs indicate that organoids lost viability after the first day of the experiment in dynamic conditions.

In comparison, intestinal organoids grown in the static control (Figure 5.22) adopted irregular shapes with evident budding starting at 24 hours. During the experiment, organoids increased in size and developed additional buds, as expected. Furthermore, organoids remained viable for the duration of the experiment. Thus, results suggest that the microfluidic device design supports intestinal organoid growth and maturation. However, the experimental parameters for dynamic experiments are not yet optimized given the loss of viability of intestinal organoids in that condition.

Comparing the results obtained in the static control to those of the 24-well plate is important to assess if the characteristics of the device, without fluid flow, influence organoid culture. By analysing the images acquired from the static control (Figure 5.22) in the device and the 24-well plate (Figure 5.23), at 60 hours of culture, it is evident that organoid morphology was different. Although organoids were viable in both conditions, their average diameter was lower in the device (265 ± 103 µm, n=22), in comparison to the organoids on the plate (336 ± 120 µm, n=28). Also, it is particularly noticeable the higher amount of apoptotic cells within the intestinal lumen of the organoids in the plate, especially in the central region of the wells, shown on the right side of Figure 5.23. That seems to be a consequence of an unintended higher seeding density of organoids on the plate, in comparison to the device, as observed in Figures 5.22 and 5.23.

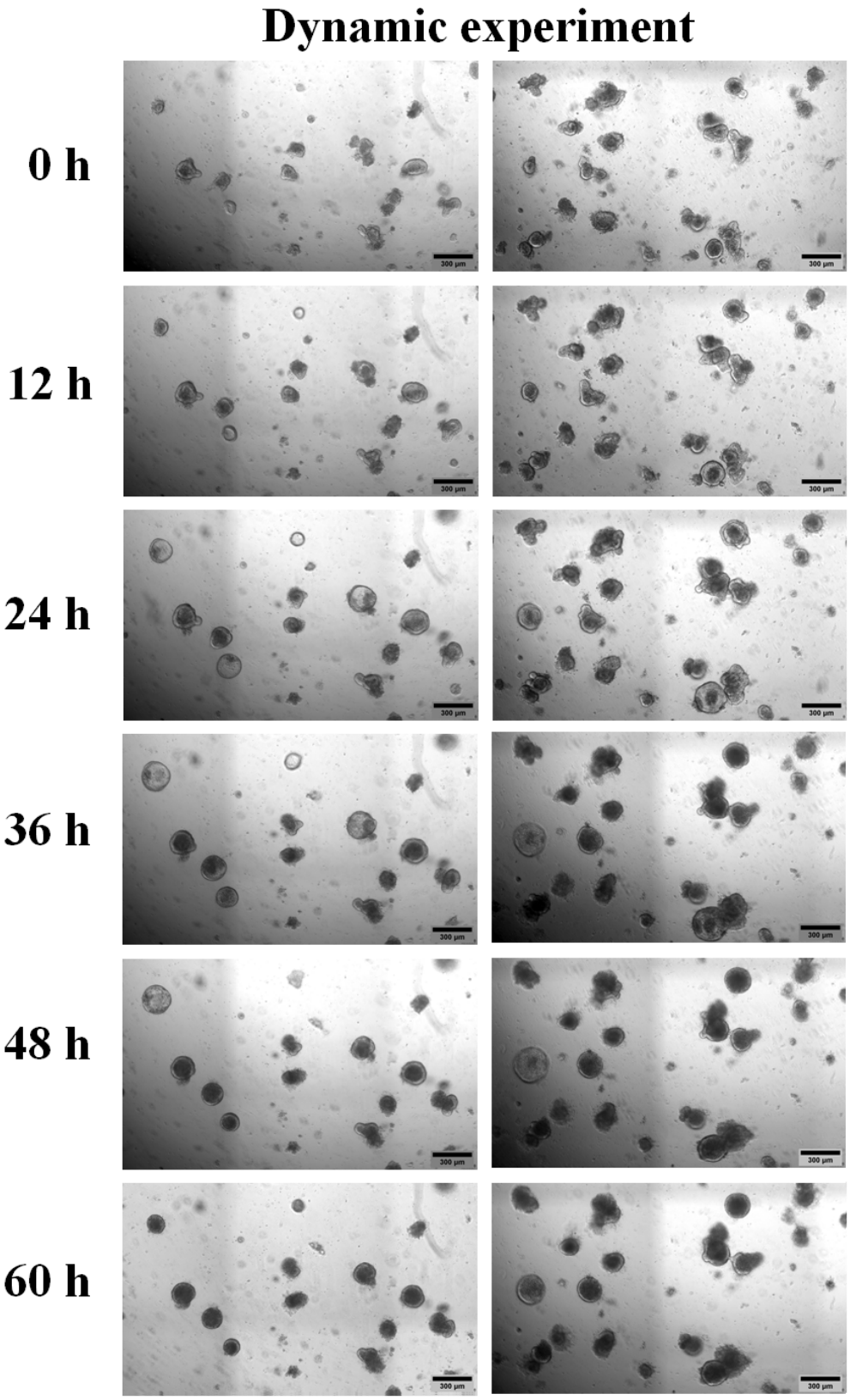

Figure 5.21: Intestinal organoid growth in dynamic conditions monitored by time-lapse microscopy over 60 hours. Two representative regions of the Matrigel domes seeded with organoids are displayed. Scale bar: 300 µm.

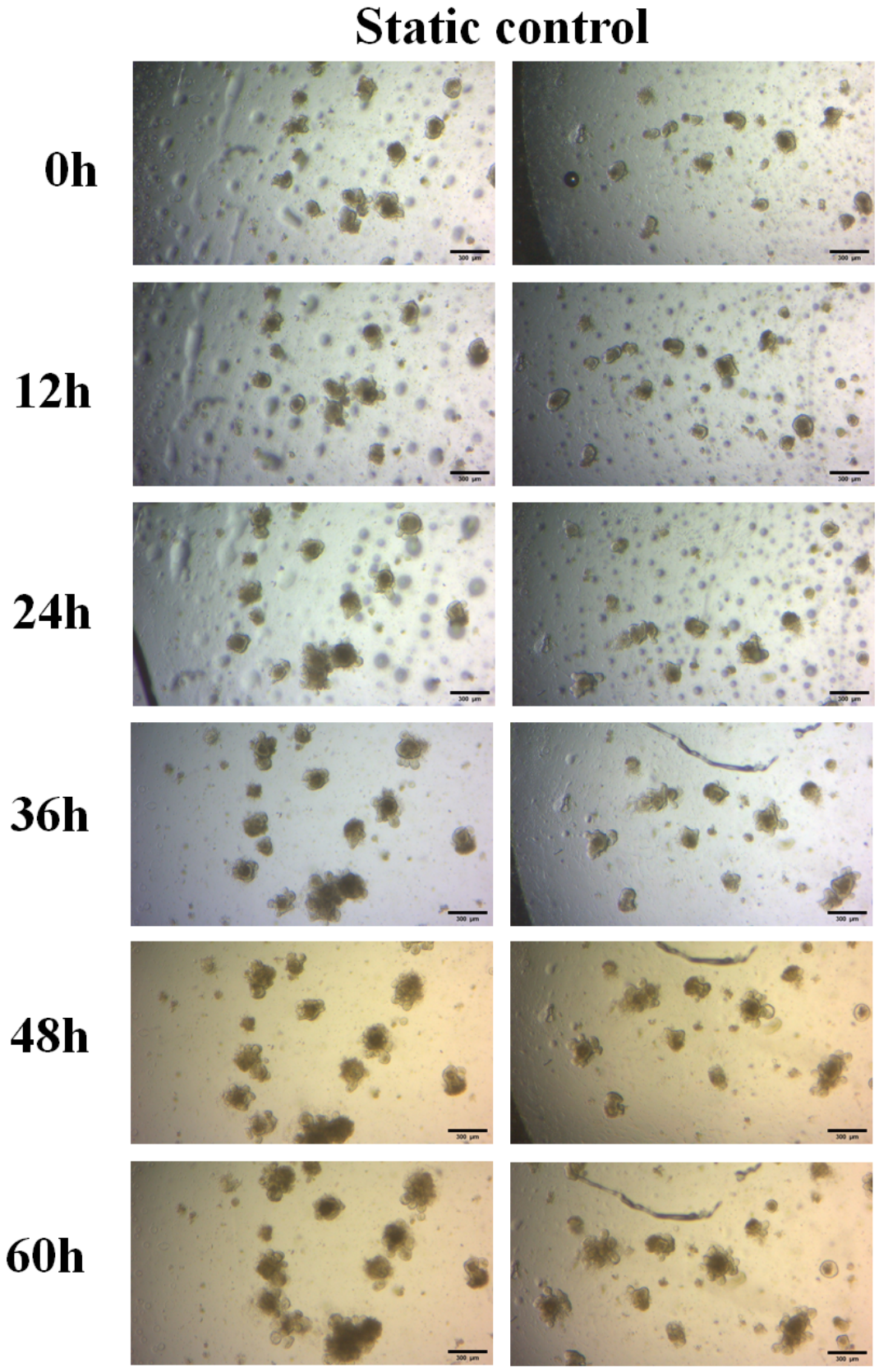

Figure 5.22: Intestinal organoid growth in static control. Images acquired in inverted microscope. Two representative regions of the culture in control conditions are displayed. Scale bar: 300 µm.

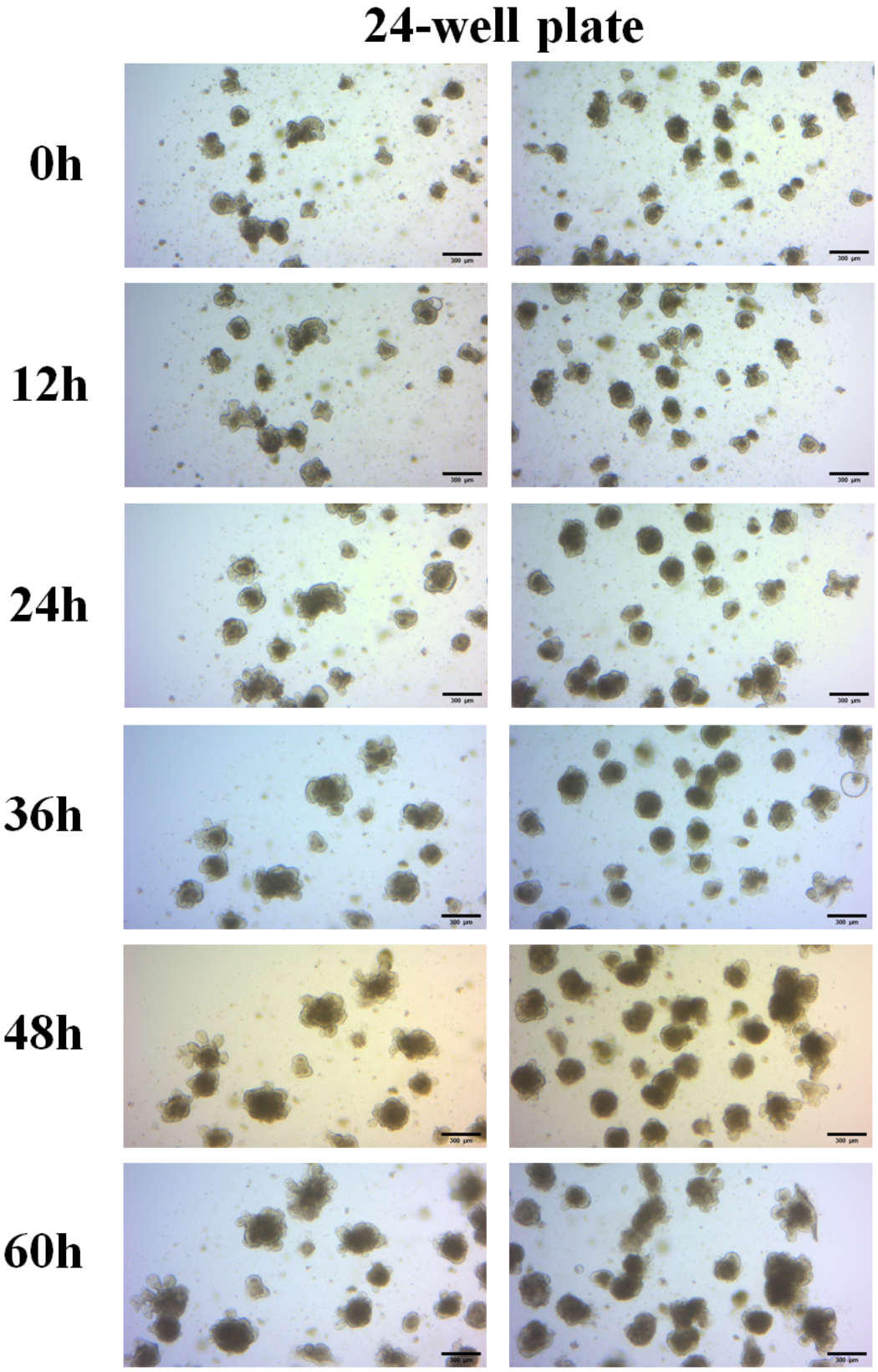

Figure 5.23: Intestinal organoid growth in the 24-well plate. Images acquired in inverted microscope. Two representative regions of the culture in standard conditions are displayed. Scale bar: 300 µm.

5.7 Real-time PCR analysis

A quantitative real-time PCR analysis was conducted to compare the expression profiles of organoids cultured in the 24-well plate according to standard protocol vs. organoids grown in device C in static condition, after 4 days. The expression of 3 genes was assessed: *Lgr5*, *Lyz1* and *Pcna*. *Lgr5* is the most established marker of ISCs [10]. *Lyz1* is a gene that encodes the protein lysozyme, specifically expressed in Paneth cells [83]. *Pcna* (proliferating cell nuclear antigen) is a gene that encodes for a co-factor of DNA polymerases, being essential in DNA replication. Thus, *Pcna* is only expressed by proliferating cells [71]. Figure 5.24 displays the results of this comparison.

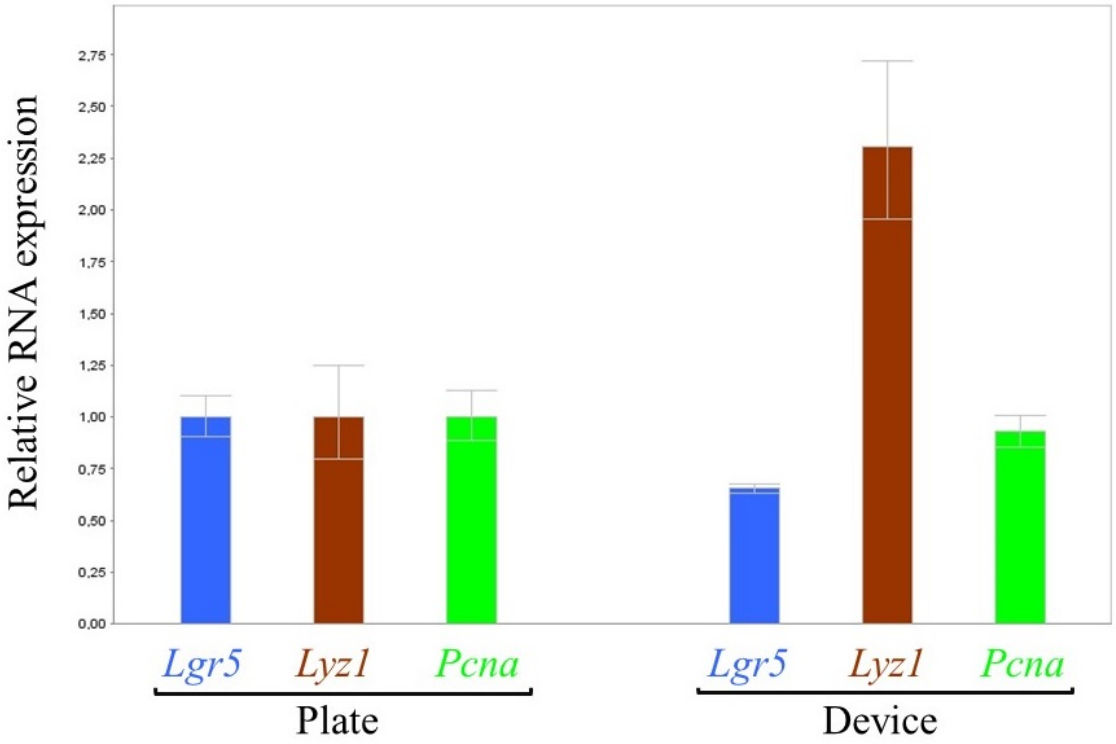

Figure 5.24: Results of quantitative real-time PCR. RNA expression of genes *Lgr5* (blue), *Lyz1* (brown) and *Pcna* (green) in intestinal organoids grown in a 24-well plate and in microfluidic device C for four days. Error bars show the standard deviation between triplicates, n=1.

Quantitative real-time PCR results indicate that proliferative activity in both conditions is equal which confirms organoids are viable and growing in both conditions. *Lgr5* expression was approximately 1.5 times lower in organoids cultured in the device while *Lyz1* expression was around 2.3 times higher than in organoids cultured in the plate. These numbers suggest that there was an enrichment of the Paneth cell lineage and a loss of ISCs in the culture in the microfluidic device. These results indicate that organoids cultured in the device were possibly in a more differentiated state than organoids cultured in the plate. This might simply reflect the higher density of organoids growing in the plate, which implies a slight delay in organoid growth and maturation when compared to the organoids in the device.

Chapter 6

Discussion

6.1 The *Lgr5^{EGFP}* model

Cell cultures derived from primary sources recapitulate more truthfully the characteristics of the native tissue. However, they are more sensitive to experimental conditions than immortalized cell lines, and therefore more challenging to work with. Throughout the development of this work, there were some setbacks with the culture of *Lgr5^{EGFP}* mice-derived organoids. Empirically, it was possible to observe that this population frequently did not survive passaging and displayed an increased sensitivity to the dissociation process. The efficiency of organoid formation from freshly isolated intestinal crypts was also lower in the *Lgr5^{EGFP}* model than in the case of wild-type mouse-derived crypts. The expression of a single *Lgr5* allele may be insufficient to maintain a healthy pool of ISCs. Since RSPOs activate the Wnt pathway by binding to LGR5 in the membrane, a downregulation of *Lgr5* expression may cause a deficient activation of the Wnt pathway. Further studies should be conducted to investigate the reason behind the problems in *Lgr5^{EGFP}*-derived organoid culture.

Another limitation of this model is the mosaic expression of EGFP. Recently, a new model with a reporter of *Lgr5* expression was developed to investigate uterine gland development [89]. The *Lgr5-2A-EGFP/CreERT2/DTR* mouse model shows a non-variegated EGFP pattern of expression, reporting all endogenous *Lgr5^{+}* cells, including stem cells in the small intestine. Moreover, physiological levels of *Lgr5* are maintained. Thus, this model could be a suitable alternative to the *Lgr5^{EGFP}* model and circumvent the two aforementioned limitations.

Given the limitations of the *Lgr5^{EGFP}* organoid culture, part of the microfluidic experiments described in Chapter 5 were performed using wild-type-derived organoids.

6.2 Establishment of intestinal organoids from single ISCs

LGR5^{+}/CD24^{+} and LGR5^{+}/CD24^{-} cells from intestinal organoids were sorted and embedded in Matrigel in an attempt to develop organoids from single ISCs. After 14 days, there was no evidence of organoid growth. This result might be a consequence of a low cell count of *Lgr5^{+}* ISCs or a deficit in stem cues to support ISC proliferation. On the other hand, the sorting process might be too aggressive for ISCs and affect their viability. In the future, organoid development

from single ISCs could be attempted by dissociating crypts or organoids into single cells and plating the entirety of dissociated cells, circumventing the sorting step.

6.3 Microfluidic culture of intestinal organoids

In this work, the introduction of fluidic flow was expected to be beneficial to organoid culture due to two factors: first, the continuous refreshment of growth factors such as NOG, RSPO1 and EGF and the elimination of metabolic waste; second, the shear stress induced on the cells. While the first was expected to enhance diffusion of nutrients and growth factors to the cells and therefore expedite organoid development, the second was hypothesized to trigger a different organization and positioning of the organoids by recapitulating part of the physical stress cells experience in the small intestine.

In the previous chapter, several microfluidic strategies for the culture of intestinal organoids were described. However, none of the approaches developed was compatible with intestinal organoid culture under fluidic conditions.

6.3.1 Limitations of device B

Device B was designed to enable the creation of a Matrigel matrix with an internal channel where culture medium could flow. Intestinal organoids cultured in device B in static conditions did not display normal development and lost viability after 4 days of culture. One of the reasons that can be pointed for this abnormality is the use of a higher concentration of Matrigel (90%), causing an alteration of matrix stiffness. Zaman *et al.*, demonstrated that a change in Matrigel concentration from 60% to 90% causes a 3-fold increase in matrix stiffness [113]. Other possible explanations are the lower concentration of growth factors RSPO1 and NOG in the matrix (2% compared to 10% in standard culture) and the fact that the gel is not immersed in medium as in the case of standard intestinal organoid culture.

In dynamic experiments, this format of Matrigel matrix did not resist to the exposure to fluid flow. Even at the minimum flow rate value (0.73 µL h^{-1}), Matrigel collapsed after a short period of perfusion. The hypothesis that Matrigel collapse was caused by a technical problem was investigated. In previous experiments, the tubing equipment (including inlet and outlet lids) was only connected to the device after Matrigel polymerization, to allow the presence of a molding line inside the device that was necessary to create an intra-matrix channel. It was possible to verify that the assembly process was creating bubbles, resulting from significant changes of pressure inside the device. The creation of bubbles and their forced passage through the intra-matrix channel was exerting too much mechanical stress on the hydrogel, destabilizing its structure prematurely. In following experiments, tubing equipment was connected to the device before Matrigel plating but the same results were observed.

Although Matrigel is a highly bioactive ECM-mimic, containing proteoglycans, laminin, collagen and growth factors, that are extremely important components for the growth of intestinal organoids, its mechanical properties were a limiting factor to the success of the aforementioned strategies. Natural and synthetic alternative matrices that support intestinal organoid growth have been reported in the literature. In 2018, Broguiere *et al.* designed a

fibrin/laminin hydrogel that supported the growth and development of intestinal organoids derived from isolated crypts as well as single $Lgr5^{+}$ cells.

In synthetic matrices, different components can be incorporated to improve mechanical stiffness, biochemical signaling and matrix degradability. A mechanically dynamic polyethylene glycol-based hydrogel (PEG) has been developed to support intestinal organoid growth and differentiation [34]. By analysing the expression pattern of YAP protein when exposed to stiffer and softer extracellular matrices, the authors concluded that an ideal matrix for intestinal organoid development should be stiffer, in an initial phase to promote ISC expansion, and get progressively softer throughout organogenesis. Further functionalization with Arginine-Glycine-Aspartate (RGD) peptides and laminin promoted cell-matrix adhesion and biochemical signaling, respectively. Another group also used a four-arm PEG macromer with maleimide groups at each terminus (PEG-4MAL) hydrogel for human intestinal organoid growth and expansion [21]. In the hydrogel, adhesive RGD sequences were incorporated and Glycine-Proline-Glutamine-Tryptophan (GPQ-W) protease degradable sequences were used for crosslinking. This matrix successfully supported organoid development from ESC and iPSC sources. Both of these studies give important insights about the impact of matrix stiffness on organoid viability and the narrow window of stiffness values compatible with organoid culture. Therefore, using a stiffer hydrogel in device B may be a complex trade-off between improving resistance to fluid flow and affecting organoid viability.

Besides, different matrices may provide distinct biochemical and mechanical cues to intestinal organoids, altering their morphology. In 2017, Sachs *et al.* reported a simple protocol for developing tubular intestinal organoids [78]. The authors discovered that embedding organoid-derived crypts in collagen I floating rings caused organoids to self-align and fuse to form macroscopic tubular hollow structures. Similarly to circular organoids, the lumen was surrounded by a simple epithelial layer and highly proliferative budding domains remained present. Applying this tissue engineering strategy to microfluidic culture systems, in particular, to microfluidic design E, could be an interesting next step in the field and improve the relevance of *in vitro* 3D models of the small intestine.

6.3.2 Static experiments in the Time-lapse microscope

Besides the limitations caused by the mechanical properties of Matrigel, other problems came across while trying to optimize microfluidic systems for intestinal organoid culture. One of the goals of this work was to monitor organoid growth in static and dynamic conditions by time-lapse microscopy. There were several attempts to perform static experiments in the Time-lapse microscope. However, all of them failed either due to premature evaporation of cell culture medium that, in these conditions, occurred at a higher rate than in a conventional incubator, or because crypt viability had been compromised in the passaging step. The characteristics of the microscope stage made it difficult to visualize the levels of cell culture medium in the devices. Also, in this experimental setup, adding medium to compensate evaporation during the experiment very frequently led to accidental moving of the devices. This was a problem because the initial positions of the organoids defined in the acquisition software would not be monitored in the exact same regions as before. Perhaps, it would be useful to increase the height of device C

so that a higher volume of intestinal organoid medium could be overlaid on top of the Matrigel dome, circumventing the necessity of medium replacement and the impact of evaporation.

6.3.3 Dynamic experiment with device D

The failure of the dynamic experiment performed in the time-lapse microscope with device D could be attributed to a number of factors. First, the injection pump, syringes and a section of the tubes had to be placed outside the temperature-controlled chamber of the microscope due to space restrictions. Although the flow rate was slow, it is possible that the temperature of the medium being continuously injected into the device was lower than 37ºC, which is the optimal temperature for organoid growth.

Secondly, internal pressures in the devices might differ from atmospheric pressure and therefore affect the response of organoids. During the experiment, it was evident that different chambers had very different volumes of medium where, out of four chambers, two were filled to the top and two seemed to have just enough medium covering the Matrigel dome (Figure 5.20c), an observation that had already been made in a preliminary test with device C. Given that all chambers were overlaid with the same amount of medium before perfusion, and flow rate was the same, the differences in medium volume could be attributed to variable internal pressures. The lack of control over this parameter has an impact on the availability of growth factors and nutrients in each chamber and on the volume of air above the medium. Pericellular oxygen levels depend on the ratio of volumes between air and medium inside the chamber and low volumes of medium are preferred, reducing the distance for oxygen diffusion from gas to liquid phase [76]. Since oxygen concentration is approximately 40 times higher in the incubator atmosphere compared to cell medium, it is important to ensure medium volume is not a limiting factor to organoid viability.

Another possible explanation for the result is the imbalance of pH levels in the system. As visible in Figure 5.20c, the culture medium showed a bright pink color. Advanced DMEM/F12 composition includes Phenol Red, a pH indicator that turns yellow in acidic solutions, orange/red in neutral solutions and bright pink in basic solutions. This information suggests intestinal organoid medium was basic because pH buffering failed. Buffering activity of sodium bicarbonate incorporated in Advanced DMEM/F12 depends on atmospheric control of CO_2 concentration (Equation 6.1) between 5-10% [33]. Although the environmentally controlled chamber maintains CO_2 levels at 5%, the device was completely isolated with a sealing material to avoid leaks, therefore preventing gas exchange between the inside of the culture chamber and the external environment, as the culture surface was glass and the device material had low gas permeability. Thus, according to the Henderson-Hasselbalch equation for the bicarbonate buffer system (Equation 6.2) [27], a lower CO_2 concentration in the internal air compartment caused the medium pH to increase.

$$CO_2 + H_2O \rightleftharpoons H_2CO_3 \rightleftharpoons {HCO_3}^- + H^+ \tag{6.1}$$

$$pH = 6.1 + log(52\frac{[NaHCO_3]}{\%CO_2} - 1) \tag{6.2}$$

The low permeability of the device also decreases oxygen circulation, which means cell culture is exposed to lower oxygen levels than in the static control or in the 24-well-plate culture. To

tackle the low gas permeability of the system that limits control over O_2 and CO_2 concentrations in cell culture, there are three solutions. The first solution is to pressurize medium vials connected to culture chambers with air containing correct percentages of O_2 and CO_2 to maintain pH and oxygen concentration at physiological values [43, 35]. This solution would require the coupling of additional equipment to the microfluidic system to use the pressure to drive fluid flow. A second strategy would consist of creating a parallel channel to the already existing channel in device D, where air with defined O_2 and CO_2 percentages would flow. The two channels would communicate through a gas permeable membrane, allowing culture medium to establish equilibrium with the gases in the channel and maintain gas concentrations compatible with long term cell-culture [63, 58]. Alternatively, the design could be changed to a PDMS-only device. PDMS is a gas-permeable polymer frequently used in microfluidic applications. Moreover, its permeability can be tuned by varying the composition ratio between the polymer base and curing agent [61]. PDMS could be casted into 3D-printed molds with the desired shapes.

Different flow rates should be tested to determine an optimal flow rate for this microfluidic strategy and also to investigate the impact of different values of shear stress in the spatial organization and morphology of organoids, as well as the expression of key differentiation and stem cell markers. In addition, the strategy for matrix and organoid plating in the device could be altered. Coating the culture surface with matrix (Matrigel or a different hydrogel) and then seeding organoids on the coating, could increase the exposure of organoids to shear stress caused by medium flow. The impact on organoid development in the coating format could be compared to the results obtained with the matrix dome format, described previously.

6.3.4 Comparison of intestinal organoid growth in the well-plate and in the device

Intestinal organoids cultured in the 24-well plate displayed a more apoptotic lumen in comparison to organoids grown in device C in static conditions that had smaller dimensions. These differences in morphology might be a reflection of an accidental difference in organoid seeding density. In a higher density, growth factor demand and use is higher and that could explain the delay in maturation of the organoids in the plate. However, other variables exist between these two conditions such as the volume of medium and consequently the volume of air in the wells, as well as the material on which the Matrigel mix is seeded. This experiment should be repeated in order to clarify the real cause of the discrepancy in organoid development and its correlation with the differences in *Lyz1* and *Lgr5* RNA expression levels. Moreover, organoid development in the device in static conditions should also be monitored by time-lapse imaging for a more complete analysis.

6.3.5 Device properties

All microfluidic devices described above were produced by Biofabics by a stereolithography process and are made of proprietary material. The devices are biocompatible, autoclavable, compatible with live cell imaging, reusable and compact and proved to support organoid growth and differentiation in static conditions.

One of the limitations of these devices is the autofluorescence of the material. Even though the culture surface is glass, the walls of the culture chamber are made of autofluorescent material, making it impossible to acquire fluorescence images of the periphery of the chamber because of the reflection of fluorescence from the walls. It would be important to determine if the material is permanently autofluorescent or if this is caused by autoclaving and, with that information, work around that limitation or replace this material for another with more desirable properties. Another observation was the occurrence of micrometric variations between two identical features in the device, so that two cultures chambers have different sizes, and the same happened with lids. Consequently, finding a perfect fit for chamber/lid or well/lid with inlet pairs was a trial-and-error process that turned into a slow and inefficient task. This is not a direct consequence of the type of material used but of the precision and resolution of the production technique. For that reason, it is preferable to work with a more compact design, like design D, that does not require as many additional parts to be functional, so fitting problems can be avoided.

These problems with fitting resulted in medium leakage from the chambers and wells and the necessity of using a sealing material in the openings of the device. The incorporation of PDMS rings in device C (and in the chamber of device D) did not completely stop medium overflow. Therefore, the design of the chamber lid needs to be readjusted to provide a more efficient isolation. Incorporating an additional ring between the lid and the base of the device could be a possible solution.

Chapter 7

Conclusions and future work

In the present thesis, microfluidic technology was coupled to intestinal organoid culture with the goal of improving the mimicking potential of this three-dimensional model, overcoming some of its shortcomings, and ultimately, developing a robust and defined intestinal-organoid-on-chip system.

The work developed consisted fundamentally on the optimization of, on one hand, microfluidic designs that would be compatible with organoid culture but also with the analysis equipment (in particular, time-lapse imaging) and, secondly, on the optimization of experimental conditions, such as Matrigel concentration, flow rate, leakage and evaporation control. It became evident during this work that translating a well-plate based culture system to a microfluidic platform is not straightforward and can be a long process of trial-and-error. Culture protocols needed to be adapted since different culture surfaces were used, media volumes were reduced and methods and frequency of media replacement were not the same. The main limiting factors in the development of a suitable protocol for these experiments were the mechanical properties of Matrigel, susceptibility to media evaporation in static experiments and to media leakage in dynamic experiments. An additional factor that delayed experimental progress was the instability of organoids derived from the *Lgr5-EGFP-IRES-creERT2* mouse model.

One of the main conclusions retrieved from this optimization process was that Matrigel is an inadequate hydrogel for application in microfluidic devices due to its softness and low resistance to shear stress. Another important conclusion is that gas permeability, often overlooked in cell culture, is essential in microfluidic devices, not just to maintain oxygen supply but to provide enough gaseous CO_2 to balance pH levels in cell culture medium. Lastly, the *Lgr5-EGFP-IRES-creERT2* model should be replaced by an alternative model that does not compromise *Lgr5* expression.

Over the duration of this dissertation, it was not possible to establish a successful protocol for intestinal organoid culture under continuous fluid perfusion in any of the microfluidic devices developed. Nonetheless, intestinal organoids were successfully cultured in a microfluidic device, without fluid flow, composed of two lateral wells and a central culture chamber were a Matrigel dome could be plated. Over 4 days, organoids grew in size and displayed a normal morphology in comparison to the organoids cultured in the 24-well plate. Analysis of RNA expression between the two conditions revealed an increase in differentiation markers and a lower expression of stemness markers in organoids grown in the device that may have been caused by different

organoid seeding densities. However, these results are not conclusive since they were retrieved from a single independent experiment.

Additionally, a microfluidic device that provided a cylindrical surface for organoid growth and the possibility of culturing other cell populations in the same chamber was designed. Organoid growth could be monitored by microscopy and histology and the study of growth factor gradients established in the organoid might uncover the triggers that drive spatial organization in the tubular organoid. If implemented successfully, this device has the potential to be the first on-chip system featuring a tubular intestinal organoid and might become a more complete and accurate *in vitro* model of the small intestine.

Since this dissertation project was conducted during the COVID-19 pandemic, access to laboratory facilities was denied or conditioned for a significant part of time. That time was invested in researching for other intestine-on-chip models reported in the literature, their main characteristics and applications. The result of that research, together with an adaptation of Chapter 2, culminated in a review paper that will be submitted during the next weeks.

Considering the results and observations reported in this dissertation, in the short-term, it would be important to repeat the static experiment in microfluidic device C, in comparison to standard culture, to draw conclusions about the effects of that culture format in organoid behavior and microarchitecture. In addition, the design of microfluidic device D needs to be modified to allow gas exchange and maintenance of oxygen and carbon dioxide levels inside the culture chamber, so that dynamic experiments in the long-term can be performed. Organoid growth in both types of experiments should be compared by analysis of RNA expression and immunohistochemistry. By immunohistochemistry, the expression of relevant cell markers such as: *Lgr5* (ISCs), lysozyme (Paneth cells), sucrase-isomaltase (absorptive lineage), mucin (Goblet cells), and chromogranin A (enteroendocrine lineage) could be analyzed to evaluate if the micro-organization of the proliferative and differentiated compartments is similar to the *in vivo* condition.

In the long-term, replacing Matrigel with a hydrogel with more easily tunable mechanical properties and a defined composition would make organoid culture more versatile for application in microfluidic approaches and overcome the disadvantages of using a variable and animal-derived matrix [56]. Also, testing organoid behavior in microfluidic settings in a coating format, instead of a dome, could result in interesting observations, given that organoids would be more exposed to shear stress. In addition, culturing organoids in a collagen I matrix, in microfluidic device E, would possibly stimulate them to acquire a tubular shape, since that phenomenon was observed before by Sachs *et al.* [78].

All in all, this dissertation describes the beginning of the development process of a microfluidic platform for the culture of intestinal organoids, aiming to build an intestinal-organoid-on-chip that is an accurate *in vitro* model of the small intestine. To further promote the physiological relevance of this model, additional features should be incorporated such as peristalsis simulation and co-culture with different cell types like mesenchymal, immune and endothelial cells.

References

[1] OrganoFlow® L | Mimetas. Cited on page 26.

[2] OrganoPlate® Caco-2 | Mimetas. Cited on page 26.

[3] OrganoTEER® | Mimetas. Cited on page 26.

[4] H. Anwar, S. Irfan, G. Hussain, M. Naeem Faisal, H. Muzaffar, I. Mustafa, I. Mukhtar, S. Malik, and M. Irfan Ullah. Gut Microbiome: A New Organ System in Body. In *Parasitol. Microbiol. Res. [Working Title]*. IntechOpen, nov 2019. Cited on page 3.

[5] R. Aoki, M. Shoshkes-Carmel, N. Gao, S. Shin, C. L. May, M. L. Golson, A. M. Zahm, M. Ray, C. L. Wiser, C. V. Wright, and K. H. Kaestner. Foxl1-Expressing Mesenchymal Cells Constitute the Intestinal Stem Cell Niche. *CMGH*, 2016. Cited on page 8.

[6] A. U. R. Aziz, C. Geng, M. Fu, X. Yu, K. Qin, and B. Liu. The role of microfluidics for organ on chip simulations, jun 2017. Cited on pages 11, 12, and 16.

[7] A. Banerjee, E. T. McKinley, J. Von Moltke, R. J. Coffey, and K. S. Lau. Interpreting heterogeneity in intestinal tuft cell structure and function, 2018. Cited on page 3.

[8] F. Baquero and C. Nombela. The microbiome as a human organ. *Clin. Microbiol. Infect.*, 18:2–4, jul 2012. Cited on page 3.

[9] N. Barker, M. V. De Wetering, and H. Clevers. The intestinal stem cell, 2008. Cited on page 4.

[10] N. Barker, J. H. Van Es, J. Kuipers, P. Kujala, M. Van Den Born, M. Cozijnsen, A. Haegebarth, J. Korving, H. Begthel, P. J. Peters, and H. Clevers. Identification of stem cells in small intestine and colon by marker gene Lgr5. *Nature*, 449(7165):1003–1007, 2007. Cited on pages 4, 5, 37, 45, 46, and 69.

[11] N. Barker, A. Van Oudenaarden, and H. Clevers. Identifying the stem cell of the intestinal crypt: Strategies and pitfalls, oct 2012. Cited on page 45.

[12] O. Basak, J. Beumer, K. Wiebrands, H. Seno, A. van Oudenaarden, and H. Clevers. Induced Quiescence of Lgr5+ Stem Cells in Intestinal Organoids Enables Differentiation of Hormone-Producing Enteroendocrine Cells. *Cell Stem Cell*, 2017. Cited on page 7.

[13] C. Beaurivage, E. Naumovska, Y. X. Chang, E. D. Elstak, A. Nicolas, H. Wouters, G. van Moolenbroek, H. L. Lanz, S. J. Trietsch, J. Joore, P. Vulto, R. A. Janssen, K. S. Erdmann, J. Stallen, and D. Kurek. Development of a gut-on-a-chip model for high throughput disease modeling and drug discovery. *Int. J. Mol. Sci.*, 20(22), nov 2019. Cited on page 26.

[14] H. Bei, W. Guang-Ce, Z. Chen-Kui, and L. Zhen-Gang. The experimental research of R-phycoerythrin subunits on cancer treatment: A new photosensitizer in PDT. *Cancer Biother. Radiopharm.*, 17(1):35–42, 2002. Cited on page 51.

[15] A. Bein, W. Shin, S. Jalili-Firoozinezhad, M. H. Park, A. Sontheimer-Phelps, A. Tovaglieri, A. Chalkiadaki, H. J. Kim, and D. E. Ingber. Microfluidic Organ-on-a-Chip Models of Human Intestine. *Cell. Mol. Gastroenterol. Hepatol.*, 5(4):659–668, jan 2018. Cited on page 34.

[16] M. J. Bull and N. T. Plummer. Part 1: The Human Gut Microbiome in Health and Disease. *Integr. Med. (Encinitas).*, 13(6):17–22, dec 2014. Cited on page 3.

[17] D. F. D. Campos, C. D. Lindsay, J. G. Roth, B. L. LeSavage, A. J. Seymour, B. A. Krajina, R. Ribeiro, P. F. Costa, A. Blaeser, and S. C. Heilshorn. Bioprinting Cell- and Spheroid-Laden Protein-Engineered Hydrogels as Tissue-on-Chip Platforms. *Front. Bioeng. Biotechnol.*, 8, apr 2020. Cited on page 54.

[18] H. Cheng and C. P. Leblond. Origin, differentiation and renewal of the four main epithelial cell types in the mouse small intestine V. Unitarian theory of the origin of the four epithelial cell types. *Am. J. Anat.*, 1974. Cited on page 4.

[19] Corning. Corning Matrigel Matrix. Cited on page 32.

[20] P. F. Costa, H. J. Albers, J. E. Linssen, H. H. Middelkamp, L. Van Der Hout, R. Passier, A. Van Den Berg, J. Malda, and A. D. Van Der Meer. Mimicking arterial thrombosis in a 3D-printed microfluidic: In vitro vascular model based on computed tomography angiography data. *Lab Chip*, 2017. Cited on page 15.

[21] R. Cruz-Acuña, M. Quirós, A. E. Farkas, P. H. Dedhia, S. Huang, D. Siuda, V. García-Hernández, A. J. Miller, J. R. Spence, A. Nusrat, and A. J. García. Synthetic hydrogels for human intestinal organoid generation and colonic wound repair. *Nat. Cell Biol.*, 19(11):1326–1335, nov 2017. Cited on page 73.

[22] A. S. Darwich, U. Aslam, D. M. Ashcroft, and A. Rostami-Hodjegan. Meta-analysis of the turnover of intestinal epithelia in preclinical animal species and humans, dec 2014. Cited on page 3.

[23] E. de Poel, J. W. Lefferts, and J. M. Beekman. Intestinal organoids for Cystic Fibrosis research. *J. Cyst. Fibros.*, 19:S60–S64, 2020. Cited on page 11.

[24] J. F. Dekkers, C. L. Wiegerinck, H. R. De Jonge, I. Bronsveld, H. M. Janssens, K. M. De Winter-De Groot, A. M. Brandsma, N. W. De Jong, M. J. Bijvelds, B. J. Scholte, E. E. Nieuwenhuis, S. Van Den Brink, H. Clevers, C. K. Van Der Ent, S. Middendorp, and J. M. Beekman. A functional CFTR assay using primary cystic fibrosis intestinal organoids. *Nat. Med.*, 2013. Cited on page 11.

[25] P. A. Doevendans, M. J. Daemen, E. D. De Muinck, and J. F. Smits. Cardiovascular phenotyping in mice, jul 1998. Cited on page 53.

[26] R. L. Drake, A. W. Vogl, and A. W. Mitchell. Gray's Anatomy for Students, Third Edition. *Gray's Anat. Students*, 2015. Cited on page 1.

[27] P. Esser. pH and Pressure in Closed Tissue Culture Vessels., 2010. Cited on page 74.

[28] J. M. Evans, L. S. Morris, and J. R. Marchesi. The gut microbiome: the role of a virtual organ in the endocrinology of the host. *J. Endocrinol.*, 218(3):R37–R47, sep 2013. Cited on page 3.

[29] A. Fatehullah, S. H. Tan, and N. Barker. Organoids as an in vitro model of human development and disease, feb 2016. Cited on page 9.

[30] M. A. Ferraz, H. H. Henning, P. F. Costa, J. Malda, F. P. Melchels, R. Wubbolts, T. A. Stout, P. L. Vos, and B. M. Gadella. Improved bovine embryo production in an oviduct-on-a-chip system: prevention of poly-spermic fertilization and parthenogenic activation. *Lab Chip*, 2017. Cited on page 15.

[31] B. K. Gale, A. R. Jafek, C. J. Lambert, B. L. Goenner, H. Moghimifam, U. C. Nze, and S. K. Kamarapu. A review of current methods in microfluidic device fabrication and future commercialization prospects, 2018. Cited on pages xv, 13, 14, 15, and 16.

[32] H. Gehart and H. Clevers. Tales from the crypt: new insights into intestinal stem cells. *Nat. Rev. Gastroenterol. Hepatol.*, 16(1):19–34, 2019. Cited on pages 5, 6, 7, and 51.

[33] Gibco™. Advanced DMEM/F-12. Cited on page 74.

[34] N. Gjorevski, N. Sachs, A. Manfrin, S. Giger, M. E. Bragina, P. Ordóñez-Morán, H. Clevers, and M. P. Lutolf. Designer matrices for intestinal stem cell and organoid culture. *Nature*, 539(7630):560–564, nov 2016. Cited on page 73.

[35] R. Gómez-Sjöberg, A. A. Leyrat, D. M. Pirone, C. S. Chen, and S. R. Quake. Versatile, fully automated, microfluidic cell culture system. *Anal. Chem.*, 79(22):8557–8563, nov 2007. Cited on page 75.

[36] S. A. N. Gowers, V. F. Curto, C. A. Seneci, C. Wang, S. Anastasova, P. Vadgama, G.-Z. Yang, and M. G. Boutelle. 3D Printed Microfluidic Device with Integrated Biosensors for Online Analysis of Subcutaneous Human Microdialysate. *Anal. Chem.*, 87(15):7763–7770, aug 2015. Cited on page 14.

[37] A. D. Gracz, M. K. Fuller, F. Wang, L. Li, M. Stelzner, J. C. Dunn, M. G. Martin, and S. T. Magness. CD24 and CD44 mark human intestinal epithelial cell populations with characteristics of active and facultative stem cells. *Stem Cells*, 31(9):2024–2030, sep 2013. Cited on page 51.

[38] G. Greicius, Z. Kabiri, K. Sigmundsson, C. Liang, R. Bunte, M. K. Singh, and D. M. Virshup. PDGFRα+ pericryptal stromal cells are the critical source of Wnts and RSPO3 for murine intestinal stem cells in vivo. *Proc. Natl. Acad. Sci. U. S. A.*, 2018. Cited on page 8.

[39] J. Groll, T. Boland, T. Blunk, J. A. Burdick, D.-W. Cho, P. D. Dalton, B. Derby, G. Forgacs, Q. Li, V. A. Mironov, L. Moroni, M. Nakamura, W. Shu, S. Takeuchi, G. Vozzi, T. B. F. Woodfield, T. Xu, J. J. Yoo, and J. Malda. Biofabrication: reappraising the definition of an evolving field. *Biofabrication*, 8(1):013001, jan 2016. Cited on page 12.

[40] Y. Guo, Z. Li, W. Su, L. Wang, Y. Zhu, and J. Qin. A Biomimetic Human Gut-on-a-Chip for Modeling Drug Metabolism in Intestine. *Artif. Organs*, 42(12):1196–1205, dec 2018. Cited on page 28.

[41] H. J. Haiser, K. L. Seim, E. P. Balskus, and P. J. Turnbaugh. Mechanistic insight into digoxin inactivation by Eggerthella lenta augments our understanding of its pharmacokinetics. *Gut Microbes*, 5(2):233–8, 2014. Cited on page 4.

[42] J. E. Hall. *Guyton and Hall: Textbook of Medical Physiology*, volume 8. 2017. Cited on page 1.

[43] S. Halldorsson, E. Lucumi, R. Gómez-Sjöberg, and R. M. Fleming. Advantages and challenges of microfluidic cell culture in polydimethylsiloxane devices, jan 2015. Cited on page 75.

[44] H. F. Helander and L. Fändriks. Surface area of the digestive tract-revisited. *Scand. J. Gastroenterol.*, 49(6):681–689, 2014. Cited on pages 1 and 2.

[45] S. Jalili-Firoozinezhad, F. S. Gazzaniga, E. L. Calamari, D. M. Camacho, C. W. Fadel, A. Bein, B. Swenor, B. Nestor, M. J. Cronce, A. Tovaglieri, O. Levy, K. E. Gregory, D. T. Breault, J. M. S. Cabral, D. L. Kasper, R. Novak, and D. E. Ingber. A complex human gut microbiome cultured in an anaerobic intestine-on-a-chip. *Nat. Biomed. Eng.*, 3(7):520–531, jul 2019. Cited on pages xiii, 25, 32, and 53.

[46] S. M. Jandhyala, R. Talukdar, C. Subramanyam, H. Vuyyuru, M. Sasikala, and D. N. Reddy. Role of the normal gut microbiota. *World J. Gastroenterol.*, 2015. Cited on pages 3 and 4.

[47] K. Kadimisetty, I. M. Mosa, S. Malla, J. E. Satterwhite-Warden, T. M. Kuhns, R. C. Faria, N. H. Lee, and J. F. Rusling. 3D-printed supercapacitor-powered electrochemiluminescent protein immunoarray. *Biosens. Bioelectron.*, 77:188–193, mar 2016. Cited on page 14.

[48] M. Kasendra, R. Luc, J. Yin, D. V. Manatakis, G. Kulkarni, C. Lucchesi, J. Sliz, A. Apostolou, L. Sunuwar, J. Obrigewitch, K.-J. Jang, G. A. Hamilton, M. Donowitz, and K. Karalis. Duodenum Intestine-Chip for preclinical drug assessment in a human relevant model. *Elife*, 9, jan 2020. Cited on pages 25 and 53.

[49] M. Kasendra, A. Tovaglieri, A. Sontheimer-Phelps, S. Jalili-Firoozinezhad, A. Bein, A. Chalkiadaki, W. Scholl, C. Zhang, H. Rickner, C. A. Richmond, H. Li, D. T. Breault, and D. E. Ingber. Development of a primary human Small Intestine-on-a-Chip using biopsy-derived organoids. *Sci. Rep.*, 8(1):2871, dec 2018. Cited on pages 24, 26, 32, and 53.

[50] G. Kaur and J. M. Dufour. Cell lines. *Spermatogenesis*, 2(1):1–5, 2012. Cited on page 19.

[51] H. J. Kim, D. Huh, G. Hamilton, and D. E. Ingber. Human gut-on-a-chip inhabited by microbial flora that experiences intestinal peristalsis-like motions and flow. *Lab Chip*, 12(12):2165, jun 2012. Cited on pages 20, 21, 22, 31, and 35.

[52] H. J. Kim and D. E. Ingber. Gut-on-a-Chip microenvironment induces human intestinal cells to undergo villus differentiation. *Integr. Biol.*, 5(9):1130, sep 2013. Cited on pages 22, 24, 31, and 35.

[53] H. J. Kim, H. Li, J. J. Collins, and D. E. Ingber. Contributions of microbiome and mechanical deformation to intestinal bacterial overgrowth and inflammation in a human gut-on-a-chip. *Proc. Natl. Acad. Sci. U. S. A.*, 113(1):E7–15, jan 2016. Cited on pages 23 and 31.

[54] T. H. Kim, S. Escudero, and R. A. Shivdasani. Intact function of Lgr5 receptor-expressing intestinal stem cells in the absence of Paneth cells. *Proc. Natl. Acad. Sci. U. S. A.*, 2012. Cited on pages 7 and 24.

[55] H. Kimura, T. Yamamoto, H. Sakai, Y. Sakai, and T. Fujii. An integrated microfluidic system for long-term perfusion culture and on-line monitoring of intestinal tissue models. *Lab Chip*, 8(5):741, may 2008. Cited on pages xiii, 19, and 20.

[56] H. K. Kleinman and G. R. Martin. Matrigel: Basement membrane matrix with biological activity, 2005. Cited on pages 32 and 78.

[57] S. Knowlton, S. Onal, C. H. Yu, J. J. Zhao, and S. Tasoglu. Bioprinting for cancer research, sep 2015. Cited on page 8.

[58] R. Koens, Y. Tabata, J. C. Serrano, S. Aratake, D. Yoshino, R. D. Kamm, and K. Funamoto. Microfluidic platform for three-dimensional cell culture under spatiotemporal heterogeneity of oxygen tension. *APL Bioeng.*, 4(1):016106, mar 2020. Cited on page 75.

[59] M. C. Kreissl, H. M. Wu, D. B. Stout, W. Ladno, T. H. Schindler, X. Zhang, J. O. Prior, M. L. Prins, A. F. Chatziioannou, S. C. Huang, and H. R. Schelbert. Noninvasive measurement of cardiovascular function in mice with high-temporal-resolution small-animal PET. *J. Nucl. Med.*, 47(6):974–980, jun 2006. Cited on page 53.

[60] M. R. Ladd, D. F. Niño, J. C. March, C. P. Sodhi, and D. J. Hackam. Generation of an artificial intestine for the management of short bowel syndrome, 2016. Cited on page 3.

[61] A. Lamberti, S. L. Marasso, and M. Cocuzza. PDMS membranes with tunable gas permeability for microfluidic applications. *RSC Adv.*, 4(106):61415–61419, 2014. Cited on page 75.

[62] M. A. Lancaster and J. A. Knoblich. Organogenesisin a dish: Modeling development and disease using organoid technologies, 2014. Cited on pages 9 and 11.

[63] E. Leclerc, Y. Sakai, and T. Fujii. Microfluidic PDMS (Polydimethylsiloxane) bioreactor for large-scale culture of hepatocytes. *Biotechnol. Prog.*, 20(3):750–755, may 2004. Cited on page 75.

[64] C. Leung, S. H. Tan, and N. Barker. Recent Advances in Lgr5+ Stem Cell Research. *Trends Cell Biol.*, 28(5):380–391, 2018. Cited on page 6.

[65] M. L. Li, J. Aggeler, D. A. Farson, C. Hatier, J. Hassell, and M. J. Bissell. Influence of a reconstituted basement membrane and its components on casein gene expression and secretion in mouse mammary epithelial cells. *Proc. Natl. Acad. Sci. U. S. A.*, 1987. Cited on page 9.

[66] N. C. Lindquist, P. Nagpal, K. M. McPeak, D. J. Norris, and S. H. Oh. Engineering metallic nanostructures for plasmonics and nanophotonics, mar 2012. Cited on page 13.

[67] D. Mandt, P. Gruber, M. Markovic, M. Tromayer, M. Rothbauer, S. R. Adam Kratz, S. F. Ali, J. Van Hoorick, W. Holnthoner, S. Mühleder, P. Dubruel, S. Van Vlierberghe, P. Ertl, R. Liska, and A. Ovsianikov. Fabrication of biomimetic placental barrier structures within a microfluidic device utilizing two-photon polymerization. *Int. J. Bioprinting*, 2018. Cited on page 14.

[68] E. Marshman, C. Booth, and C. S. Potten. The intestinal epithelial stem cell, 2002. Cited on page 4.

[69] M. Maurer, M. S. Gresnigt, A. Last, T. Wollny, F. Berlinghof, R. Pospich, Z. Cseresnyes, A. Medyukhina, K. Graf, M. Gröger, M. Raasch, F. Siwczak, S. Nietzsche, I. D. Jacobsen, M. T. Figge, B. Hube, O. Huber, and A. S. Mosig. A three-dimensional immunocompetent intestine-on-chip model as in vitro platform for functional and microbial interaction studies. *Biomaterials*, 220:119396, nov 2019. Cited on pages 29, 30, 32, and 53.

[70] A. L. Mescher. *Junqueira's Basic Histology: Text and Atlas, Fourteenth Edition*. 2015. Cited on pages 1, 2, and 3.

[71] G. L. Moldovan, B. Pfander, and S. Jentsch. PCNA, the Maestro of the Replication Fork, may 2007. Cited on page 69.

[72] L. Ogiolda, R. Wanke, O. Rottmann, W. Hermanns, and E. Wolf. Intestinal dimensions of mice divergently selected for body weight. *Anat. Rec.*, 250(3):292–299, mar 1998. Cited on page 53.

[73] A. Ootani, X. Li, E. Sangiorgi, Q. T. Ho, H. Ueno, S. Toda, H. Sugihara, K. Fujimoto, I. L. Weissman, M. R. Capecchi, and C. J. Kuo. Sustained in vitro intestinal epithelial culture within a Wnt-dependent stem cell niche. *Nat. Med.*, 2009. Cited on page 10.

[74] S. E. Park, A. Georgescu, and D. Huh. Organoids-on-a-chip, 2019. Cited on pages 16 and 17.

[75] B. Pereira, A. L. Amaral, A. Dias, N. Mendes, V. Muncan, A. R. Silva, C. Thibert, A. G. Radu, L. David, V. Máximo, G. R. van den Brink, M. Billaud, and R. Almeida. MEX3A regulates Lgr5 + stem cell maintenance in the developing intestinal epithelium . *EMBO Rep.*, 21(4), 2020. Cited on page 10.

[76] T. L. Place, F. E. Domann, and A. J. Case. Limitations of oxygen delivery to cells in culture: An underappreciated problem in basic and translational research, dec 2017. Cited on page 74.

[77] K. Pocock, L. Delon, V. Bala, S. Rao, C. Priest, C. Prestidge, and B. Thierry. Intestine-on-a-Chip Microfluidic Model for Efficient in Vitro Screening of Oral Chemotherapeutic Uptake. *ACS Biomater. Sci. Eng.*, 3(6):951–959, jun 2017. Cited on pages 27 and 28.

[78] N. Sachs, Y. Tsukamoto, P. Kujala, P. J. Peters, and H. Clevers. Intestinal epithelial organoids fuse to form self-organizing tubes in floating collagen gels. *Dev.*, 144(6):1107–1112, mar 2017. Cited on pages 73 and 78.

[79] M. S. Sadabad, J. Z. Von Martels, M. T. Khan, T. Blokzijl, G. Paglia, G. Dijkstra, H. J. Harmsen, and K. N. Faber. A simple coculture system shows mutualism between anaerobic faecalibacteria and epithelial Caco-2 cells. *Sci. Rep.*, 5, 2015. Cited on page 19.

[80] Y. Sambuy, I. De Angelis, G. Ranaldi, M. L. Scarino, A. Stammati, and F. Zucco. The Caco-2 cell line as a model of the intestinal barrier: Influence of cell and culture-related factors on Caco-2 cell functional characteristics, 2005. Cited on page 19.

[81] A. Sato. Tuft cells, 2007. Cited on page 3.

[82] T. Sato, D. E. Stange, M. Ferrante, R. G. Vries, J. H. Van Es, S. Van Den Brink, W. J. Van Houdt, A. Pronk, J. Van Gorp, P. D. Siersema, and H. Clevers. Long-term expansion of epithelial organoids from human colon, adenoma, adenocarcinoma, and Barrett's epithelium. *Gastroenterology*, 2011. Cited on page 7.

[83] T. Sato, J. H. Van Es, H. J. Snippert, D. E. Stange, R. G. Vries, M. Van Den Born, N. Barker, N. F. Shroyer, M. Van De Wetering, and H. Clevers. Paneth cells constitute the niche for Lgr5 stem cells in intestinal crypts. *Nature*, 469(7330):415–418, jan 2011. Cited on pages 10, 51, and 69.

[84] T. Sato, R. G. Vries, H. J. Snippert, M. Van De Wetering, N. Barker, D. E. Stange, J. H. Van Es, A. Abo, P. Kujala, P. J. Peters, and H. Clevers. Single Lgr5 stem cells build crypt-villus structures in vitro without a mesenchymal niche. *Nature*, 459(7244):262–265, 2009. Cited on pages 6, 9, 10, 38, 48, and 51.

[85] K. Schneeberger, B. Spee, P. Costa, N. Sachs, H. Clevers, and J. Malda. Converging biofabrication and organoid technologies: The next frontier in hepatic and intestinal tissue engineering?, 2017. Cited on page 12.

[86] School of Anatomy and Human Biology - The University of Western Australia. Blue Histology - Gastrointestinal Tract, 2009. Cited on page 2.

[87] J. Schuijers, L. G. Van Der Flier, J. Van Es, and H. Clevers. Robust cre-mediated recombination in small intestinal stem cells utilizing the Olfm4 locus. *Stem Cell Reports*, 3(2):234–241, aug 2014. Cited on page 45.

[88] R. Seishima and N. Barker. A contemporary snapshot of intestinal stem cells and their regulation. *Differentiation*, 108(November 2018):3–7, 2019. Cited on page 6.

[89] R. Seishima, C. Leung, S. Yada, K. B. A. Murad, L. T. Tan, A. Hajamohideen, S. H. Tan, H. Itoh, K. Murakami, Y. Ishida, S. Nakamizo, Y. Yoshikawa, E. Wong, and N. Barker. Neonatal Wnt-dependent Lgr5 positive stem cells are essential for uterine gland development. *Nat. Commun.*, 10(1), dec 2019. Cited on page 71.

[90] P. Shah, J. V. Fritz, E. Glaab, M. S. Desai, K. Greenhalgh, A. Frachet, M. Niegowska, M. Estes, C. Jäger, C. Seguin-Devaux, F. Zenhausern, and P. Wilmes. A microfluidics-based in vitro model of the gastrointestinal human–microbe interface. *Nat. Commun.*, 7(1):11535, sep 2016. Cited on page 29.

[91] W. Shin, C. D. Hinojosa, D. E. Ingber, and H. J. Kim. Human Intestinal Morphogenesis Controlled by Transepithelial Morphogen Gradient and Flow-Dependent Physical Cues in a Microengineered Gut-on-a-Chip. *iScience*, 15:391–406, may 2019. Cited on pages 25 and 32.

[92] W. Shin and H. J. Kim. Intestinal barrier dysfunction orchestrates the onset of inflammatory host–microbiome cross-talk in a human gut inflammation-on-a-chip. *Proc. Natl. Acad. Sci.*, 115(45):E10539–E10547, nov 2018. Cited on pages 23 and 31.

[93] B. Sidar, B. R. Jenkins, S. Huang, J. R. Spence, S. T. Walk, and J. N. Wilking. Long-term flow through human intestinal organoids with the gut organoid flow chip (GOFlowChip). *Lab Chip*, 19(20):3552–3562, oct 2019. Cited on pages 30, 31, 32, 35, and 53.

[94] S. Singh, M. Sasikala, G. V. Rao, and D. N. Reddy. Intestinal stem cells in homeostasis and cancer. In *Regen. Med. - from Protoc. to Patient 2. Stem Cell Sci. Technol. Third Ed.* 2016. Cited on pages 7 and 8.

[95] N. R. Smith, A. C. Gallagher, and M. H. Wong. Defining a stem cell hierarchy in the intestine: markers, caveats and controversies. *J. Physiol.*, 594(17):4781–4790, 2016. Cited on page 6.

[96] R. G. Spurrier, A. L. Speer, C. N. Grant, D. E. Levin, and T. C. Grikscheit. Vitrification preserves murine and human donor cells for generation of tissue-engineered intestine. *J. Surg. Res.*, 190(2):399–406, 2014. Cited on page 10.

[97] W. T. Stott, M. D. Dryzga, and J. C. Ramsey. Blood-flow distribution in the mouse. *J. Appl. Toxicol.*, 1983. Cited on page 53.

[98] F. Tournoux, B. Petersen, H. Thibault, L. Zou, M. J. Raher, B. Kurtz, E. F. Halpern, M. Chaput, W. Chao, M. H. Picard, and M. Scherrer-Crosbie. Validation of noninvasive measurements of cardiac output in mice using echocardiography. *J. Am. Soc. Echocardiogr.*, 24(4):465–470, apr 2011. Cited on page 53.

[99] S. J. Trietsch, E. Naumovska, D. Kurek, M. C. Setyawati, M. K. Vormann, K. J. Wilschut, H. L. Lanz, A. Nicolas, C. P. Ng, J. Joore, S. Kustermann, A. Roth, T. Hankemeier, A. Moisan, and P. Vulto. Membrane-free culture and real-time barrier integrity assessment of perfused intestinal epithelium tubes. *Nat. Commun.*, 8(1), dec 2017. Cited on pages 26 and 27.

[100] A. M. Valdes, J. Walter, E. Segal, and T. D. Spector. Role of the gut microbiota in nutrition and health. *BMJ*, 2018. Cited on page 3.

[101] T. Valenta, B. Degirmenci, A. E. Moor, P. Herr, D. Zimmerli, M. B. Moor, G. Hausmann, C. Cantù, M. Aguet, and K. Basler. Wnt Ligands Secreted by Subepithelial Mesenchymal Cells Are Essential for the Survival of Intestinal Stem Cells and Gut Homeostasis. *Cell Rep.*, 2016. Cited on page 8.

[102] M. Van de Wetering, E. Sancho, C. Verweij, W. De Lau, I. Oving, A. Hurlstone, K. Van der Horn, E. Batlle, D. Coudreuse, A. P. Haramis, M. Tjon-Pon-Fong, P. Moerer, M. Van den Born, G. Soete, S. Pals, M. Eilers, R. Medema, and H. Clevers. The β-catenin/TCF-4 complex imposes a crypt progenitor phenotype on colorectal cancer cells. *Cell*, 2002. Cited on page 4.

[103] L. G. Van der Flier, J. Sabates-Bellver, I. Oving, A. Haegebarth, M. De Palo, M. Anti, M. E. Van Gijn, S. Suijkerbuijk, M. Van de Wetering, G. Marra, and H. Clevers. The Intestinal Wnt/TCF Signature. *Gastroenterology*, 2007. Cited on page 4.

[104] J. H. van Es, A. Haegebarth, P. Kujala, S. Itzkovitz, B.-K. Koo, S. F. Boj, J. Korving, M. van den Born, A. van Oudenaarden, S. Robine, and H. Clevers. A Critical Role for the Wnt Effector Tcf4 in Adult Intestinal Homeostatic Self-Renewal. *Mol. Cell. Biol.*, 2012. Cited on page 6.

[105] J. Vaskovic and A. Osika. Goblet cells: Definition, location, function | KenHub, 2020. Cited on page 2.

[106] J. H. Wang, T. C. Liu, Y. C. Cao, X. F. Hua, H. Q. Wang, H. L. Zhang, X. Q. Li, and Y. D. Zhao. Fluorescence resonance energy transfer between FITC and water-soluble CdSe/ZnS quantum dots. *Colloids Surfaces A Physicochem. Eng. Asp.*, 302(1-3):168–173, jul 2007. Cited on page 51.

[107] C. L. Watson, M. M. Mahe, J. Múnera, J. C. Howell, N. Sundaram, H. M. Poling, J. I. Schweitzer, J. E. Vallance, C. N. Mayhew, Y. Sun, G. Grabowski, S. R. Finkbeiner, J. R. Spence, N. F. Shroyer, J. M. Wells, and M. A. Helmrath. An in vivo model of human small intestine using pluripotent stem cells. *Nat. Med.*, 2014. Cited on page 10.

[108] G. Weisgrab, A. Ovsianikov, and P. F. Costa. Functional 3D Printing for Microfluidic Chips, 2019. Cited on page 14.

[109] I. A. Williamson, J. W. Arnold, L. A. Samsa, L. Gaynor, M. DiSalvo, J. L. Cocchiaro, I. Carroll, M. A. Azcarate-Peril, J. F. Rawls, N. L. Allbritton, and S. T. Magness. A High-Throughput Organoid Microinjection Platform to Study Gastrointestinal Microbiota and Luminal Physiology. *Cell. Mol. Gastroenterol. Hepatol.*, 6(3):301–319, 2018. Cited on page 12.

[110] M. J. Workman, J. P. Gleeson, E. J. Troisi, H. Q. Estrada, S. J. Kerns, C. D. Hinojosa, G. A. Hamilton, S. R. Targan, C. N. Svendsen, and R. J. Barrett. Enhanced Utilization of Induced Pluripotent Stem Cell–Derived Human Intestinal Organoids Using Microengineered Chips. *Cell. Mol. Gastroenterol. Hepatol.*, 5(4):669–677.e2, 2018. Cited on pages 24 and 32.

[111] A. Yadegari, F. Fahimipour, M. Rasoulianboroujeni, E. Dashtimoghadarm, M. Omidi, H. Golzar, and M. Tahriri. Specific considerations in scaffold design for oral tissue engineering. *Biomater. Oral Dent. Tissue Eng.*, pages 157–183, jan 2017. Cited on page 13.

[112] K. S. Yan, L. A. Chia, X. Li, A. Ootani, J. Su, J. Y. Lee, N. Su, Y. Luo, S. C. Heilshorn, M. R. Amieva, E. Sangiorgi, M. R. Capecchi, and C. J. Kuo. The intestinal stem cell markers Bmi1 and Lgr5 identify two functionally distinct populations. *Proc. Natl. Acad. Sci. U. S. A.*, 109(2):466–471, 2012. Cited on page 6.

[113] M. H. Zaman, L. M. Trapani, A. Siemeski, D. MacKellar, H. Gong, R. D. Kamm, A. Wells, D. A. Lauffenburger, and P. Matsudaira. Migration of tumor cells in 3D matrices is governed by matrix stiffness along with cell-matrix adhesion and proteolysis. *Proc. Natl. Acad. Sci. U. S. A.*, 103(29):10889–10894, jul 2006. Cited on page 72.